Sphingomyelin d18:1/14:0 and TLR4: Fueling the Fire in Metaflammation

Doctoral Thesis
to obtain a doctorate (PhD)
from the Faculty of Medicine
of the University of Bonn

Friederike Sophie Gorki
from Grevesmühlen, Germany

2024

Written with authorization of
the Faculty of Medicine of the University of Bonn

First Reviewer: PD Dr. Peter Düwell
Second Reviewer: Prof. Dr. Matthias Geyer
Supervisor: Prof. Dr. Eicke Latz

Day of oral examination: 19.02.2024

From the Institute of Innate Immunity
Director: Prof. Dr. Eicke Latz

TABLE OF CONTENTS

ABBREVIATIONS

x g	gravitational constant (centrifugal force)
β-Me	β-Mercaptoethanol (2-Mercaptoethanol)
ABCA	ATP-binding cassette-subfamily A
ABCG	ATP-binding cassette-subfamily G
ALR	AIM2-like receptor
AP-1	activator protein 1
Apo	apolipoprotein
ASC	apoptosis-associated speck-like protein containing a CARD
AT	adipose tissue
ATMs	adipose tissue macrophages
ATP	adenosine triphosphate
AUC	area under the curve
BCA	bicinchoninic acid assay
BIR	baculovirus-inhibitor-of-apoptosis protein repeat
BMDMs	bone marrow-derived macrophages
BMI	body-mass-index
BSA	bovine serum albumin
CAD	coronary artery disease
CARD	caspase activation and recruitment domain
CCL	C-C motif ligand
CD	chow diet
CD14	cluster of differentiation 14
CDase	ceramidase
cDNA	complementary DNA
Cer	ceramide
CerS	ceramide synthase
CERT	ceramide transport protein
CLR	C-type lectin receptor
CM(R)	chylomicron (remnants)
CO_2	carbon dioxide
CoA	coenzyme A
CREB	cyclic AMP-responsive element-binding protein
CRID3	cytokine release inhibitory drug 3
C_T	threshold cycle
CTB	CellTiter^{TM} Blue
CVD	cardiovascular disease
CXCL	C-X-C motif ligand
d	day
DAMP	damage associated molecular pattern

DC	dendritic cell
ddH_2O	double-distilled water
DMEM	Dulbecco's Modified Eagle's Medium
DMSO	dimethyl sulfoxide
DNA	deoxyribonucleic acid
dNTP	deoxynucleoside triphosphate
dsDNA	double-stranded DNA
dsRNA	double-stranded RNA
e.g.	*example gratia* (latin); for example
ECAR	extracellular acidification rate
EDTA	ethylenediaminetetraacetic acid
ELISA	enzyme-linked immunosorbent assay
ER	endoplasmic reticulum
EU	endotoxin unit
eWAT	epididymal WAT
FACS	fluorescence-activated cell sorting
FADD	Fas-associated death domain
FCCP	fluoro-carbonyl cyanide phenylhydrazone
FCS	fetal calf serum
FI	fluorescence intensity
fw	forward (used for primers)
g	gram
GO	gene ontology
GSDMD	gasdermin D
GSL	glycosphingolipid
h	hour
HCD	hypercaloric diet
HDL	high-density lipoprotein
HFD	high-fat diet
hMDMs	human monocyte-derived macrophages
HPRT	hypoxanthine phoshporibosyltransferase
HSP	heat-shock protein
HTRF	homogeneous time-resolved fluorescence
i.p.	intraperitoneal
IBMX	isobutylmethylxanthine
IFN	interferon
IgG	immunoglobulin G
IKK	IκB-kinase
IL	interleukin
IL-1R	interleukin 1 receptor
incMSE	increase in mean squared error
iNOS	inducible nitric oxide synthase

IRAK	interleukin-1 receptor-associated kinase 1
IRF	interferon regulatory factor
JNK	JUN N-terminal kinase
kDa	kilodalton
KO	knock-out
L	liter
LBP	LPS-binding protein
LC-MS	liquid chromatography-mass spectrometry
LCAT	lecithin-cholesterol acyltransferase
LCD	low-caloric diet
lcSFAs	long-chain saturated fatty acids
LDL	low-density lipoprotein
LDLR	LDL receptor
LPL	lipoprotein lipase
LPS	lipopolysaccharide
LRR	leucine-rich repeat
LXR	liver X receptor
m	meter
M	molar
M-CSF	macrophage colony-stimulating factor
MACS	magnetic-activated cell sorting
MAL	MyD88 adaptor-like protein
MAPK	mitogen-activated protein kinase
MCP-1	monocyte chemoattractant protein 1
MD	molecular dynamic
MD-2	myeloid differentiation factor 2
MHC	major histocompatibility complex
min	minute(s)
mol	mole(s)
MPL	monophosphoryl lipid A
mRNA	messenger RNA
mt	mitochondrial
MyD88	myeloid differentiation primary-response 88
ND	not determined
NEK7	NIMA-related kinase 7
NF-κB	nuclear factor 'kappa-light-chain-enhancer' of activated B-cells
Nig	Nigericin
NK cell	natural killer cell
NLR	NOD-like receptor
NLRP	NOD, LRR and pyrin domain-containing protein
NOD	nucleotide-binding oligomerization domain
ns	not significant

o/n	overnight
ob	obese
OCR	oxygen consumption rate
oxLDL	oxidized LDL
PAGE	polyacrylamide gel electrophoresis
Pam3CSK4	Pam3CysSerLys4
PAMP	pathogen-associated molecular pattern
PBMCs	peripheral blood mononuclear cells
PBS	phosphate-buffered saline
PDK	pyruvate dehydrogenase kinase
PEG	polyethylene glycol
PFA	paraformaldehyde
PMSF	phenylmethylsulfonyl fluoride
PRR	pattern recognition receptor
PUFA	polyunsaturated fatty acid
PVDF	polyvinylidene difluoride
PYD	pyrin domain
qPCR	quantitative polymerase chain reaction
r^2	coefficient of determination
RCT	reverse cholesterol transport
REE	resting energy-expenditure
rev	reverse (used for primers)
rh	recombinant human
RIP	receptor-interacting protein
RLR	RIG-I-like receptor
RLR	RIG-I-like receptor
rm	recombinant mouse
RMSD	root mean square deviation
RNA	ribonucleic acid
ROS	reactive oxygen species
rpm	revolutions per minute
RPMI	Roswell Park Memorial Institute Medium
RT	room temperature
s	second
S14	sphingomyelin d18:1/14:0
S1P	sphingosine-1-phosphate
SARS-Cov-2	severe acute respiratory syndrome coronavirus 2
SASA	solvent-accessible surface area
SB	sample buffer
scWAT	subcutaneous WAT
SD	standard deviation
SDS	sodium dodecyl sulfate

SEM	standard error of the mean
Seq	sequencing
SM	sphingomyelin
SMase	sphingomyelinase
SMS	sphingomyelin synthase
SphK	sphingosine kinase
SPT	serine palmitoyltransferase
SR	scavenger receptor
ssRNA	single-stranded RNA
t	time(point)
T2D	type 2 diabetes
TAK	transforming growth factor-β (TGF-β)-activated kinase
TBK1	TANK-binding kinase 1
TBS	Tris-buffered saline
TG	triglyceride
TIR	Toll-Interleukin-1 receptor homology
TLR	Toll-like receptor
TNF	tumor necrosis factor
TNFR	TNF receptor
TRAF	TNF receptor-associated factor
TRAM	TRIF-related adaptor molecule
TRIF	TIR-domain-containing adaptor protein inducing interferon-β
UT	untreated
v	version
V	volts
Veh	vehicle
VLCD	very low-calorie diet
VLDL	very low-density lipoprotein
VSMCs	vascular smooth muscle cells
W	watt
WAT	white adipose tissue
WD	Western-type diet
WHO	world health organization
WT	wild type

1 INTRODUCTION

1.1 The Immune System

We are continuously surrounded by allergens, toxic substances, bacteria, viruses and other pathogens. To protect us from potential harm, we have evolved a complex immune system. Its main function is to distinguish self from non-self, using a repertoire of different host-defense mechanisms (Chaplin, 2010). The first line of defense is formed by physical and chemical barriers such as skin, mucosal surfaces and gastric acid. If these barrier sites are breached, an intricate system of recognition and response mechanisms takes over, including humoral (e.g. complement system) as well as cellular defense factors (Eyerich et al., 2018). To generate a fully functional immune response, two branches of the immune system usually need to cooperate: the innate and adaptive (acquired) immune system (Medzhitov, 2007).

The principal function of the mammalian immune system is the effective clearance of pathogens and toxic molecules, while maintaining self-tolerance and avoiding excessive tissue damage (Chaplin, 2010). A tightly controlled synergism between the two branches of the immune system is essential for an adequate and successful response. The initial rapid, but unspecific, response is navigated by the innate immune system. Hereby, a limited number of germline-encoded pattern recognition receptors (PRRs) that are expressed on innate immune cells are essential (Chaplin, 2010). A second wave of response is coordinated by the slightly slower, but more specific, adaptive immune system, which mainly relies on T- and B-cells that can be activated by innate immune cells. Their defense mechanisms rely on the expression of clonally selected, highly specific antigen-binding receptors that are generated via somatic gene rearrangement (Medzhitov, 2007). Activation of the adaptive immune system can additionally lead to immunological memory through the generation of pathogen-specific memory cells that allow for a faster response upon re-infection (Chaplin, 2010).
Over the past decade, numerous studies have shown that the innate immune system also displays certain memory characteristics, termed ‘trained immunity’ (Netea et al., 2020). Similar to what has been observed in plants and invertebrates lacking an adaptive immune

system, an enhanced unspecific response can be elicited in innate immune cells during a secondary infection with the same or even a different stimulus (cross-protection) (Netea et al., 2011). Mechanistically, trained immunity is conferred by long-term metabolic and epigenetic reprogramming of cells such as monocytes and macrophages (Fanucchi et al., 2021).

As this thesis will only focus on the innate branch of the immune system, more detail on it will be provided in the following sections, whereas the adaptive immune system will not be described any further.

1.2 Innate Immunity and its Recognition Principles

1.2.1 Pattern Recognition Receptors (PRRs)

The innate immune system is responsible for the initial host defense in response to potentially harmful threats. It has evolved to quickly detect invading pathogens and, if necessary, to initiate appropriate defense mechanisms. Once innate immune cells become activated, they initiate the transcription and secretion of various proinflammatory effector cytokines, chemokines and interferons, as well as cause the recruitment of more immune cells to the site of infection (Kumar et al., 2011; Takeuchi & Akira, 2009). Mechanisms used by the recruited cells include phagocytosis or release of antimicrobial peptides and reactive oxygen species (ROS) (Alberts et al., 2002). If a pathogen is not effectively cleared, innate immune cells instruct cells of the adaptive immune system, which can then aid in eliminating the threat, before the resolution and repair phase is entered. Cells associated with the innate immune response mainly originate from the myeloid lineage and include granulocytes, mast cells, monocytes, macrophages and dendritic cells (Janeway et al., 2001). Moreover, cells at barrier sites such as fibroblasts are also capable of contributing to the innate immune response and are, therefore, considered to be non-professional immune cells (Janeway et al., 2001; Eyerich et al., 2018).

As mentioned previously, innate immune cells sense danger by employing PRRs that recognize highly conserved molecules. These molecules usually contain a common structural motif that is preserved across specific pathogen families (Barton, 2008; Medzhitov, 2007). Therefore, these structures are generally regarded to as pathogen-associated molecular patterns (PAMPs) (Chaplin, 2010). In addition, PRRs can also detect endogenous proteins or metabolites that are host-derived and are released when cells are damaged or dying, for example as a consequence of infection. Due to their non-microbial origin, these molecules are termed damage-associated molecular patterns (DAMPs) (Takeuchi & Akira, 2010). To maintain immune homeostasis, it is essential that a correct discrimination between self and non-self, as well as altered self, pathogen-associated non-self and harmless non-self (i.e. commensal bacteria that constitute our

microbiome) takes place (Matzinger, 2002; Medzhitov & Janeway, 1997). Errors in the regulation of the innate immune system can lead to severe tissue damage, drive immunopathology or even cause persisting auto-inflammation and inflammatory disease (Chaplin, 2010).

PRRs only recognize conserved structures. Based on their protein domain homology, there are five distinct families of PRRs (Iwasaki & Medzhitov, 2015). They are either located on the cell surface or within the endosomal compartment and include:

- C-type lectin receptors (CLRs)
- Toll-like receptors (TLRs)

Others are found in the cytoplasm of the cell and include:

- AIM-2-like receptors (ALRs)
- Nucleotide-binding oligomerization (NOD)-leucine-rich repeat-containing receptors (NLRs)
- RIG-I-like receptors (RLRs)

The NLR family is the largest group to date, and its members have been assigned various functions such as the recognition of bacterial peptidoglycans (e.g. NOD1 and NOD2) as well as initiating the nucleation of macromolecular signaling complexes termed ‘inflammasomes’ (NLRP proteins) (Broz & Monack, 2013). ALRs, similar to NLRs, are also involved in inflammasome assembly, in addition to their ability to recognize intracellular bacterial dsDNA (Li & Wu, 2021). RLRs are mainly involved in innate antiviral immunity due to their specificity for viral nucleic acids, whereas CLRs bind carbohydrate structures found in fungal cell walls (Kumar et al., 2011; Takeuchi & Akira, 2009). TLR family members have been extensively studied and a broad range of ligands have been identified to date, including microbial nucleic acids as well as membrane components such as lipids or lipoproteins (Akira et al., 2001).

The significance of PRRs in the innate immune regulatory network is indisputable, as their engagement allows the cell to initiate host defense against infection. In the following sections, TLRs and inflammasomes (specifically TLR4 and NLRP3) will be discussed in further detail due to their relevance for the work presented in this thesis.

1.2.2 Toll-like receptors (TLRs)

1.2.2.1 The TLR Family

TLRs were first discovered in the 1990s and are probably the best described PRR family (O'Neill et al., 2013). To this date, 10 functional TLRs (TLR 1-10) have been identified in humans and 12 in mice (TLR 1-9, 11-13) (Kumar et al., 2011). All TLRs are transmembrane glycoproteins that contain an extracellular ligand-binding domain with tandem leucine-rich repeats (LRRs) that recognize distinct patterns, a membrane-spanning domain and a cytoplasmic Toll-IL-1 Receptor homology (TIR) domain. The TIR domain initiates downstream signaling via homotypic TIR-TIR interactions with various adaptor proteins (Akira et al., 2001). The localization of TLRs as homo- or heterodimers either at the cell surface or the endosome, determines the type of ligand recognized (Table 1.1) (Kumar et al., 2011).

Table 1.1: Human TLR Localization and Typical Ligands

TLR	Localization	Ligands
TLR1-TLR2	Cell surface	Triacylated lipopeptides, Pam3CSK4
TLR3	Endosomal compartment	dsRNA, polyI:C
TLR4 (Co-receptor MD2)	Cell surface Endosomal compartment	LPS (Lipid A), Plant-derived Paclitaxel, Heat-shock proteins
TLR5	Cell surface	Flagellin
TLR6-TLR2	Cell surface	Diacylated lipopeptides
TLR7	Endosomal compartment	Viral/Bacterial ssRNA, Imidazoquinolines (e.g. R848)
TLR8	Endosomal compartment	Viral ssRNA, Imidazoquinolines (e.g. R848)
TLR9	Endosomal compartment	CpG DNA
TRL10 (orphan receptor)	unclear	dsRNA (*in vitro data* only)

(Adapted from Broz and Monack (2013); Kawai and Akira (2010); Akira (2006))

TLR signaling generally employs two major pathways that are either myeloid differentiation primary-response protein 88 (MyD88)-dependent or MyD88-independent, as depicted in Figure 1.1. The MyD88-dependent pathway leads to activation of mitogen-activated protein kinases (MAPKs) and nuclear factor-κB (NF- κB), whereas the MyD88-independent pathway instead relies on the TIR-domain-containing adaptor protein

inducing IFNβ (TRIF) (Broz & Monack, 2013). All TLRs except TLR3 utilize MyD88 as an adaptor for signal transduction, whereby TLR4 is the only TLR that can additionally also signal in a TRIF-dependent manner (Figure 1.1) (Kumar et al., 2011). Upon ligand binding, TLRs dimerize and recruit, in case of the MyD88-dependent pathway, the MyD88 adaptor-like protein (MAL or TIRAP) (Gay et al., 2014). MyD88 in turn recruits IL-1R-associated kinase (IRAK) family members that interact with its death domain, which subsequently leads to formation of a complex that activates TNF receptor-associated factors (TRAFs) and TGFβ-activated kinase 1 (TAK1) (Figure 1.1, left side). JUN N-terminal kinase (JNK) and p38, both MAPKs, are activated, along with induction of the release of lκB-kinases (IKKs) from cytoplasmic NF-κB, causing its nuclear translocation, where it initiates transcription of proinflammatory cytokines such as interleukin-1 (IL-1), tumor necrosis factor (TNF) and IL-6. Further transcription factors being activated include cyclic AMP-responsive element-binding protein (CREB) and activator protein 1 (AP-1) (Kawasaki & Kawai, 2014; Takeda & Akira, 2004).

On the other hand, the TRIF-dependent signaling cascade, which is triggered by TLR3 or TLR4 ligation, is directed towards an antiviral response (Figure 1.1, right side) (Creagh & O'Neill, 2006). Upon receptor activation, the TRIF-related adaptor molecule (TRAM) is recruited, which allows downstream activation of TRAFs, TANK-binding kinase 1 (TBK1) and the receptor-interacting protein 1 (RIP1), which rewires signaling through the NF-κB pathway. TRAF3 downstream of TRIF however, leads to activation of Interferon-regulatory factors (IRFs), which induce the expression of type I IFN genes (IFNα and IFNβ), and stimulates expression of genes involved in the regulation of the adaptive immune response (Kawasaki & Kawai, 2014; Takeda & Akira, 2004).

Whilst the signaling cascades downstream of TLR activation and their importance in shaping an adequate immune response have been well characterized, their crosstalk as well as the pathways connecting TLRs with other PRRs, are not yet fully understood.

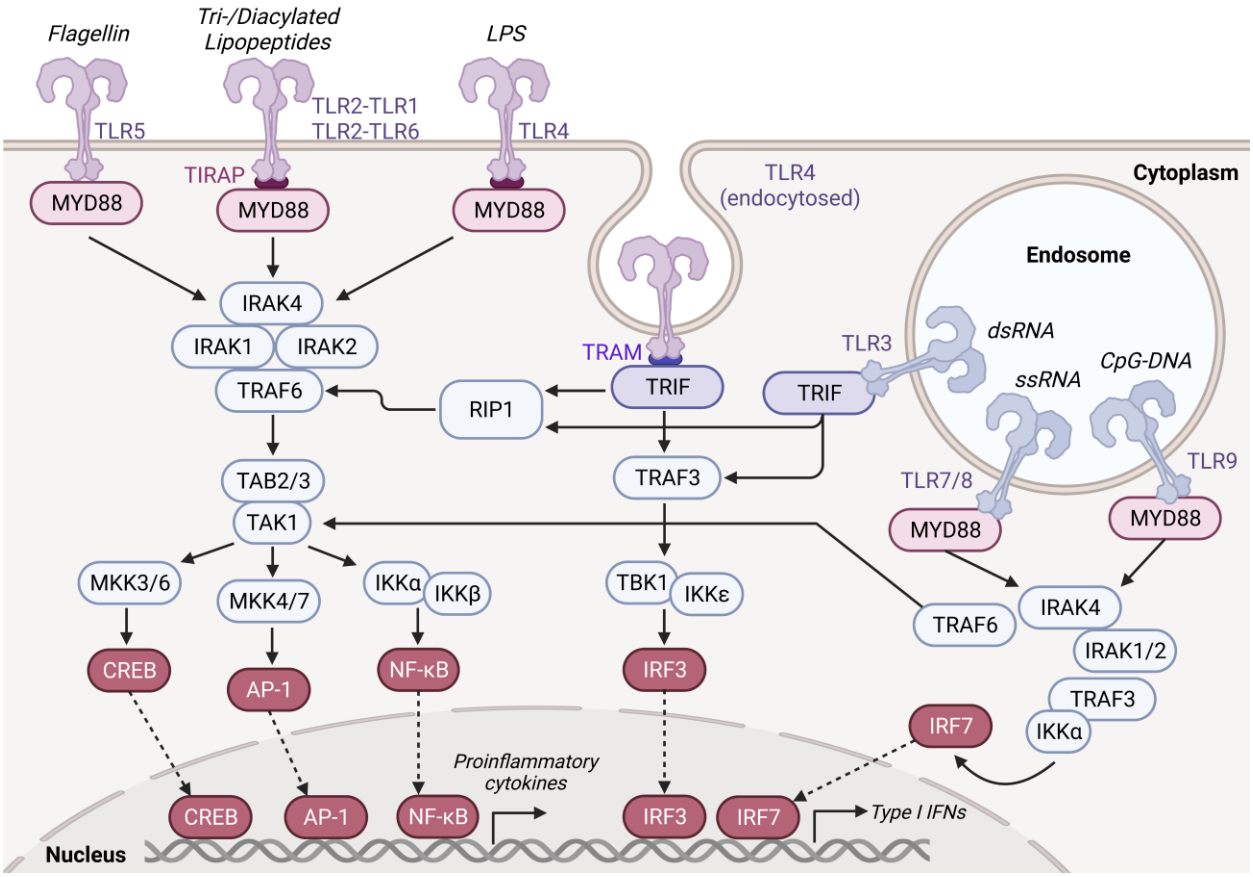

Figure 1.1: Human TLR activation and signaling pathways
Schematic overview of human TLRs, including the activation and main downstream signaling hubs involved. Human TLR 1-9 (TLR10 is not shown) are either expressed at the cell surface or within the endosome. Upon ligand binding, signaling is initiated by the adaptor molecules MyD88 and/or TRIF. Ultimately, these signaling events induce activation of transcription factors such as NF-κB, IRF3 and IRF7, which leads to the expression of proinflammatory cytokines, chemokines and type I IFNs. This figure was created with BioRender.com under a department license.

1.2.2.2 Toll-like receptor 4 (TLR4)

In 1997 Medzhitov and Janeway officially identified TLR4 (Medzhitov et al., 1997), one of the most extensively studied TLRs to date. Its importance was recognized with the Nobel Prize in 2011, which was awarded to Jules Hoffmann and Bruce Beutler (together with Ralph Steinmann) for their respective contributions towards the role of the Toll protein in innate immune responses (1996) and the subsequent demonstration of lipopolysaccharide (LPS) as a ligand for TLR4 (1998) (Lemaitre et al., 1996; O'Neill et al., 2013; Poltorak et al., 1998). LPS, an endotoxin component and the causative agent of Gram-negative bacteria-induced sepsis, remains until today the prototypical activator of TLR4. Specifically, the lipid moiety of LPS – lipid A – is important for this highly inflammatory activity (Raetz & Whitfield, 2002). LPS signaling is mediated by LPS-binding

protein (LBP) and Cluster of Differentiation 14 (CD14). They cooperate to extract LPS from the bacterial cell wall and monomerize it before presenting it to TLR4 (Park & Lee, 2013). Of note, TLR4 also possesses a co-receptor, myeloid differentiation factor 2 (MD-2), which is indispensable for LPS recognition (Shimazu et al., 1999), although studies have shown that TLR4 activation by other ligands can also function independent of MD-2 (Raghavan et al., 2012). In the inactive state, extracellular TLR4 and MD-2 form a heterodimer (TLR4/MD-2_2), which dimerizes upon ligand binding, forming a symmetrically arranged, M-shaped receptor multimer (TLR4/MD-$2_2)_2$ (Park et al., 2009; Park & Lee, 2013).

The exact binding mechanism of LPS to TLR4/MD-2 with its essential structural features was only recently uncovered, when the crystal structure of the TLR4/MD-2/LPS (type Ra, *E. coli*) complex was solved by Park *et al*. (Park et al., 2009). While Lipid A binds directly with five out of its six acyl chains to the large hydrophobic cavity in MD-2, the sixth acyl chain, together with hydrophobic residues in MD-2, provides secondary bridging to TLR4. This core hydrophobic interface is supported by the F126 loop in MD-2, which undergoes a structural change that subsequently provides hydrophilic interactions with TLR4 (Park et al., 2009). Additionally, several studies have noted the importance of the glucosamine phosphate groups in LPS. They facilitate receptor dimerization by formation of hydrogen bonds and ionic interactions with positively charged residues in TLR4 and MD-2 (Maeshima & Fernandez, 2013; Park & Lee, 2013). Removal of the phosphate group, such as in monophosphoryl lipid A (MPL), greatly decreases the inflammatory activity (Maeshima & Fernandez, 2013). These seemingly minor changes have the potential to drastically alter endotoxicity, illustrating a high degree of specificity and sensitivity for the receptor, as well as complex structural requirements for potential TLR4/MD-2 activators.

It is therefore not surprising that lipid A structures derived from families of bacteria other than *E. coli*, are considered only weak TLR4 agonists, or even antagonists of TLR4. TLR4 antagonizing lipids include lipid IVa (in human cells), LPS from *Rhodobacter sphaeroides* (RS-LPS) or the potent synthetic lipid A derivative Eritoran (E5564) (Maeshima & Fernandez, 2013; Mullarkey et al., 2003). Moreover, for certain lipids (i.e. lipid IVa), TLR4/MD-2 activation has been proven to only occur species-specifically (Maeshima &

Fernandez, 2013). Whereas LPS is a well-known ligand of TLR4, recent literature has proposed novel activators such as host-derived C12/C16 sulfatides (Su et al., 2021), bacterial ornithine lipids (Pizzuto et al., 2022) or the secreted cryptococcal protein CPL1 (Dang et al., 2022). However, most studies are either lacking a clear physiological relevance or, more importantly, the structural evidence supporting a direct interaction between the proposed ligand and TLR4/MD-2. The same holds also true for host-derived (endogenous) molecules that many studies regard as TLR4 agonists, including S100 proteins (Foell et al., 2013), heat-shock proteins (HSPs) (Fang et al., 2011) or fatty acids such as palmitate (Kochumon et al., 2018). In fact, not long ago it was shown that palmitate-induced inflammation was actually not mediated by direct TLR4 agonism, but rather by a dependence on TLR4 priming and subsequent metabolic rewiring (Lancaster et al., 2018).

Due to its relevance in many disease settings, targeting TLR4 holds an immense therapeutic potential. Knowledge of the molecular details regarding the interaction of the TLR4/MD-2 receptor complex with its ligands, offers possibilities for the discovery and design of novel, safe therapies. Given the extensive research into TLR4, a TLR4 drug pipeline has already been established, and several preclinical candidates have been identified or even be approved for use in clinics (O'Neill et al., 2010). Based on their ability to enhance the immune response, TLR4 agonists are particularly interesting as vaccine adjuvants. Indeed, MPL has been approved as an adjuvant in vaccines against human papilloma virus and hepatitis B (MacLeod et al., 2011). Additionally, the lipid A analogue OM-174 was tested in clinical trials for the induction of tumor regression in cancer patients (Isambert et al., 2013). On the other hand, significant focus has been put on the development of TLR4 antagonists for the treatment of inflammatory diseases such as sepsis, asthma or Alzheimer's disease, in an attempt to dampen the TLR4-induced cytokine storm (O'Neill et al., 2010).

Overall, it is clear that TLR4 constitutes an essential signaling hub at the heart of innate immunity, and striving to continue uncovering its role in specific disease settings and to identify novel ligands, will surely open up a number of new opportunities to target innate immune signaling.

1.2.3 NOD-like receptors (NLRs) and Inflammasomes

1.2.3.1 The NLR Family

Next to TLRs, the over 23 NLR family members have received a considerable amount of attention. They are cytosolic receptors that not only respond to pathogens, but are also involved in other biological processes such as cell death and embryonic development (Meunier & Broz, 2017). Moreover, aberrant activation of NLRs plays a role in various autoimmune and inflammatory diseases (Zhong et al., 2013).

Most NLR proteins share a conserved structure of three domains (Wilmanski et al., 2008):

- a distinguished N-terminal effector domain that contains protein-protein motifs (pyrin domain [PYD] or caspase activation and recruitment domain [CARD])
- a central nucleotide binding domain (also known as NACHT domain) that facilitates self-oligomerization and NLR activation
- a C-terminal LRR that aids in ligand recognition (not present in NLRP10)

Based on their different effector domains, NLRs can be divided into five subfamilies (Elinav et al., 2011). The NLRA proteins contain an acidic domain and a CARD, NLRB proteins (also referred to as NAIPs) possess an effector domain with baculovirus-inhibitor-of-apoptosis protein repeats (BIRs), and NLRC proteins, to which NOD1 and NOD2 belong, predominantly contain a CARD domain. Moreover, there are also NLRX proteins as well as NLRPs, the largest subfamily, comprising 14 members (NLRP1-14) that all contain a conserved PYD that is similar to the CARDs (Elinav et al., 2011). The NLRPs are sensors of pathogen-derived structures and molecules such as anthrax lethal toxin, microbial nucleic acids or viral proteins. In addition, various sterile activators were identified, including cholesterol crystals, silica, monosodium urate crystals or amyloid β (Schroder & Tschopp, 2010). As mentioned previously, some of the NLRs participate in the assembly of an oligomeric inflammasome complex, which regulates maturation and release of the pro-inflammatory cytokines IL-1β and IL-18, as well as initiates a distinct form of cell death called pyroptosis (Schroder & Tschopp, 2010). Assembly of the inflammasome generally involves the NLR protein that is responsible for PAMP or DAMP recognition, the adaptor protein apoptosis-associated speck-like protein containing a CARD (ASC) as well as the effector protein caspase-1 (or caspase-11), which

proteolytically cleaves the immature pro-forms of IL-1β and IL-18 (Dinarello & Fantuzzi, 2003; Latz et al., 2013). The detailed mechanism will be described in the following section using one of the most extensively studied receptors - NLRP3 - as an example.

1.2.3.2 The NLRP3 Inflammasome

Since inflammasomes were first described twenty years ago, numerous studies have investigated NLRP3 (NOD-, LRR- and pyrin domain-containing 3) and its role as an inflammasome nucleator. Reported activators of NLRP3 cover a wide range of PAMPs (e.g. *C. albicans*), DAMPs (e.g. extracellular ATP, fibrillar amyloid β, mitochondrial stress) and environmental stimuli (e.g. ultraviolet light) (Schroder & Tschopp, 2010). A common mechanism of how exactly NLRP3 senses these clearly diverse stimuli has not been established yet. It has been proposed, amongst others, that efflux of intracellular potassium or the generation of ROS may be the common downstream event that these stimuli converge in, to ultimately trigger NLRP3 activity (Broz & Dixit, 2016). However, with new activators continuously being proposed, there always appears to be one that is not consistent with a specific theory.

Although some mechanistic details remain to be elucidated, we know that priming via TLR activation is generally, but not necessarily, required for NLRP3 activity. In this first step, TLR activation leads to the induction of genes that are not constitutively expressed in the cell, but that are essential for the inflammasome response, such as NLRP3, pro-IL-1β and pro-IL-18 (Figure 1.2) (Creagh & O'Neill, 2006). In the canonical model, a second stimulus subsequently leads to assembly and activation of the complex. During assembly, ASC is recruited via homotypic PYD-PYD interactions. ASC then binds the catalytically inactive caspase-1 via its C-terminal CARD domain, which allows for caspase-1 autocatalytic processing and subsequent activation. Once activated, caspase-1 processes and cleaves the immature precursors of IL-1β and IL-18 into their mature forms. Conventional NLRP3 activation further leads to caspase-1-(or -11)-dependent pyroptosis, a form of cell death that protects the host cell from infection (Bauernfeind et al., 2009; He et al., 2015). Hereby, Gasdermin D is cleaved and its N-terminal fragment is inserted into the cell membrane, which causes pore formation in the membrane and allows for the release of pro-

inflammatory IL- 1β and IL-18 (Latz et al., 2013; Liu et al., 2016). As the released IL-1β is highly pyrogenic, it can contribute to immunopathology (Latz et al., 2013).

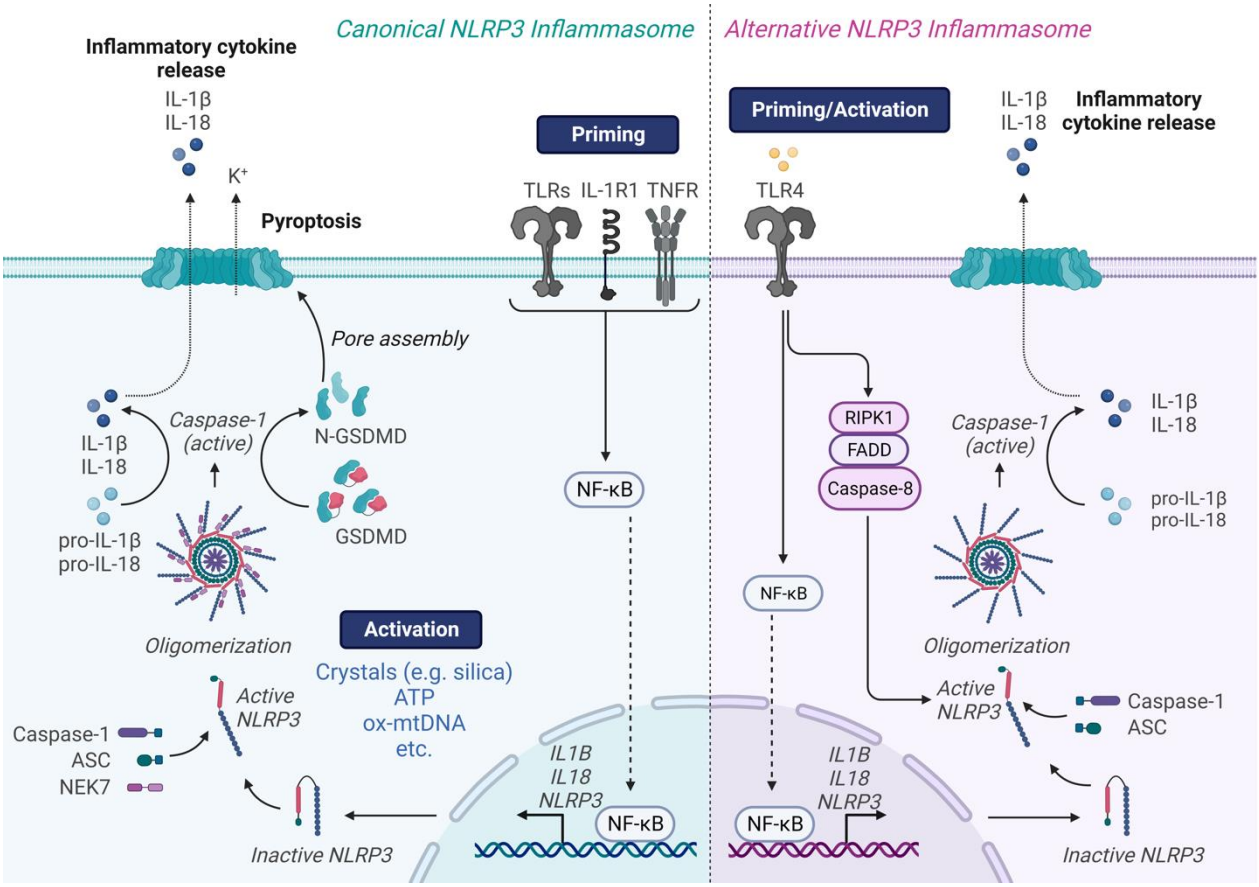

Figure 1.2: Activation mechanism of the NLRP3 inflammasome
Simplified overview of NLRP3 inflammasome activation in a conventional (canonical) and alternative manner. Whereas the canonical NLRP3 inflammasome is only fully activated in a two-step model, first by TLR-mediated 'priming' and then by a second 'activation' stimulus, the alternative route only requires TLR4 stimulation, which provides both 'priming' and 'activation' at the same time. Both modes of inflammasome activation rely on the NLRP3-ASC-Caspase-1 axis for the generation and release of mature pro-inflammatory IL-1β and IL-18. This figure was created with BioRender.com under a department license.

An alternative NLRP3 activation mechanism has been described in human monocytes, where activation of the inflammasome occurs in a one-step model (Figure 1.2) (Gaidt & Hornung, 2017). Whereas the alternative NLRP3 inflammasome, similar to the conventional inflammasome, relies on the NLRP3-ASC-caspase-1 axis, it neither requires activation by a classical inflammasome stimulus nor does it induce pyroptosis. Instead, signaling is promoted by a pathway dependent on TLR4, TRIF, RIPK1, the Fas-associated death domain (FADD) adaptor protein and Caspase-8 (Gaidt et al., 2016).

While NLRP3 is beneficial in detecting and fighting infection, its hyper-activation, as evident in patients with NLRP3 gain-of-function mutations, can have detrimental consequences (Cordero et al., 2018). However, in the contemporary ageing society, NLRP3 is primarily involved in non-genetic, non-communicable diseases that are becoming increasingly prevalent. Hereby, an accumulation of DAMPs leads to sterile chronic inflammation that is, in many cases, associated with NLRP3 activation (Gritsenko et al., 2020). The range of conditions and inflammatory diseases that have been linked to aberrant NLRP3 activation is broad and includes metabolic diseases such as diabetes, aggregate-mediated pathology observed in gout or atherosclerosis, as well as several autoimmune diseases (Mangan et al., 2018).

Similar to TLR4, NLRP3 is also a central signaling hub of the immune system, and, as such, inhibition or activation of the NLRP3 inflammasome could potentially be beneficial for various disease settings.

1.3 Metaflammation

1.3.1 Concept of Metaflammation

‘Metaflammation’ is an emerging concept that refers to metabolically-triggered, chronic low-grade inflammation. The term was coined because metabolic diseases are in fact not necessarily accompanied by the typical hallmarks of inflammation (namely: swelling, pain, redness and fever) (Hotamisligil, 2006, 2017a; McNelis & Olefsky, 2014). With dramatically rising incidences of obesity in adults and children worldwide, obesity-related metabolic diseases such as type 2 diabetes (T2D), cardiovascular diseases (CVDs) or fatty liver disease have become a major health concern (Agha & Agha, 2017; Grundy, 2004). Metaflammation can be linked to the more and more sedentary lifestyle as well as to ageing and pollution (Christ & Latz, 2019; Egger & Dixon, 2011; Hosseini et al., 2016). An accumulation of lipids in the circulation and in tissues can cause alterations in cellular metabolism that lead to endoplasmic reticulum stress, cell hypertrophy and hypoxia, amongst others. These factors can culminate in an aberrant production of cytokines and acute phase molecules, that together, contribute to the development of disease or disease-related complications (McNelis & Olefsky, 2014). The following sections will shed light on important metaflammation-related processes in obesity and atherosclerosis.

1.3.2 Obesity and Inflammation

1.3.2.1 Obesity – a prevalent health problem

Overweight and obesity are defined by the unhealthy excessive accumulation of adipose tissue in the body that is caused by an imbalance between energy intake and expenditure. Based on body-mass-index (BMI), overweight is defined by a BMI ≥ 25 kg/m^2 and obesity at BMI ≥ 30 kg/m^2 (Panuganti et al., 2023). According to the WHO European Regional Report 2022, almost 60 % of adults and nearly 30 % of children are affected by overweight and obesity (Wickramasinghek et al., 2022). Obesity has, therefore, become a major liability, as it is amongst the most common risk factors for the development of non-communicable diseases (Hotamisligil, 2017b; McNelis & Olefsky, 2014). Complications

associated with obesity such as insulin resistance and type 2 diabetes (T2D), are causally linked to the chronic inflammatory signaling observed in these patients (McNelis & Olefsky, 2014). Individuals with insulin resistance display an impaired ability of insulin to suppress glucose output from the liver and to increase glucose uptake in peripheral tissues such as muscle and adipose tissue. Ultimately, insulin resistance can lead to the development of T2D due to the inability of the pancreas to compensate and normalize blood glucose levels (Lebovitz, 2001).

The predominant site of inflammation in obesity is the white adipose tissue (WAT), however, other metabolically active organs such as the liver are also involved (Hildebrandt et al., 2023). It is important to distinguish WAT based on two anatomical locations: subcutaneous (scWAT) and visceral (epididymal; eWAT) (Khan et al., 2020). Whereas expansion of scWAT has been shown to be protective, expansion of visceral fat mass is closely associated with obesity-derived pathology such as insulin resistance or liver steatosis. These effects are likely mediated by different mechanisms, including the preferential expansion of eWAT through adipocyte hypertrophy, as well as the fact that eWAT uses the hepatic portal vein as its draining system, and that a high-fat diet leads to adipocyte death in eWAT but not scWAT (Hildebrandt et al., 2023). Furthermore, adipocytes of the visceral WAT have been shown to be crucial in the interaction with other immune cells and for the generation of pro-inflammatory mediators. For example, they constitutively express TNFα and increase their release of fatty acids upon adipose tissue (AT) expansion (Ahmed et al., 2021; Hildebrandt et al., 2023). Moreover, adipocytes produce adipokines, and obesity correlates with increased concentrations of the energy-regulating hormone leptin and decreased release of adiponectin, which has multiple homeostatic functions including promotion of fatty acid oxidation, glucose uptake and control over liver gluconeogenesis (Chait & den Hartigh, 2020). Although in humans not a classical adipokine, resistin is another crucial metabolic hormone associated with obesity (Chait & den Hartigh, 2020). As opposed to rodents, human resistin is predominantly expressed in peripheral blood mononuclear cells (PBMCs) and monocyte-derived macrophages (Nagaev et al., 2006). Despite the fact that the mechanism of how resistin exerts its functions remains obscure, studies have acknowledged its role in amplifying inflammation in metabolic disorders (Chait & den Hartigh, 2020).

1.3.2.2 The Role of Macrophages in Obesity

Macrophages are the most abundant type of leukocytes in the adipose tissue (Weisberg et al., 2003). The population of macrophages in fat tissue is diverse and depending on the metabolic status and localization, it can be highly phenotypically heterogeneous and also vary in numbers (Li et al., 2020). In both mice and humans, an infiltration of macrophages into the AT is observed in obese compared to lean individuals (Weisberg et al., 2003). The pool of resident adipose tissue macrophages (ATMs) is hereby expanded by recruitment of monocyte-derived macrophages as well as by local proliferation (Haase et al., 2014; Weisberg et al., 2003). In obesity, ATMs are often found in close proximity to dying cells (Hildebrandt et al., 2023), suggesting that they are both phagocytosing material as well as sensing the release of DAMPs via TLRs and NLRP3 (Ruggiero et al., 2021). The latter has indeed been shown to be involved in mediating Western-type diet-induced inflammation and trained immunity via reprogramming of myeloid progenitors in mice (Christ & Latz, 2019).

Although there is a myriad of literature, our understanding of the extent and mechanistic details of macrophage involvement in obesity-induced inflammation and its complications is still incomplete. It is known that ATMs are a major source of TNFα and IL-6, and highly express inducible nitric oxide synthase (iNOS) in mice (Boutens & Stienstra, 2016; McNelis & Olefsky, 2014). These pro-inflammatory mediators are capable of directly affecting insulin sensitivity as well as the regulation of glucose- and lipid metabolism. Further, studies have proposed that the increased presence of free fatty acids triggers TLR2 and TLR4 signaling (Rogero & Calder, 2018). Indeed, mice deficient in either of these receptors are protected from obesity-induced inflammation and insulin resistance (Ehses et al., 2010; Shi et al., 2006). A role for TLR4 in driving inflammation is in fact a reasonable theory, as high-fat diet-induced presence of microbiota-derived LPS has also been associated with AT inflammation during obesity (Hersoug et al., 2018). However, it is possible that other, not yet identified mechanisms also play a role.

1.3.3 Cardiovascular Disease (CVD)

1.3.3.1 Atherosclerosis

Cardiovascular diseases remain the leading cause of morbidity and mortality globally (Vaduganathan et al., 2022). Amongst the most relevant CVDs are coronary artery disease (CAD), peripheral artery disease, myocardial infarction and stroke. Most of these diseases are driven by atherosclerosis (Frostegård, 2013), which is characterized by the development of arterial lesions (also referred to as 'plaques'), accompanied by a continuous low-grade inflammation. In advanced disease stages, atherosclerotic plaques are subject to erosion or rupture, leading to the occlusion of large and medium-sized arteries (Epstein et al., 1992; Hansson & Hermansson, 2011). The pathogenesis of atherosclerosis can, in part, be attributed to hypercholesterolemia and dyslipidemia, which are both associated with genetic factors, lifestyle as well as with the presence of metabolic disorders such as obesity or T2D (Crowther, 2005). Therefore, most therapies are aimed at controlling circulating low-density lipoprotein (LDL)-cholesterol in CVD patients (Masana et al., 2023). However, these therapies are often not sufficient to completely abolish the occurrence of adverse cardiovascular events, as a residual risk is likely also rooted in the persisting inflammation. Indeed, inhibition of the highly inflammatory disease-associated IL-1β (CANTOS trial) successfully reduced the rate of recurrent cardiovascular events, independent of lipid-lowering (Ridker et al., 2017).

The development of atherosclerosis is initiated by lipid deposition and accumulation of immune cells in the vessel wall. In early disease stages, predominantly cholesterol-rich apolipoprotein B (ApoB)-LDL enters the intima of the artery, where it is retained and modified by chemical, enzymatic and oxidative reactions (e.g. oxLDL). Oxidation of LDL leads to the generation of 'oxidation-specific epitopes', which facilitates their uptake by phagocytes via receptors such as CD36 and scavenger receptor A (SR-A) (Hansson & Hermansson, 2011; Miller et al., 2011). The evolving plaque harbors a core rich in lipids and activated immune cells, mainly macrophages, dendritic cells and T cells. The activated immune cells, supported by endothelial cells and vascular smooth muscle cells (VSMCs), further evoke influx of bone marrow-derived myeloid subsets (e.g. monocytes),

due to an upregulated expression of adhesion molecules as well as increased release of chemokines (CCL2, CCL5, CX3CL1, etc.) (Hansson & Hermansson, 2011).
Circulating monocytes enter the site of inflammation and differentiate into macrophages. As such, they face excessive levels of native and modified lipoproteins. In an attempt to induce clearance of these lipids, macrophages transform into cholesteryl-ester loaded 'foam cells' (Hansson & Hermansson, 2011; Jonasson et al., 1986). Foamy macrophages have been shown to not be pro-inflammatory per se. However, continued exposure to lipoproteins and oxidative stress leads to a rewiring of macrophage metabolism and epigenetic reprogramming (Bekkering et al., 2014). As a result, these macrophages exhibit an upregulation of fatty acid synthesis, glycolysis and the pentose phosphate pathway, as well as an increased expression of co-stimulatory molecules (e.g. CD80, CD86) and pro-inflammatory cytokines (Wculek et al., 2022). The core of activated immune cells, together with extracellular lipids and cholesterol crystals, is contained by a fibrous cap composed of VSMCs and collagen (Hansson & Hermansson, 2011).

Throughout plaque progression, the core can become necrotic due to cell death along with insufficient efferocytosis. DAMPs released from dying cells as well as aforementioned cholesterol crystals provide signals for TLRs and NLRP3, which further contributes to inflammation (Duewell et al., 2010). As more and more immune cells are being attracted, the plaque continues to grow. Importantly, growth and stability of the plaque have been shown to greatly influence disease severity. Thinning of the fibrous cap due to the ongoing inflammation, renders the plaque unstable, causing erosion or rupture, and prompting the formation of a thrombus. The consequence is an obstruction of blood flow, which can lead to severe organ damage (Bentzon et al., 2014).

1.3.3.2 Lipoproteins in CVD

Plasma lipoproteins are intricately linked to the severity of, and susceptibility to CVDs (Grundy, 2004; Hegele, 2009). Lipids such as cholesterol or triglycerides (TGs) are water-insoluble and thus, need to be associated with proteins for transport in the circulation. Generally, lipoproteins are spheroidal molecules with a hydrophilic outer layer consisting of free cholesterol, apolipoproteins and phospholipids, that coats a hydrophobic core of

cholesteryl esters and TGs (Hegele, 2009). Dietary lipid transport occurs directly from the small intestine to the liver, adipose tissue and muscles, and from the liver towards peripheral tissues. The process of cholesterol transport from peripheral tissues back to the liver, the only organ with the ability to clear cholesterol via bile, is referred to as reverse cholesterol transport (RCT) (Lewis & Rader, 2005). Certain types of lipoproteins are key risk factors in augmenting disease, whereas others play an important role in reducing inflammation and CVD development (Hegele, 2009). For example, high-density lipoprotein (HDL)-mediated RCT is an important mechanism in the counter-regulation of atherogenesis (Lewis & Rader, 2005). Hence, it is not surprising that targeting lipoproteins and their metabolism is immensely interesting regarding future potential for therapeutic interventions.

There are several classes of lipoproteins based on different size, density and composition. The mainly cholesterol-carrying lipoproteins include LDL and HDL, whereas chylomicrons (CMs) and very low-density lipoproteins (VLDLs) mostly carry TGs. Lipoprotein assembly and metabolism is complex, however, it is relevant to understand in context of its role in disease development and progression (Figure 1.3) (Hegele, 2009). Dietary lipids or sterols in the small intestine are transported into intestinal cells (enterocytes), where they are reconstituted and packaged, together with ApoB, into CMs. CMs are subsequently secreted via the lymph into the vena cava. Here, they are processed by the lipoprotein lipase (LPL) into CM remnants (CMRs), whereby free fatty acids enter peripheral cells such as adipocytes. CMRs are then taken up by the liver and catabolized (Hegele, 2009). Hepatocytes synthesize VLDL by packaging of triglycerides and ApoB (isoform B100) together with *de novo* synthesized or recycled cholesterol. In the circulation, VLDL is processed by LPL into free fatty acids and VLDL remnants (IDL), which are further hydrolyzed yielding LDL. LDL then transports cholesterol to peripheral cells, where it is taken up via the LDL receptor (LDLR) (Hegele, 2009). As mentioned previously, LDL is subject to modifications in the periphery, for example the arterial wall. These modifications result in enhanced uptake by non-hepatic cells such as macrophages, which is beneficial in certain situations, for example to fuel inflammation when fighting an infection, but can also drive pathology like atherosclerosis (Hansson & Hermansson, 2011; Miller et al., 2011).

The main responsibility of HDL is to recycle cholesterol back to the liver (Figure 1.2; blue arrows). Apolipoprotein A1 (ApoA1), a main component of HDL, is secreted from enterocytes or hepatocytes and assembled into a relatively lipid-poor pre-β-HDL particle (Lewis & Rader, 2005). During RCT, macrophage transport proteins ATP-binding cassette (ABC)-subfamily A member 1 (ABCA1) and ABCG1 mediate cholesterol efflux onto pre-β-HDL and HDL particles, respectively (Khera & Rader, 2010). The expression of both transporters is highly induced via activation of the transcription factor Liver X Receptor (LXR) in response to cholesterol accumulation. In mature HDL, free cholesterol is esterified to form cholesteryl esters by the enzyme lecithin-cholesterol acyltransferase (LCAT) (Hegele, 2009; Khera & Rader, 2010). The cholesterol transported on HDL is then selectively removed via scavenger receptor B1 (SR-B1) on hepatocytes. Hereby, the protein moiety of HDL is maintained and released back into the circulation. The cholesterol deposited in hepatocytes can then be recycled in form of VLDL, or can be secreted via the bile facilitated by ABCG5 and ABCG8 (Hegele, 2009; Khera & Rader, 2010).

There is a plethora of epidemiological and experimental studies suggesting an inverse association between HDL-cholesterol levels and CVDs, however a definitive causal relationship has, to date, not been established (Gordon et al., 1989a; Gordon et al., 1977; Lewis & Rader, 2005). In fact, there are even studies reporting that HDL is not only anti-atherogenic but also has pro-inflammatory capacity (Hahn et al., 2008; van der Vorst et al., 2017). Research in the field of HDL metabolism in context of disease is complex, given that there are multiple subpopulations of HDL particles that vary not only in size, shape and composition but also in their functional properties (Camont et al., 2011). While it is indisputable that HDL, similar to LDL, has an essential role in atherosclerosis, new metric approaches regarding HDL biology are required to enhance our understanding of HDL and its association with disease risk.

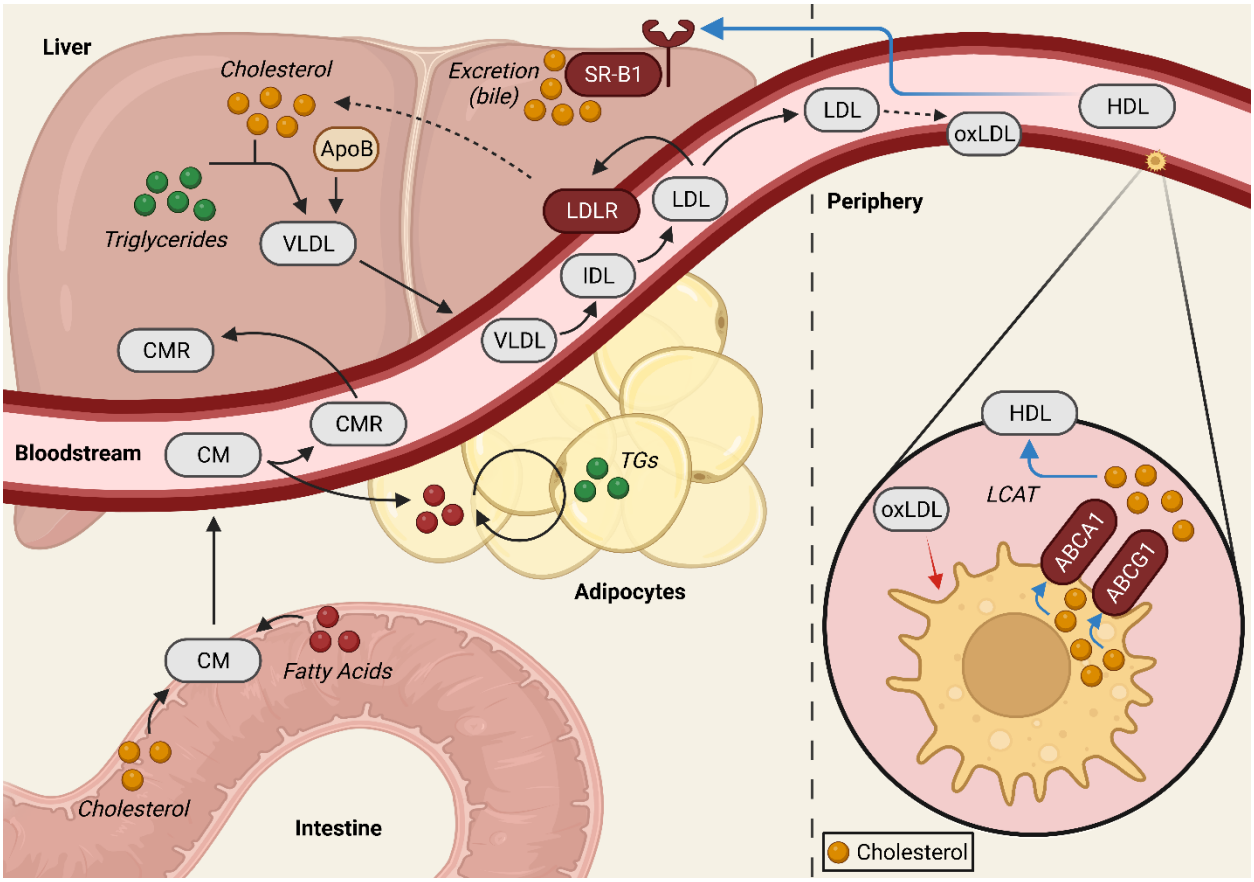

Figure 1.3: Lipoprotein Metabolism
Schematic and simplified overview of key steps in lipoprotein metabolism, including assembly, secretion, processing and catabolism of different lipoproteins. The main organs involved are the small intestine, the liver, adipose tissue and peripheral cells such as arterial macrophages. Processes related to reverse cholesterol transport are indicated with blue arrows. This figure was created with BioRender.com under a department license.

1.4 Lipids in health and disease

1.4.1 Bioactive Lipids

Over the past years there has been an increased appreciation of the role of lipids beyond being solely membrane components and an effective source of energy (Wymann & Schneiter, 2008). In fact, dietary and endogenous lipids possess bioactive properties, as they have the capacity to not only maintain tissue homeostasis, but also regulate host immune functions and contribute to, or suppress inflammation. Changes in the relative abundance of intra- and extracellular lipid species can have far-reaching functional consequences for the host (Radzikowska et al., 2019). Given their prevailing relevance, cutting-edge lipidome analysis has become more and more essential for the research into

lifestyle- and diet-associated disorders (Murphy & Nicolaou, 2013). However, the network of bioactive lipids is highly intertwined and its analysis is complex, owing to temporal and spatial aspects in the engagement of different lipid species.

Fatty acids function as precursors for several classes of bioactive lipids such as eicosanoids, (lyso-)phospholipids, sphingolipids and special pro-resolving lipids. These lipids can either start and fuel the fire by coordinating host inflammatory processes, or function as resolvents of inflammation, mediating resolution and tissue regeneration (Wymann & Schneiter, 2008). Various studies support the notion that omega-3 polyunsaturated fatty acids (PUFAs) are beneficial to human health. Indeed, we know that eicosapentaenoic acid and docosahexaenoic acid and their derivatives, possess potent resolving and anti-inflammatory properties in various disease settings such as Alzheimer's disease, asthma or CVD (Serhan et al., 2008). On the other hand, looking at obesity or CVD, we know that certain lipids are also positively associated with disease pathology (Wymann & Schneiter, 2008). The Western-type diet of our society has shifted more and more towards an increase in the amount of omega-6 PUFAs, whilst simultaneously being reduced in "good" omega-3 PUFAs. Subsequently, more linoleic acid and arachidonic acid (AA)-derivatives are being produced. Excessive amounts of omega-6 PUFAs and their metabolites promote pathogenesis in many of our modern diseases (Radzikowska et al., 2019; Simopoulos, 2008). Another important example of such a bioactive lipid family that functions as more than just mere membrane lipids, are sphingolipids (Green et al., 2021; Wymann & Schneiter, 2008). They have been described to modulate a plethora of biological processes in various diseases, and remain, to date, exceptionally intriguing to many researchers.

1.4.2 Sphingolipids

The family of sphingolipids comprises hundreds of different members ranging from a simple sphingoid base backbone (sphingosine) to more complex lipids such as ceramide, sphingomyelin or glycosphingolipids (Figure 1.4). As we progress to understand the intricate network of sphingolipid metabolism, we comprehend their importance not only as membrane components, but as signaling molecules in a vast variety of cellular processes

(Green et al., 2021; Hannun & Obeid, 2018). Due to the plethora of different lipids, the functions attributed to sphingolipids cover almost all aspects of cell biology. Not only are they essential for membrane organization and dynamics, they also play a role in processes like cell migration, adhesion, apoptosis, autophagy and cellular senescence as well as inflammation and immunity (MacEyka & Spiegel, 2014).

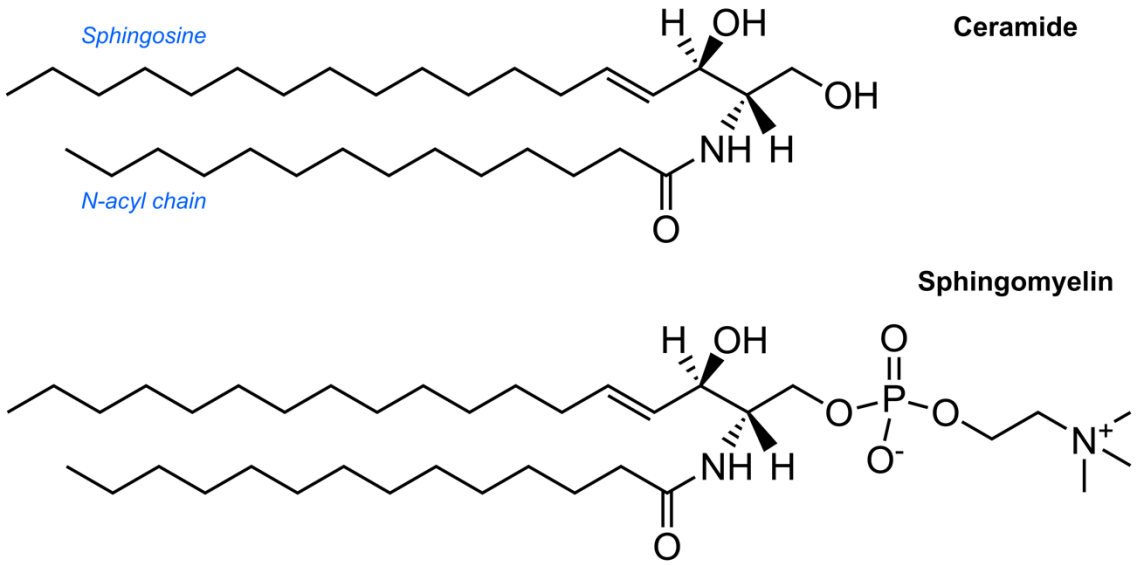

Figure 1.4: Structure of sphingolipids
Representative structure of the central sphingolipid ceramide and its relative, sphingomyelin that is synthesized from ceramide by the enzymatic action of sphingomyelin synthase (SMS). Indicated in blue are the sphingosine backbone, which in humans is mostly an 18:1 amino alcohol, and the highly variable N-acyl chain. Sphingolipids are usually named according to the species and the lengths of the sphingosine and fatty acid chain (including any double bonds). Shown here, are Ceramide d18:1/14:0 and Sphingomyelin d18:1/14:0. Chemical structures were created using ChemDraw v21.0.0.

Ceramide is the central hub of mammalian sphingolipid metabolism, and its *de novo* synthesis is the unique entry point into a highly intricate network of lipids that are synthesized, catabolized, interconverted and recycled. The only metabolic 'exit' point from sphingolipid metabolism is mediated by sphingosine-1-phosphate (S1P) lyase, leading to the irreversible degradation of S1P into non-sphingolipid molecules (MacEyka & Spiegel, 2014). A basic overview of main pathways and subcellular compartmentalization of sphingolipid metabolism is depicted in Figure 1.5. *De novo* synthesis of ceramide starts in the endoplasmic reticulum (ER) with the condensation of the amino acid serine and palmitoyl coenzyme A (CoA), facilitated by the enzyme serine palmitoyltransferase (SPT) (MacEyka & Spiegel, 2014). The newly formed 3-ketosphinganine is then reduced to sphinganine, which is subsequently acylated by one of six ceramide synthases (CerS1-CerS6) that are each specific to certain acyl chains of typically 14-26 carbons in length

(Stiban et al., 2010). In a last step, dihydroceramide is dehydrogenated to form ceramide. Ceramide is then transported in vesicles or by ceramide transport protein (CERT) to the Golgi for the synthesis of more complex sphingolipids such as glucosylceramide (GluCer) and glycosphingolipids (GSLs), galactosylceramide (GalCer) or sphingomyelin (SM). Newly synthesized sphingomyelin or GSLs are then delivered to the plasma membrane by vesicular transport (Gault et al., 2010; MacEyka & Spiegel, 2014; Nixon, 2009).

At the plasma membrane, sphingolipid signaling is mediated by the conversion of sphingomyelin into ceramide by sphingomyelinase (SMase), the subsequent formation of sphingosine by ceramidase (CDase), and finally the conversion into sphingosine-1-phosphate (S1P) by the enzyme sphingosine kinase (SphK) (MacEyka & Spiegel, 2014). The highly bioactive S1P can then either exit sphingolipid metabolism by S1P lyase-mediated degradation, or it can be recycled via sphingosine. To exert its functions, it is transported across the membrane, where it can bind to one of five G-protein-coupled S1P receptors (Nixon, 2009). Other membrane sphingolipids such as SM can also be internalized by endocytosis and degraded in the lysosome. Here, acidic SMase and CDase can again propagate the formation of sphingosine. Phosphorylated sphingosine (S1P) can subsequently be re-utilized in the salvage pathway for the synthesis of ceramide in the ER (MacEyka & Spiegel, 2014).

Alterations in sphingolipid metabolism can be detrimental, as exemplified by patients harboring mutations in the SMase gene, *SMPD1* (Brady et al., 1966). Also known as Niemann-Pick disease (type A and B), deficiency in acidic SMase activity leads to aberrant accumulation of sphingomyelin, especially in myeloid cells. Amongst the severe consequences are hyperlipidemia, pulmonary disease, hepatosplenomegaly and neurologic pathology, which emphasizes the importance of maintaining homeostasis of sphingolipid metabolism (McGovern et al., 2017).

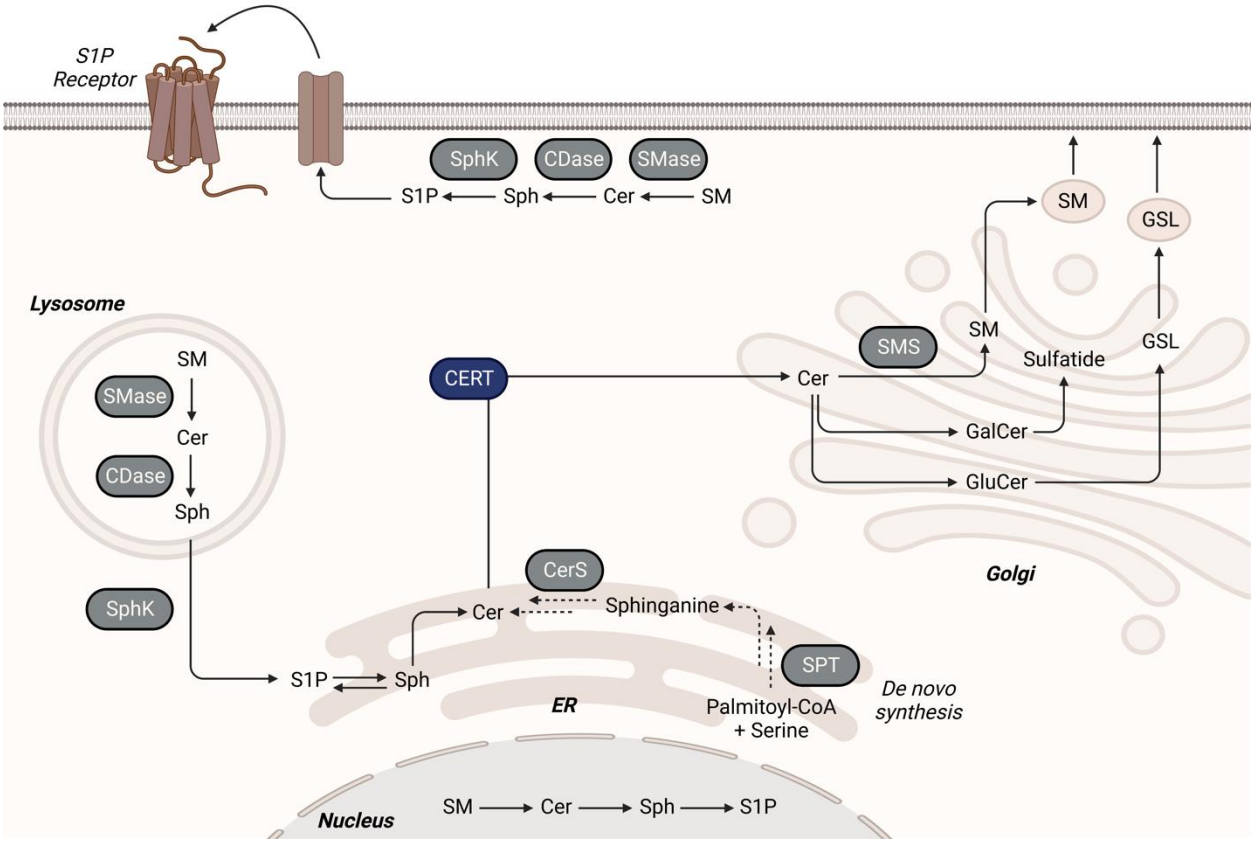

Figure 1.5: Sphingolipid Metabolism
Schematic and simplified overview of key steps in sphingolipid metabolism with ceramide as a central hub for the conversion and recycling into other, more complex, sphingolipids. Dashed arrows indicate multiple conversion steps. Some reactions are depicted one-way only, although most reactions are in fact reversible. This figure was created with BioRender.com under a department license.

1.4.3 Sphingomyelin in Inflammation

Different bioactive sphingolipids have emerged as key molecules in initiating and sustaining inflammation in various disease settings. Due to their relevance for this thesis, this section will, however, focus on sphingomyelins, and to less extent also ceramides, in context of different inflammatory disorders.

Sphingomyelin (SM) is the major sphingolipid species in mammalian cell membranes, where it is part of lipid-rich microdomains (also referred to as ‘lipid rafts’) that are essential in signal transduction processes (Slotte, 2013). They are considered pro-inflammatory, as their plasma levels are not only associated with cardiometabolic conditions such as obesity, atherosclerosis and coronary artery disease, but because they are also known to

elicit cellular inflammatory responses (Jiang et al., 2000; Kikas et al., 2018; Turpin et al., 2014). In the past decade, many studies have demonstrated that both serum and tissue SM concentrations are altered in context of obesity in both mice and humans (Im et al., 2019; Turpin et al., 2014). In fact, inhibition of the *de novo* synthesis of ceramides or SMs was shown to be beneficial regarding parameters such as glucose homeostasis or insulin resistance (Turpin et al., 2014). It is not surprising, therefore, that the abundance of SM also represents as risk factor in different cardiovascular diseases. Studies in mice have shown, that inhibition of sphingomyelin synthase reduces atherogenesis (Park et al., 2004). Moreover, in humans, plasma SM levels were found to be positively and independently related to coronary artery disease as well as potential inducers of atherosclerotic plaque inflammation and instability (Jiang et al., 2000).

The mechanisms underlying this profound positive correlation between metaflammation and SM are not completely understood. Both exogenously added ceramides and SMs are known to induce pro-inflammatory cytokines in macrophages and arterial smooth muscle cells (Fischer et al., 2007; Peters et al., 2022). In fact, it has been suggested that the SM catabolite ceramide plays a role in TLR4- and NLRP3-mediated inflammation (Scheiblich et al., 2017), both important signaling pathways in metaflammation-associated conditions. Moreover, it should be considered that SM is also the most abundant sphingolipid in lipoproteins (Iqbal et al., 2017), which are, as discussed previously, essential players in CVDs. There is evidence that SM-rich lipoproteins may promote foam cell formation or negatively influence cholesterol efflux capacity (Schlitt et al., 2006). It is, however, interesting to note that most studies don’t focus on specific sub-species, but rather on the family of SMs or ceramides as an entity, hereby neglecting the possibility that specific lipids or a change in their ratios might have a relevant impact.

1.5 Research Objectives

In the last few decades our environment has vastly changed and with it the diseases we live with. Apart from the recent corona virus (SARS-CoV-2) pandemic, infectious diseases have diminished while the prevalence of lifestyle-associated disorders continues to rise. Chronic low-grade inflammation, also referred to as metaflammation, is causally associated with the development of many of such non-communicable diseases, including obesity, atherosclerosis and type 2 diabetes. Although they are major health concerns of our modern society, specific underlying triggers of the subclinical inflammation observed in these diseases, remain yet to be elucidated. The identification of novel targets will provide a rationale for the development of preventative as well as interventional strategies that may hamper metaflammation processes.

Previous data from our laboratory indicates that there is a high degree of phenotypic variability in a mouse model of atherosclerosis, leading us to hypothesize that non-genetic environmental factors contribute to and drive metaflammation. Based on these preliminary observations, three specific aims were set for this thesis:

- To investigate metabolites that potentially contribute to inflammation and disease progression in atherosclerotic mice
- To study the effect of novel pro-inflammatory metabolite(s) on innate immune cells
- To understand the underlying mechanism of how inflammation is exacerbated, and to comprehend its physiological relevance

2 MATERIALS AND METHODS

2.1 Materials

2.1.1 Cell Lines and Primary Cells

HEK293T: Human embryonic kidney (HEK) cell line. HEK293T cells used in this study stably express either human TLR4 (HEK-TLR4) or both human TLR4 and MD-2 (HEK-TLR4/MD-2). Both cell lines were kindly provided by Prof. Sandra van Vliet (VUmc, Amsterdam, Netherlands).

3T3-L1: Mouse fibroblast cell line that can be induced to undergo a pre-adipocyte to adipocyte conversion. 3T3-L1 cells were kindly provided by Prof. Thiele (LIMES Institute, Bonn, Germany) and Prof. Wachten (Institute of Innate Immunity, Bonn, Germany).

Human Monocyte-Derived Macrophages (hMDMs): hMDMs were generated by *in vitro* differentiation of primary human monocytes that were isolated by CD14-positive selection from buffy coats purchased from Sanquin blood bank (Amsterdam, Netherlands).

Bone Marrow-Derived Macrophages (BMDMs): BMDMs were generated by *in vitro* differentiation of bone marrow cells that were isolated from wild-type C57BL/6 mice, or mice of the indicated genotype.

2.1.2 Cell Culture Media

Media	Composition	
Complete DMEM	DMEM (high glucose)	
	FCS	10 %
	Penicillin/Streptomycin	1 %
Complete RPMI	RPMI-1640	
	FCS	10 %
	Penicillin/Streptomycin	1 %
hMDM RPMI	RPMI-1640	
	FCS	10 %
	Penicillin/Streptomycin	1 %
	GlutaMAX	1 %
	Sodium pyruvate	1 mM
Basal Adipocyte Medium	DMEM (high glucose)	
	FCS	10 %
	Penicillin/Streptomycin	1 %
	GlutaMAX	1 %
Adipocyte Induction Medium	Basal Adipocyte Medium	
	Insulin	0.85 µM
	Dexamethasone	1 µM
	Rosiglitazone	1 µM
	IBMX	100 µM
Adipocyte Maintenance Medium	Basal Adipocyte Medium	
	Insulin	0.175 µM
Seahorse Assay Medium	Seahorse XF Base Medium	
	Glutamine	2 mM

2.1.3 Equipment

Device	Manufacturer
Azure Sapphire Biomolecular Imager	Azure Biosystems
Benchtop pH meter	Mettler Toledo
Bioanalyzer 2100	Agilent Technologies
Centrifuges	Eppendorf
Counting chamber (Neubauer)	Brand
Cytation 5	BioTek Instruments
Gel preparation equipment	Bio-Rad
iMark microplate reader	Bio-Rad
Incubator (non-CO_2)	Fisher Scientific
Incubator for tissue culture	Fisher Scientific
JESS™	Protein Simple
LSRFortessa X-20 Cell Analyzer	BD Biosciences
MacBook	Apple
Microplate Washer	Thermo Fisher Scientific
NanoDrop 1000	Thermo Fisher Scientific
NextSeq2000	Illumina
Pipettes (0.1 µL – 1 mL)	Gilson
Pipetting device	Integra Biosciences
QuadroMACS separator	Miltenyi Biotec
QuantStudio™ 5 Real-Time PCR System	Applied Biosystems
Seahorse XFe96 Analyzer	Agilent Technologies
SpectraMax i3 multimode reader	Molecular Devices
Sterile tissue culture hood	Fisher Scientific
Thermal Cycler SimpliAmp™	Applied Biosystems
ThermoMixer	Eppendorf

Tissue culture microscope	Leica Microsystems
Trans-Blot Turbo Transfer System	Bio-Rad
Tube rotator	MRC Laboratory Instruments
Ultrasonic bath sonicator	Fisher Scientific
Vacuum concentrator	Labconco
Water bath	Memmert
WES™	Protein Simple

2.1.4 Disposables

Material	**Manufacturer**
Cell scrapers	Greiner bio-one
EASYstrainer (70 µm)	Greiner bio-one
Falcon tubes (15 mL, 50 mL)	Greiner bio-one
Flow cytometry tubes	Sarstedt
MACS LS columns	Miltenyi Biotec
MicroAmp™ Endura™ 384-well plate (PCR)	Applied Biosystems
Microcentrifuge tubes	Eppendorf
Mini 0.2 µm PVDF Transfer Packs	Bio-Rad
Needles	Braun
Nunclon™ Delta-Surface, 6-well plates	Thermo Fisher Scientific
PCR plate	Applied Biosystems
Pipette tips (sterile and unsterile)	Gilson
Pipettes (2 mL, 5 mL, 10 mL, 25 mL)	Greiner bio-one
Seahorse 96-well Culture Microplate	Agilent Technologies
Seahorse XF Sensor Cartridge	Agilent Technologies
Small volume HTRF 384-well plate	Labomedic
Syringe filters (0.22 µm)	Millipore

Syringes	BD Biosciences
Tissue culture plastics (plates, dishes, flasks)	Greiner bio-one

2.1.5 Chemicals and Reagents

All reagents listed in the table below that were used under sterile conditions, were either obtained in tissue culture grade, or alternatively filtered (0.22 µm) before use. Moreover, all reagents used for lipid extraction and lipidomic analysis were obtained in mass spectrometry (MS) grade quality.

Reagent	**Manufacturer**
2-Mercaptoethanol	Sigma-Aldrich
3-Hydroxybutyrylcarnitine (3-HBC)	Sigma-Aldrich
4-Hydroxy-L-proline (4-HLP)	Sigma-Aldrich
Acetic acid	Roth
ACK Lysing Buffer	Thermo Fisher Scientific
Acrylamide/Bis solution 30 %	Bio-Rad
Ammonium persulfate (APS)	Sigma-Aldrich
Antimycin A	Sigma-Aldrich
Bovine Serum Albumin (BSA)	Sigma-Aldrich
BSA, fatty acid-free, low endotoxin	Sigma-Aldrich
CD14 MicroBeads, human	Miltenyi Biotec
Ceramide d18:1/14:0 (Cer14)	Avanti Polar Lipids
Ceramide d18:1/16:0 (Cer16)	Avanti Polar Lipids
Chenodeoxycholate (CDA)	Sigma-Aldrich
Chloroform	Roth
Cholestenone	Cayman-Chemical
cOmplete™ EDTA-free Protease Inhibitor	Roche Life Science
CRID3 (MCC950)	Pfizer

D-(+)-Glucose solution 45 %	Sigma-Aldrich
Dimethyl sulfoxide (DMSO)	AppliChem
DMEM (high glucose)	Gibco
EDTA solution 0.5 M, pH 8.0	Gibco
Ethanol	AppliChem
Fast SYBR™ Green Master Mix	Applied Biosystems
Fetal calf serum (FCS)	Thermo Fisher Scientific
Ficoll-Paque® PLUS	GE Healthcare Life Sciences
Fixable Viabiliy Dye eFluor™ 780	Invitrogen
Fluoro-carbonyl cyanide phenylhydrazone	Tocris Bioscience
GlutaMAX	Thermo Fisher Scientific
Glycine	Sigma-Aldrich
Intercept (TBS) Blocking Buffer	LI-COR
L-Glutamine	Capricorn Scientific
L929-conditioned medium	produced in-house
Laemmli Sample Buffer (4x)	Bio-Rad
Lipopolysaccharide from *E.coli* (0111:B4) (LPS)	InvivoGen
Methanol	Roth
N-Acetylneuraminate (NANA)	Sigma-Aldrich
N-Formylmethionine (F-Met)	Cayman Chemical
Nigericin, free acid	Invitrogen
Nudifloramide (NFA)	Cayman Chemical
Oligomycin	Tocris Bioscience
OptiMEM	Gibco
Pam3CSK4	InvivoGen
Paraformaldehyde 16 % (PFA)	Thermo Fisher Scientific
Penicillin-Streptomycin 100x	Capricon Scientific
Phenol sulfate (PheSulf)	Sigma-Aldrich

Phosphate-buffered saline (PBS)	Thermo Fisher Scientific
PhosSTOP™ Phosphatase Inhibitor	Roche Life Science
PMSF	AppliChem
Poly-L-Lysine	Sigma-Aldrich
Polyethyleneglycol (PEG) 8000	Fisher Scientific
Precision Plus Protein Dual Color Standard	Bio-Rad
Pyridine-2,3-dicarboxylic acid (2,3-PDC)	Selleckchem
Resolving Gel Buffer (PAGE)	Bio-Rad
rh Interferon γ (IFN γ)	Immunotools
rh Interleukin 10 (IL-10)	Immunotools
rhM-CSF	Immunotools
Rotenone	Tocris Bioscience
RPMI-1640	Gibco
Sandoz 58-035	Sigma-Aldrich
Saponin	Sigma-Aldrich
Sodium azide	Sigma-Aldrich
Sodium deoxycholate	Sigma-Aldrich
Sodium dodecyl sulfate (SDS)	Sigma-Aldrich
Sodium pyruvate	Life Technologies
Sphingomyelin d18:1/14:0 (S14)	Avanti Polar Lipids
Sphingomyelin d18:1/16:0 (S16)	Avanti Polar Lipids
Sphingomyelin d18:1/18:0 (S18)	Avanti Polar Lipids
Sphingomyelin d18:1/20:0 (S20)	Cayman Chemicals
Sphingomyelin d18:1/26:0 (S26)	Avanti Polar Lipids
Stacking Gel Buffer (PAGE)	Bio-Rad
T0901317 (LXR Agonist)	Tocris Bioscience
TAK-242	InvivoGen
Tetramethylethylenediamine (TEMED)	Sigma-Aldrich

TopFluor® Cholesterol	Avanti Polar Lipids
Trypan blue	Thermo Fisher Scientific
Trypsin-EDTA 10x	Capricorn Scientific
Tween-20	Sigma-Aldrich
UltraComp eBeads™ Compensation Beads	Thermo Fisher Scientific
VX-765 (Belnacasan)	Selleckchem
Water (sterile)	Fresenius Kabi AG
XF Base Medium	Agilent Technologies
XF Calibrant	Agilent Technologies

2.1.6 Commercial Reagent Kits

Kit	**Manufacturer**
Anti-Rabbit Detection Module	Protein Simple
cDNA Reverse Transcription Kit	Applied Biosystems
CellTiter-Blue® Cell Viability Assay	Promega
Chromogenic Endotoxin Quant Kit	Thermo Fisher Scientific
DC Protein Assay	Bio-Rad
EZ Standard Pack 1 (WES)	Protein Simple
Human IL-1 beta/IL-1F2 DuoSet	R&D Systems
Human IL-6 DuoSet	R&D Systems
Human IL-8 DuoSet	R&D Systems
Human LegendPLEX™ Inflammation Panel 1	Biolegend
Human LegendPLEX™ Metabolic Panel 1	Biolegend
Human MCP-1 DuoSet	R&D Systems
Human TNF alpha DuoSet	R&D Systems
Mouse IFN beta DuoSet	R&D Systems
Mouse IL-1 beta/IL-1F2 DuoSet	R&D Systems
Mouse IL-6 DuoSet	R&D Systems

Mouse IL-6 Kit HTRF	Cisbio
Mouse IP-10 DuoSet	R&D Systems
Mouse TNF alpha DuoSet	R&D Systems
Mouse TNF alpha Kit HTRF	Cisbio
RePlex™ Module for JESS™	Protein Simple
RNase-free DNase Set	Qiagen
RNeasy® Mini Kit	Qiagen
WES™ Separation Module (12-230 kDa)	Protein Simple

2.1.7 Buffers

Buffer/Solution	**Composition**	
Resolving Gel Solution (12%)	MilliQ H_2O	6.6 mL
(for two gels)	30 % Acrylamide Mix	8 mL
	Resolving Gel Buffer	5 mL
	20 % SDS	0.1 mL
	10 % APS	0.2 mL
	TEMED	0.008 mL
Stacking Gel Solution (5 %)	MilliQ H_2O	4.5 mL
(for two gels)	30 % Acrylamide Mix	1.3 mL
	Stacking Gel Buffer	2 mL
	20 % SDS	0.08 mL
	10 % APS	0.08 mL
	TEMED	0.008 mL
Electrophoresis Buffer	ddH_2O	
	Tris-glycine buffer (10x)	10 %
	20 % SDS solution	0.5 %

Tris-buffered Saline with Tween	1x TBS	
(TBS-T)	Tween-20	0.1 %
ELISA Wash Buffer	PBS	
	Tween-20	0.05 %
ELISA Reagent Diluent	PBS	
(filtered, 0.2 µm)	BSA	1 %
ELISA Stop Solution	Sulfuric Acid	2 N
MACS Buffer	PBS	
(sterile-filtered, 0.2 µm)	BSA	0.5 %
	EDTA	2 mM
Cell Detachment Buffer	PBS	
	EDTA	5 mM
FACS Staining Buffer	PBS	
	BSA	0.5 %
	Sodium azide	0.02 %
RIPA Lysis Buffer	ddH_2O	
	Tris-HCl, pH 8	50 mM
	NaCl	150 mM
	EDTA	1 mM
	NP-40	1 %
	Sodium Deoxycholate	0.5 %
	SDS	0.1 %
	PMSF	1 mM
	cOmplete™ Protease Inhibitor	1x
	PhosSTOP™ Phosphatase Inhibitor	1x

2.1.8 Antibodies

All antibodies used in this work are listed in the tables below, grouped per application.

Antibody (Flow Cytometry)	Clone	Provider	Dilution
Anti-mouse TLR4-PE-Cy7	MTS510	Biolegend	1:200
Anti-mouse TLR4-APC	SA 15-21	Biolegend	1:50
Anti-mouse CD16/CD32	93	Invitrogen	1:100
Anti-mouse CD80-BV650	16-10A1	Biolegend	1:100
Anti-mouse CD86-BV510	GL-1	Biolegend	1:100
Anti-mouse CD40-APC	3/23	Biolegend	1:100
Anti-mouse MHCII-PerCP-Cy5.5	M5/114.15.2	Biolegend	1:200
Anti-mouse iNOS-PE	CXNFT	Invitrogen	1:150

Antibody (Immunoblotting)	Clone	Provider	Dilution
Anti-mouse SAPK/JNK	-	Cell Signaling	1:20
Anti-mouse phospho-SAPK/JNK	81E11	Cell Signaling	1:20
Anti-mouse NF-kB p65	C22B4	Cell Signaling	1:20
Anti-mouse phospho-NF-kB p65	93H1	Cell Signaling	1:20
Anti-human beta-Actin	926-42212	LI-COR	1:5000
Anti-human IL-1 beta/IL-1F2	-	R&D Systems	1:1000

Antibody (Detection)	Provider	Dilution
Goat anti-mouse IR700 and IR800	Azure Biosystems	1:15,000
Goat anti-rabbit IR700 and IR800	Azure Biosystems	1:15,000
Donkey anti-goat IR800	Azure Biosystems	1:15,000

Antibody (Neutralization)	Clone	Provider	Dilution
Anti-human TLR4-IgG	W7C11	Invivogen	1:20

2.1.9 Synthetic Oligonucleotides (Primers)

All primers were individually designed and obtained from Invitrogen.

Target	Sequence
Human HPRT-1 fwd	AGCCCTGGCGTCGTGATTAGT
Human HPRT-1 rev	CGAGCAAGACGTTCAGTCCTGTCC
Human IL1B fwd	AAGATGCTGGTTCCCTGC
Human IL1B rev	GTTCAGTGATCGTAGAGGTGC
Human IL6 fwd	GAGTAGTGAGGAACAAGCCAG
Human IL6 rev	TTGTCATGTCCTGCAGCC
Human TNFα fwd	GGCGTGGAGCTGAGAGAT
Human TNFa rev	TGGTAGGAGACGGCGATG
Human NLRP3 fwd	TCGGAGACAAGGGGATCAAA
Human NLRP3 rev	AGCAGCAGTGTGACGTGAGG
Human PYCARD fwd	GAGCTCACCGCTAACGTGCT
Human PYCARD rev	ACTGAGGAGGGGCCTGGAT
Human CASP1 fwd	ACAACCCAGCTATGCCCACA
Human CASP1 rev	GTGCGGCTTGACTTGTCCAT
Human GSDMD fwd	ATGAGGTGCCTCCACAACTTCC
Human GSDMD rev	CCAGTTCCTTGGAGATGGTCTC

2.1.10 Software

Software/Application	Supplier
Affinity Designer v1.9.3	Serif
BioRender (License: VUmc, MCBI, Netherlands)	BioRender
ChemDraw® v21.0.0.28	Perkin Elmer
ClueGO v2.5.8	Bindea *et al*., 2009
Compass (Automated Western Blot)	Protein Simple
Cytoscape v3.9.1	Institute for Systems Biology
FlowJo v10	BD Biosciences
LegendPLEX™ Data Analysis Software	Biolegend
Prism 9	GraphPad
QuantStudio™ 5 RT-PCR System Software	Applied Biosystems
RStudio v1.4.1106	Ihaka and Gentleman, 1996
Sapphire Capture	Azure Biosystems
SoftMax Pro v6.3	Molecular Devices
Wave (Seahorse Assay)	Agilent Technologies

2.2 Methods

2.2.1 Animal Models

Atherosclerosis model

This *in vivo* model was performed under the lead of PD Dr. Peter Düwell and Dr. Anette Christ, preliminary to and independent of the preparation of this thesis. However, the rationale of the experiments performed in the present work, relies substantially on the dataset generated from this study. Animal experiments were approved by the Institutional Animal Care and Use Committee (IACUC; protocol ID 1945-14 and 1945-17) of the University of Massachusetts Medical School, Worcester, MA. The LDLR KO mouse colony was bred internally, maintained on a C57BL/6 background and frequently genotyped (Transnetyx Inc., Cordova, TN, USA). With an average age of 10 weeks, mice were fed a high fat and high cholesterol western diet ad libitum (Teklad TD.88137; 42% calories from fat, 0.2% cholesterol) for 8 weeks. Mice were kept on a regular day-night rhythm, which was maintained throughout the entire study duration. All analysis and data, including cytokine measurements, lipidomics analysis, plasma lipoprotein analysis and bioinformatics evaluation presented in this thesis were provided by Christoph A. Thaiss, Lenka Dohnalová (both Department of Microbiology, Perelman School of Medicine, University of Pennsylvania, Philadelphia, PA, USA) and Santu K. Singha, Michael L. Fitzgerald (both Lipid Metabolism Unit, Centre for Computational and Integrative Biology, Massachusetts General Hospital, Harvard Medical School, Boston, USA).

Lipid-induced acute peritonitis model

This animal experiment was conducted after approval by the Committee for Animal Welfare (University of Amsterdam, VU University Amsterdam) under work protocol 0750-MCB19-01A3 with all animals being handled and sacrificed by Eelco Keuning. Acute peritonitis was induced by intraperitoneal injection of 8 week old, male wild type C57BL/6 mice (n=5 per group) with 5 mg/kg bodyweight LPS or sphingomyelin d18:1/14:0, or vehicle control. Mice were sacrificed 3 h after injection and blood was collected by cardiac

puncture with EDTA-coated syringes. Plasma was obtained by centrifugation of the blood at 300 x g for 6 min. Peritoneal lavage was performed by injection of 5 mL PBS supplemented with 2 mM EDTA into the peritoneal cavity, followed by careful re-collection of the maximum volume lavage fluid possible. Both plasma and peritoneal lavage fluid were aliquoted and stored at -70 ºC.

Mice used for Cell Isolations

All animal experiments were approved by the Committee for Animal Welfare of the VU University Amsterdam and the University of Bonn. Male and female wild type C57BL/6J mice were 8-16 weeks of age, unless stated otherwise, purchased from Charles River and housed under specific pathogen-free conditions. TLR4 KO mice were initially supplied by Prof. Kurts (University of Bonn) and subsequently bred in house at the University of Bonn. IRF3 KO, MYD88 KO or TRIF KO mice were bred in house at the University of Bonn. All animals were kept on a regular day-night rhythm with food and water ad libitum. All live mice were handled and sacrificed by either Maximilian Rothe (University of Bonn) or Kyra de Goede (VU Amsterdam) according to local ethics regulations.

2.2.2 Human Subject Details

All cohort data generated in this study originates from serum and plasma biospecimens kindly provided by study coordinators of third-party registered clinical studies. All study participants had previously given their written consent to the respective clinical study coordinators for use of the material.

The ***DESIRE cohort*** (ClinicalTrials.gov ID: NCT02628301) consists of 15 healthy male volunteers (age 18-30 years) from the Netherlands with a BMI of 20-25 kg/m^2. In short, participants were exposed to a hypercaloric diet (HCD) consisting of a normal ad libitum diet with 60 % surplus kilocalories. The HCD intake was calculated as resting energy expenditure (REE)x1.3x1.6. Once a 5 % gain in body weight was achieved, participants were switched to a low-caloric diet (LCD) consisting of 1.0xREE until returning to their baseline body weight.

The ***300-Obesity (300-OB) cohort***, established by Radboud University Medical Center, Nijmegen (NL) between 2014-2016, consists in total of 302 overweight and obese individuals aged 55-81 years with a BMI of >27 kg/m^2. The study was approved by the IRB CMO Regio Arnhem-Nijmegen (nr. 46846.091.13) and further details can be found at the Human Functional Genomics Project (HFGP) website. For the present study, only samples of male participants were considered.

The ***FAIR cohort*** (ClinicalTrials.gov ID: NCT05295160), for which recruitment started in 2020, consists of individuals aged 28 to 73 with diabetes mellitus type 2 and a BMI of >27 kg/m^2. In brief, study subjects received a very low-calorie diet (VLCD; 600-800 kcal/day) over a period of three months or until successful loss of 15 kg body weight. This study is still ongoing and therefore, some study parameters are classified and not published yet. For the present study, only samples of male participants were considered.

The study ***"Sphingomyelins in CVD"*** (ClinicalTrials.gov ID: NCT03539133) has been established by the Cardiovascular Research Institute Düsseldorf (CARID) University Duesseldorf, Medical Faculty, Duesseldorf (Germany) between 2019-2022 and consists of both male and female individuals with a mean age of 63.5±10.7 with coronary artery disease (CAD) and a mean BMI of 28.7±4.6 kg/m^2. The healthy control cohort consists of individuals with a mean age of 30.7±4.4 and a mean BMI of 24.8±2.8 kg/m^2.

2.2.3 Cell Culture

All cells were cultured and incubated during stimulation periods at 37 °C, 5 % CO_2 in a humidified atmosphere. Unless stated otherwise, culture media were warmed to 37 °C before use. All tissue culture work was performed in tissue culture hoods under sterile conditions.

For permanent storage, cell lines or isolated bone marrow was frozen in cryo-vials in designated freezing containers for 24 h at -70 °C and subsequently transferred into liquid nitrogen tanks. When required for experiments, frozen cells were quickly thawed at 37 °C in a water bath and immediately transferred into pre-warmed medium. After pelleting the cells at 340 x g for 5 min, cells were re-suspended in fresh medium for culturing.

2.2.3.1 Cultivation of HEK293T Cells

HEK293T cells were continuously cultured in complete DMEM in 75 cm^2 flasks. For passaging, cells were washed once with PBS and detached with trypsin-EDTA before re-suspending an appropriate amount of cells (split ratio 1:10 – 1:20 every second to third day) in fresh medium. For experiments, 40.000 cells were seeded per well into a poly-L-Lysine coated 96-well plate and left to attach for 6 h before stimulation.

2.2.3.2 Cultivation of 3T3-L1 Cells

3T3-L1 cells were continuously cultured in basal adipocyte medium until reaching maximum 70 % confluence. Prior to experiments, 3T3-L1 cells were seeded at $5x10^3$ cells per well in 48-well plates in basal adipocyte medium (d-2). Two days post-seeding (d0), differentiation of cells was induced by exchanging the medium for adipocyte induction medium. Two days later (d2), the medium was exchanged again, maintaining the cell for additional 2 days (d4) in adipocyte maintenance medium. On day 4 and thereafter, cells were maintained in basal adipocyte medium, refreshing the medium every two days. On day 7, cells were kept for 1 h in serum-free DMEM before re-stimulating cells with 10 nM human insulin or medium control for 24 h.

2.2.3.3 Human Monocyte-Derived Macrophages (hMDMs)

Buffy coats from healthy donors were purchased from Sanquin blood bank (Amsterdam, Netherlands). Primary hMDMs were generated through differentiation of monocytes in medium supplemented with recombinant human M-CSF (rhM-CSF). In brief, human peripheral blood mononuclear cells (PBMCs) were isolated by density gradient centrifugation using Ficoll-Paque® PLUS (700 x g, 20 min). Monocytes were obtained from PBMCs by CD14 positive selection using CD14 microbeads. In short, PBMCs were incubated with magnetic microbeads conjugated to anti-human CD14 antibodies for 20 min at 4 °C before being washed and run over a MACS column placed in a magnetic field. In a final step, $CD14^+$ monocytes were washed off the column and plated at $2x10^6$ cells/mL in hMDM RPMI. Differentiation was subsequently induced by addition of 50 U/mL rhM-CSF to the culture medium. After 3 days of incubation, cells were harvested and plated for experiments in hMDM RPMI with 25 U/mL rhM-CSF. On day 4, experiments were performed in hMDM RPMI without additional M-CSF supplementation.

2.2.3.4 Human Whole Blood Stimulation

Whole Blood from healthy donors collected in ethylene-diamine-tetraacetate (EDTA) tubes was purchased from Sanquin blood bank (Amsterdam, Netherlands). Shortly after collection, the blood was processed by diluting 100 µL of whole blood 1:5 with the indicated stimuli in RPMI-1640 without further supplements. The diluted blood was then incubated for the times indicated (usually 8 or 24 h) in a thermal shaker at 37 °C. After stimulation, the blood was centrifuged at 400 x g for 5 min at RT and the “supernatant” (plasma mixed with medium) was immediately stored at -70 °C for cytokine or adipokine analysis.

2.2.3.5 Bone Marrow-Derived Macrophages (BMDMs)

Bone marrow was isolated from femurs and tibias of WT, TLR4 KO, IRF3 KO, MYD88 KO or TRIF KO mice. Briefly, bones were disinfected with 70 % ethanol before flushing the bone marrow cavity with ice-cold PBS and filtering the cell suspension through 70 µm cell strainers. BMDMs were generated by culturing the isolated bone marrow cells in complete DMEM supplemented with 15 % L929 cell-conditioned medium (LCM) in 15 cm tissue culture dishes. On day 6 of differentiation, BMDMs were collected using cold cell detachment buffer, live cells were counted using trypan blue and plated for experiments in appropriate flat-bottom plates. Experiments were performed in complete DMEM, unless stated otherwise.

2.2.3.6 Stimulation of Cells

Sphingolipid Preparation: Sphingomyelin and ceramide lyophilized stocks were initially prepared under sterile conditions in 95 % methanol. For cell culture experiments, the organic solvent was evaporated under vacuum before dissolving the dried lipid film in the appropriate cell culture medium containing fatty-acid free BSA to a final molar ratio of 1 to 2.75 (Sphingolipid:BSA) and incubating the mix for 45 min at 40 °C whilst shaking and with occasional vortexing. For the *in vivo* injection protocol, sphingomyelin was coupled to sterile-filtered mouse serum albumin in PBS, instead of BSA in cell culture medium.

Stimulations: Unless stated otherwise, BMDMs were generally treated with 100 ng/mL LPS, 30 µM sphingomyelin (e.g. S14) or ceramide, or the corresponding vehicle control (BSA without being coupled to sphingolipid) for 3 h or 18 h, or the time indicated. For Extracellular Flux Experiments using BMDMs, 20 ng/mL LPS in combination with 50 ng/mL recombinant mouse IFNγ was used. HEK293T cells were stimulated with 10 ng/mL LPS, 30 µM S14 or vehicle control for 18 h. Unless stated otherwise, hMDMs were generally treated with 10 ng/mL LPS, 30 µM S14 or vehicle control for 6 h or 18 h, or the time indicated. Human whole blood was incubated for either 8 h or 24 h with 30 µM S14 or vehicle control. Details on more complex experiments are outlined in the stimulation scheme below.

Experiment	Pre-treatment			Stimulation		
	Compound	***Concentration***	***Time***	***Compound***	***Concentration***	***Time***
Sphingomyelinase inhibition in BMDMs	GW4869 ARC39	10 µM 5 µM	30 min 30 min	Vehicle S14	- 30 µM	18 h 18 h
TLR4 Inhibition in BMDMs	TAK-242	2 µM	30 min	Vehicle S14	- 30 µM	18 h 18 h
TLR4 Neutralization in hMDMs	Anti-hTLR4 IgG	5 µg/mL	1 h	Vehicle S14	- 30 µM	18 h 18 h
Inflammasome assay in human whole blood	untreated CRID3 VX-765	- 2.5 µM 8 µM	15 min 15 min 15 min	Vehicle LPS S14	- 10 ng/mL 30 µM	8 h 8 h 8 h

2.2.4 Endotoxin Quantification

Potential endotoxin contamination (e.g. LPS) was assessed using the Chromogenic Endotoxin Quant Kit according to the manufacturer's instructions. Briefly, 50 µL of amebocyte lysate reagent was added to 50 µL of each sample, blank or endotoxin standard dilution and incubated for the time indicated on the reagent vial. After exactly incubating for this time, 100 µL of pre-warmed chromogenic substrate solution was added for 6 min, before stopping the reaction with 50 µL of stop solution (25 % acetic acid). The optical density at 405 nm was determined immediately after performing the assay and sample endotoxin concentration were determined based on a standard curve generated.

2.2.5 Cytokine Measurement

2.2.5.1 Homogenous Time-Resolved Fluorescence (HTRF®) Assay

The mouse HTRF assays for detection of IL-6 and TNFα in cell culture supernatants were performed according to the manufacturer's instructions. Antibodies and standard provided in the kit were initially reconstituted and stored at -80 °C. Per sample, 1.5 µL of cryptate- (donor) and XL-antibody (acceptor) were mixed with 12 µL of appropriately diluted cell-free supernatant or standard. The samples were incubated in the dark for cytokine-specific time periods (usually overnight) at RT, before measuring the fluorescence of donor and acceptor at 620 nm and 668 nm using a SpectraMax Plate Reader.

2.2.5.2 Enzyme-linked Immunosorbent Assay (ELISA)

ELISA kits from R&D Systems were used for the detection of various murine and human cytokines in cell culture supernatants or blood plasma. All component of each kit were prepared according to manufacturer instructions. One day prior to the assay, NuncMaxiSorp 96-well plates were coated with 50 µL/well capture antibody in PBS and incubated overnight at RT. The next day, the plate was washed three times with ELISA Wash Buffer using an autowasher, before adding 150 µL/well Reagent Diluent for 1 h at RT. After washing again three times, 50 µL of a dilution series of standard or the appropriately diluted samples were added to the plate in duplicates. After incubating for either 2 h at RT or overnight at 4 °C (to increase sensitivity), the plate was again washed three times and the remaining liquid was removed. Subsequently, 50 µL/well of 1:40 diluted Streptavidin-HRP was added and incubated for 20 min in the dark. Finally, the plate was washed four times, all residual liquid was removed thoroughly before incubating with 50 µL/well of substrate solution. The reaction was stopped as soon as a stable blue color change was observed, by adding 25 µL/well of 2 N sulfuric acid under the fume hood. The optical density (corrected reading = $OD_{450\ nm} - OD_{570\ nm}$) was determined using a microplate reader.

2.2.5.3 LegendPLEX™ Multiplex Assay

Multiplex cytokine and adipokine analysis were performed using the following LegendPLEX™ kits according to manufacturer instructions: Human Inflammation Panel 1, Human Metabolic Panel 1 (both V-bottom plate format). Analysis was performed using a LSRFortessa X-20 flow cytometer and obtained data was evaluated using the LegendPLEX™ Data Analysis Software Suite (online application).

2.2.5.4 Griess Assay (Quantification of Nitric Oxide)

Concentrations of nitrite (a direct stable breakdown product of nitric oxide) in cell culture supernatants were determined using a standard Griess Assay. It relies on two consecutive chemical reactions that first use sulfanilamide and then N-1-naphthylethylenediamine

dihydrochloride in presence of phosphoric acid (all components of Griess Reagent) to produce a pink-colored azo dye in the presence of nitrite. Briefly, equal amounts of cell culture supernatant or a sodium nitrite standard are incubated 1:1 with Griess Reagent for 5 min before measuring absorbance values at 540 nm.

2.2.6 Cell Viability Assay (CellTiter-Blue®)

The CellTiter-Blue® Cell (CTB) Assay provides a measure of cell viability based on the metabolic capacity of living cells, converting the redox dye resazurin into the fluorescent product resorufin. After cells were stimulated and culture supernatants were harvested, 50 µL culture medium containing 10 % CTB reagent was added per well of the 96-well plate. Subsequently, cells were incubated at 37 ºC for 30-60 min before measuring the fluorescence at an excitation wavelength of 530-570 nm and an emission wavelength of 580-620 nm.

2.2.7 Flow Cytometry

All flow cytometry samples were acquired on the same day at the O|2 Core Facility at Amsterdam UMC (Netherlands) on a LSRFortessa X-20 flow cytometer, which was calibrated daily using CS&T calibration beads (BD Biosciences). Data was analyzed using FlowJo, gating on live, single cells and using single stains with UltraComp eBeads™ as compensation controls and fluorescence minus one samples as gating controls.

Macrophage Phenotyping: BMDMs were stimulated as indicated and subsequently harvested. After washing the cells in cold FACS buffers, cells were stained for surface markers for 30 min at 4 ºC in the dark. Unspecific binding was blocked using an anti-CD16/CD32 antibody and fixable viability dye (1:1000) was added to discriminate live cells. If applicable, cells were subsequently washed with PBS, fixed with 1.6 % PFA for 10 min at RT and permeabilized in FACS Buffer supplemented with 0.1 % Saponin for 15 min at 4 ºC. Subsequently, cells were stained with antibodies against intracellular target proteins for 30 min at 4 ºC in FACS Buffer with 0.1 % Saponin. For the assessment of

inflammatory macrophage markers, cells were stained with the following fluorescently-labeled antibodies: CD80, CD86, MHC-II, CD40 and iNOS.

TLR4 Dimerization Assay: TLR4 dimerization and endocytosis were assessed and calculated as published previously (Tan et al., 2015a; Zanoni et al., 2011, 2017a). Briefly, BMDMs were left untreated and harvested immediately (t=0 min), or treated for 15 min and 120 min with LPS or S14 before harvesting cells. Subsequently, cells were stained as described in the section above, using antibodies against surface TLR4 that allow analysis of either dimerization status (TLR4-PE-Cy7, clone MTS510) or receptor endocytosis (TLR4-APC, clone SA15-21). Clone MTS510 binds to a specific epitope of TLR4/MD-2 that is lost after ligand-induced receptor activation, whereas clone SA15-21 binds to another distinct epitope. These antibodies don't cross block each other.

2.2.8 Seahorse Extracellular Flux Analysis

One day prior to the assay, $8x10^4$ BMDMs were plated in a XF-96 cell culture microplate and stimulated either overnight for 18 h or on the assay day for 3 h with 20 ng/mL LPS in combination with 50 ng/mL IFNγ, 30 µM S14 or vehicle only. Furthermore, the sensor cartridge was already hydrated by adding 200 µL/well sterile water and placing it in a non-CO_2 incubator overnight. The next day, the water in the sensor cartridge was replaced by 200 µL/well Seahorse XF calibrant, before placing it back in the non-CO_2 incubator. Upon completion of the stimulation, the cell culture medium in the culture microplate was replaced by warm Seahorse XF base medium supplemented with 2 mM glutamine, adjusted to pH 7.4. Subsequently, the cells were further incubated for approximately 1 h in a non-CO_2 incubator. Meanwhile, the sensor cartridge was prepared by filling the four injection ports A-D and was then placed into the Extracellular Flux Analyzer for calibration. After additionally inserting the cell culture microplate into the machine, measurement of oxygen consumption rate (OCR) and extracellular acidification rate (ECAR) were first performed under basal conditions (5 cycles). Further, OCR and ECAR were monitored for 3 cycles each upon the sequential injection of glucose (final 10 mM), the ATP-synthase inhibitor oligomycin A (final 1 µM), the mitochondrial uncoupler fluoro-carbonyl cyanide phenylhydrazone (FCCP, final 2 µM) together with sodium pyruvate (final 1 mM) and

finally, the electron transport chain complex I and III inhibitors rotenone and antimycin A (both 0.5 µM). Calculations were performed according to the scheme below (Figure 2.1).

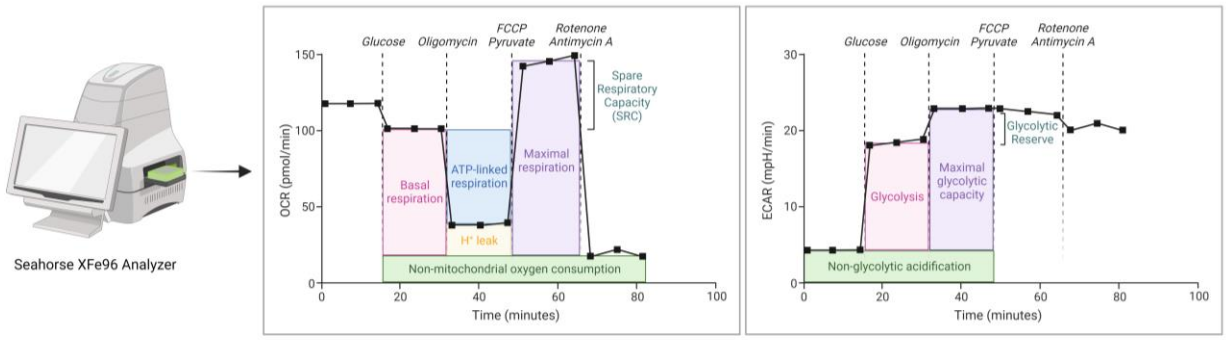

Figure 2.1: Seahorse Extracellular Flux Analysis
The figure depicts a schematic overview of the data obtained during Seahorse Extracellular Flux Analysis. OCR and ECAR graphs are shown with the individual metabolic parameters that can be calculated from the data generated over time with the indicated injection strategy. This figure was created with BioRender.com under a department license.

2.2.9 Cholesterol Efflux Capacity (*in vitro*)

ApoB-depletion from human plasma: Whole Blood from healthy donors collected in EDTA tubes was purchased from Sanquin blood bank (Amsterdam, Netherlands). The blood was centrifuged for 10 min at 2000 x g, RT. Meanwhile, a 200 mM glycine buffer supplemented with 20 % (w/w) PEG 8000 was prepared and then mixed with the collected plasma at 40 parts to 100 parts, respectively. After gently mixing, the plasma was incubated for 20 min at RT before centrifugation at 4 ºC for 30 min at 10,000 rpm. The "supernatant" was then recovered, aliquoted and frozen at -20 ºC.

Cholesterol Efflux Assay: This assay was designed to determine the rate of efflux of externally added cholesterol from cultured cells *in vitro* following sphingomyelin treatment. On day 0 (d0), $6x10^4$ BMDMs were plated per well in black 96-well plates with a clear flat bottom. Once the cells were attached, they were incubated overnight with 3 µM TopFluor® Cholesterol in RPMI-1640 containing 0.2 % BSA, 2 µg/mL Sandoz 58-035 (Acetyl-CoA Acetyltransferase inhibitor) and 1 % FCS. The next day (d1), cells were washed once with OptiMEM and then stimulated for 18 h with 30 µM S14 or vehicle only, diluted in RPMI-1640 containing 0.2 % BSA, 2 µg/mL Sandoz 58-035 and 5 µM T0901317 (LXR agonist). For each condition, triplicate wells were included for a lysis control and a "no acceptor"

control. After stimulation (d2), cells were washed with warm OptiMEM, meanwhile preparing the efflux medium by supplementing OptiMEM with 2 µg/mL Sandoz 58-035 and 2 % ApoB-depleted plasma (not added for the “no acceptor” controls). Subsequently, the cells were either incubated for 6 h with complete efflux medium or efflux medium without acceptor present (to determine background cholesterol efflux), whereas the cells for the lysis control were incubated with 1 % Sodium Deoxycholate (to determine the initial amount of cholesterol present after labeling, corresponding to 100 % TopFluor® Cholesterol). After 6 h, supernatants and lysates were recovered and transferred to a new black plate with an optical clear bottom. The fluorescence intensity (FI) of all samples including the controls was determined (495 nm/507 nm) and the % efflux calculated:

$$\% \text{ Efflux} = \frac{\text{FI (supernatants)-FI ("no acceptor")}}{\text{FI (lysis control)}} \text{ x } 100$$

2.2.10 Immunoblot Analysis

2.2.10.1 Sample Preparation

For analysis of protein expression, $1x10^6$ hMDMs or BMDMs were seeded in 6-well plates and stimulated as described in section 2.2.3.6. After completion of the stimulation, cells were washed once with cold PBS, lysed in RIPA buffer and the cell lysates were collected using a cell scraper. The lysates were then transferred to 1.5 mL tubes, ensuring to work on ice the whole time. Subsequently, the samples were centrifuged at 13,000 rpm for 15 min at 4 ºC, to pellet the DNA. The supernatants were then transferred to new tubes to proceed with quantitation of the protein concentration. The concentration of protein in total cell lysates was determined using the DC Protein Assay according to the manufacturer’s instructions. After incubating the diluted samples or the albumin standard with the assay reagents for 15 min, the absorbance was determined at 750 nm and the sample concentrations calculated from the standard curve.

2.2.10.2 Gel Preparation

12 % Tris-glycine gels were prepared freshly before use. Using a gel preparation system (Bio-Rad) with clean glass plates (1.5 mm gel thickness), a resolving gel was initially poured (ca. 7.5 mL) and left to polymerize for 20 min at RT. Then, around 2 mL of stacking gel solution was poured on top and a 10-well comb immediately inserted into the liquid. After polymerization, the gel, left between the glass plates, was either immediately used or kept for maximum two days at 4 ºC wrapped in wet paper towels.

2.2.10.3 Gel Electrophoresis (SDS PAGE)

For SDS Polyacrylamide Gel Electrophoresis (SDS PAGE) of hMDM lysates, all samples were diluted with ddH_2O to obtain equal protein concentrations and a final amount of 25 µg protein. All samples were then mixed accordingly with 4x Laemmli Sample Buffer (final 1x) and 10 % β-Mercaptoethanol (β-Me). To denature the proteins, samples were heated for 5 min at 95 ºC and cooled down before loading them onto the prepared 12 % gels. To determine the size of the proteins analyzed, a pre-stained protein ladder was included as a molecular weight standard. The loaded gels were placed in an electrophoresis chamber filled with electrophoresis buffer and a voltage of 80 V was applied for around 10 min before increasing the voltage to 120 V until completion.

2.2.10.4 Western Blotting

After gel electrophoresis, the proteins were transferred onto a PVDF membrane in a semi-dry manner, utilizing the Trans-Blot Turbo Transfer System together with the Mini 0.2 µm PVDF Transfer Packs according to the manufacturer's instructions. Either one or two mini gels were ran at the same time using the low molecular weight program. Upon completion, the membranes were blocked for at least 1 h in a 1:1 mix of Intercept (TBS) blocking buffer with TBS (1x) at RT. Afterwards, the blocking buffer was removed and the membrane was incubated at 4 ºC overnight with 5 mL of primary antibody diluted in a 1:1 mix of Intercept (TBS) blocking buffer with TBS-T. To remove unbound primary antibody, the membranes were washed three times with TBS-T for 10 min each, before incubating with secondary

antibody diluted in a 1:1 mix of Intercept (TBS) blocking buffer with TBS-T for 1 h in the dark on a tube roller. Before imaging using the Azure Sapphire Biomolecular Imager, the membranes were washed again three times with TBS-T and then once with TBS for 10 min each.

2.2.10.5 Immunoblotting by WES™ and JESS™

Samples were prepared as described above and 12-230 kDa Separation Modules as well as RePlex Modules were prepared according to the manufacturer's instructions (ProteinSimple). Shortly, four units of equally concentrated samples were mixed with one unit of fluorescent master mix and incubated for 10 min at 95°C. Samples were loaded twice per plate and analysed for SAPK/JNK (Cell Signaling #9252) or phospho-SAPK/JNK (Cell Signaling #4668) on the WES. Expression levels of phosphorylated NF-κB p65 (Cell Signaling #3033) and total NF-κB p65 (Cell Signaling #4764) per sample were sequentially analyzed in the same capillaries using the RePlex module on the JESS. Proteins were detected using the anti-rabbit chemiluminescence detection module. Protein separation and analysis was performed using the compass simple western software with the following program: 25 min separation at 375 V, 5 min washing, 90 min (WES) or 60 min (JESS) primary antibodies, 30 min secondary antibody. Per sample, the ratio of phosphorylated to total protein expression was calculated using the AUC of the respective chemiluminescent signals.

2.2.11 Quantitative Polymerase Chain Reaction (qPCR)

2.2.11.1 Sample Preparation

For qPCR analysis, $1x10^6$ hMDMs were left untreated (vehicle only) or stimulated for 6 h with 30 µM S14. Subsequently, cells washed once with cold PBS and then collected in 700 µL RLT Buffer (RNeasy Mini Kit, Qiagen) containing freshly added 10 % β-Me. The total cell lysates were homogenized 5-10x using a 23G-needle attached to a plastic syringe, followed by a vortexing step. Total RNA was extracted using the RNeasy Mini Kit together with the RNase-free DNase Set for DNA digestion according to manufacturer

instructions. A NanoDrop spectrophotometer was utilized to assess the quality of the isolated RNA and to determine its concentration. The ratio of the absorbance values at 260 nm and 280 nm as well as 230 nm were indicative of potential contaminations, and only RNA of adequate quality was further processed.

2.2.11.2 Complementary DNA (cDNA) Synthesis

Approximately 0.5 µg of isolated total RNA from each sample was used for synthesis of cDNA using the high-capacity cDNA reverse transcription kit according to manufacturer instructions. Briefly, equal amounts of (diluted) RNA were mixed with a cDNA synthesis master mix containing nuclease-free water, buffer, dNTPs, random primers and the reverse transcriptase enzyme. The mix was then placed in a thermal cycler and subjected to the following program: 10 min at 25 ºC, 120 min at 37 ºC, 5 min at 85 ºC and finally, cooling down to and maintaining 4 ºC until removing samples from the thermal cycler.

2.2.11.3 Quantitative real-time PCR (qPCR)

qPCR analysis was performed using the fluorescent probe SYBR® Green, which intercalates with the DNA and can, therefore, be used to monitor dsDNA amplification. For the qPCR reaction, the appropriate amount of cDNA was mixed with 10 µM working solution of gene specific forward and reverse primers (see section 2.1.9), SYBR® Green and nuclease-free water. In addition, a “no template” control was included as a quality control. The qPCR was performed in 384-well plates on a QuantStudio™ 5 Real-Time PCR System. The relative mRNA expression of the genes of interest was calculated based on the expression of the housekeeping gene using the $\Delta\Delta C_T$ method.

2.2.12 3’ mRNA-Sequencing Analysis

2.2.12.1 Sample Preparation

For RNA Sequencing, $1x10^6$ BMDMs were stimulated for 3 h or 18 h with 100 ng/mL LPS, 30 µM S14 or vehicle only. Subsequently, cells washed once with cold PBS and then

collected in 700 µL RLT Buffer (RNeasy Mini Kit, Qiagen) containing freshly added 10 % β-Me. The total cell lysates were homogenized 5-10x using a 23G-needle attached to a plastic syringe, followed by a vortexing step. Total RNA was extracted using the RNeasy Mini Kit together with the RNase-free DNase Set for DNA digestion according to manufacturer instructions.

2.2.12.2 Sample Processing

RNA quality assessment, library preparation and sequencing were performed by Lexogen GmbH (Vienna, Austria). In short, libraries were prepared using the QuantSeq 3' mRNA-Seq FVD Library Prep Kit according to manufacturer's instructions. Briefly, 150 ng total RNA were reverse transcribed with oligo(dT) primer containing an Illumina-compatible 5' end sequence (first strand) and random priming (second strand). Finally, individual sample barcodes were introduced via 15 cycles of PCR. All libraries were then analysed for adapter dimers, size distribution and concentration on a Fragment Analyzer (Agilent). Sequencing was performed on an Illumina NextSeq 2000 sequencer at Lexogen GmbH.

2.2.12.3 Quality Control, Alignment, Quantification and Analysis

Quality control of the FastQ files was performed using cutadapt version 1.18 (https://cutadapt.readthedocs.io/en/stable/) for adapter trimming and reads of the samples were analysed using FastQC version v0.11.7 prior to and after adapter trimming (https://www.bioinformatics.babraham.ac.uk/projects/fastqc/). The read alignment to the spike-in complemented Ensembl release 101 of the Mus musculus high coverage assembly GRCm38 was performed with splice-aware aligner STAR version 2.6.1a (Dobin et al., 2013). The featureCounts software program version 1.6.4 was used for quantification of gene expression using the annotations of Ensembl GRCm38.101 and spike-in specific annotations of Lexogen as reference (http://subread.sourceforge.net). A differential gene expression analysis was conducted using DESeq2 version v1.18.1 using the counts of unique alignments. Further individual analysis was carried out by Johanna Luise Gorki and myself using RStudio and ClueGO (Bindea et al., 2009, 2013). The raw

data files for the RNA sequencing reported in this thesis have been deposited at NCBI GEO: GSE221910.

2.2.13 Lipidomics

Lipid extractions and analyses were performed by myself, Jelena Zurkovic, Arslan Hamid or Mohamed H. Yaghmour at the LIMES Institute (Bonn, Germany) or Philip Wollnitzke (Heinrich Heine University, Düsseldorf, Germany) using only HPLC or LC-MS-grade solvents.

Lipid Extraction: In short, to 2 µL serum or plasma sample, or 2 mg white adipose tissue (exact weight was determined) or cultured cells, 500 µL extraction mix (CHCl3/MeOH 1/5 containing internal standards: 210 pmol PE(31:1), 396 pmol PC(31:1), 98 pmol PS(31:1), 84 pmol PI(34:0), 56 pmol PA(31:1), 51 pmol PG (28:0), 28 pmol CL(56:0), 39 pmol LPA (17:0), 35 pmol LPC(17:1), 38 pmol LPE (17:0), 32 pmolCer(17:0), 99 pmol SM(17:0), 55 pmolGlcCer(12:0), 14 pmol GM3 (18:0- D3), 359 pmol TG(50:1-d4), 111 pmol CE(17:1), 64 pmol DG(31:1), 103 pmol MG(17:1), 724 pmol Chol(d6), 45 pmol Car(15:0)) was added. Samples (in Eppendorf tube or cell culture plate) were sonicated in the bath sonicator for 10 s and subsequently lipids were collected. After centrifugation at 20,000 x g for 2 min, supernatants were retrieved and mixed with 200 µL CHCl3 and 800 µL of 1 % acetic acid. The samples were briefly shaken and centrifuged for 2 min at 20,000 x g. The upper aqueous phase was removed, and the entire lower phase was transferred into a new tube and evaporated in a speed vacuum concentrator (45°C, 10 min). Spray buffer (8/5/1 2-propanol/MeOH/water, 10 mM ammonium acetate) was added and samples were sonicated for 5 min.

Lipidomics analysis: All samples were separately infused at 10 µL/min into a Thermo Q Exactive Plus spectrometer equipped with the HESI II ion source for shotgun lipidomics. MS1 spectra (resolution 280 000) were recorded in 100 m/z windows from 250 to 1200 m/z (positive mode) followed by recording MS/MS spectra (resolution 70 000) by data independent acquisition in 1 m/z windows from 250 to 1200 (positive mode). Raw files were converted to .mzml files and imported into and analyzed by LipidXplorer software

using custom mfql files to identify sample lipids and internal standards. For further data processing, absolute amounts were calculated using the internal standard intensities and normalized to the amount of extracted serum or tissue.

2.2.14 Molecular Dynamic (MD) Simulations

MD Simulations were performed in collaboration by Jan K. Marzinek and Peter J. Bond (Bioinformatics Institute A*STAR, Singapore). All atom simulations were performed using the GROMACS 2018.3 simulation package (Van Der Spoel et al., 2005) with the CHARMM36m (Huang et al., 2016) force field and TIP3P water model (Jorgensen et al., 1983). The experimental structure (PDB: 3FXI) (Park et al., 2009) of the $(TLR4:MD\text{-}2)_2$ dimer bound to *E. coli* Re-LPS was used. All lipid structures and topologies were taken from CHARMM-GUI membrane builder (Jo et al., 2008). Given that *E. coli* Re-LPS is typically composed of six acyl tails, three sets of double-tailed lipid molecules as studied in experiments were modelled bound to each MD-2 monomer. Four simulation systems were set up, composed of $(TLR4:MD\text{-}2)_2$ complexes bound to a given lipid type, namely: i) CER 18:1/14:0 ii) CER 18:1/16:0; iii) SM d18:1/14:0; and iv) SM d18:1/16:0. Lipids were aligned such that their headgroups overlaid with the crystallographically resolved Re-LPS lipid A headgroup. Each dimeric construct was placed in a dodecahedron box with ~16 nm box edge. Approximately 90,000 TIP3P water molecules were added to the box, along with 150 mM NaCl salt whilst neutralizing the overall system charge. Energy minimization was performed using the steepest descent minimization algorithm with a 0.01 nm energy step size. The system was equilibrated in a step wise fashion: i) 1 ns with position restraints on protein alpha carbons and lipid headgroups in the NVT ensemble; ii) 10 ns with position restraints on protein alpha carbons and lipid headgroups in the NPT ensemble; and iii) 20 ns with position restraints on protein alpha carbons in the NPT ensemble. All position-restrained simulations were run with a force constant of 1000 kJ mol^{-1} nm^{-2}. Unrestrained production runs were set to 1000 ns in the NPT ensemble. A temperature of 310 K was maintained using the velocity rescaling thermostat with an additional stochastic term using a time constant of 1 ps. Pressure was maintained semi-isotropically at 1 atm using the Parrinello-Rahman barostat (Parrinello & Rahman, 1981) and a time constant of 5 ps. All bonds which involved hydrogens were constrained using

the LINCS algorithm. Equations of motion were integrated using the leap-frog algorithm with a time step of 2 fs. Long-range electrostatic interactions were described using the particle mesh Ewald method (Essmann et al., 1995). The short-range electrostatics reals pace cut-off was 1.2 nm and the short-range van der Waals cut-off was also 1.2 nm. Periodic boundaries conditions were applied in all directions. Simulations were performed on an in-house Linux cluster composed of 8 nodes containing 2 GPUs (Nvidia GeForce RTX 2080 Ti) and 24 CPUs (Intel® Xeon® Gold 5118 CPU @ 2.3 GHz) each.

All simulation snapshots were generated using VMD (Humphrey et al., 1996). The root mean square deviation (RMSD) of the MD-2 backbone was calculated with respect to the experimental structure after alignment onto the TLR4 dimer backbone. The RMSD of the TLR4 dimer backbone was calculated with respect to the experimental structure after alignment onto the same set of atoms. The RMSD of the F126 loop encompassing backbone atoms of residues 120-129 was calculated with respect to the experimental structure after alignment onto each MD-2 monomer backbone. Protein-lipid hydrogen bonds were calculated based on a 0.35 nm donor-acceptor cut-off distance and 30° hydrogen-donor-acceptor cut-off angle. The buried solvent accessible surface area (SASA) between MD-2/lipid and TLR4 was calculated by summing the constituent SASAs of each MD-2/lipid complex and TLR4 chain, before subtracting the SASA of the entire TLR4-MD-2-lipid complex. RMSDs, hydrogen bonds, and buried SASA values were calculated as a mean of two parts of the $(TLR4:MD\text{-}2)_2$ dimer and averaged over the final 200 ns of each trajectory.

2.2.15 Protein – Protein Interaction Native PAGE

Native PAGE experiments were performed in collaboration by Umeharu Ohto (Graduate School of Pharmaceutical Sciences, The University of Tokyo, Tokyo, Japan). S14 and S16 were initially dissolved at 2.5 mg/mL in water before mixing with purified protein. The de-glycosylated recombinant protein for the extracellular domain of mouse (m) TLR4 (residues 22-627) was prepared as described previously (Ohto et al., 2012). Purified extracellular domains of mTLR4/MD-2 (25 μM) were mixed with either Re-LPS (125 μM), S14 (0.25, 0.5, 1.0, and 1.5 mM), or S16 (0.25, 0.5, 1.0, and 1.5 mM) in 20 mM Tris-HCl

pH 8.0, 0.15 M NaCl, and 0.1% Triton X-100 and incubated for 3 h at 37 ºC. After incubation, samples were subjected to 12.5% native PAGE and stained with Coomassie Brilliant Blue.

2.2.16 Statistical Analysis

Unless stated otherwise, paired or unpaired two-tailed Student's t-test (as indicated) or one-/two-way ANOVA with Bonferroni post-test correction for multiple testing was performed to determine significance of the difference between groups. P-Values of $p<0.05$ were considered to be statistically significant and are denoted by asterisks (*$p<0.05$, **$p<0.01$, ***$p<0.001$), while data not reaching significance (not significant; ns) is, unless stated, left without notation. For the biological process gene ontology-enrichment analysis (GOEA) using Cytoscape and ClueGO (Bindea et al., 2009, 2013), visualization networks were created by performing right sided hypergeometric test including Benjamini-Hochberg correction. Cluster names represent GO terms with highest significance inside the individual cluster. All statistical analyses were performed using Prism 9.

3 RESULTS

3.1 Unbiased analysis of atheroprogression mice

Cardiovascular diseases have been associated with chronic low-grade inflammation, termed ‘metaflammation’, however, the immediate triggers remain largely unknown. Previously, our laboratory has performed an unbiased *in vivo* discovery approach (unpublished) with the aim of uncovering non-genetic factors that influence cardiovascular disease in mice. Using machine learning, the data obtained from the analysis of the microbiome, systemic and portal vein blood as well as tissue samples from mice of various genetic backgrounds were integrated to identify factors that affect disease severity (Fig.3.1A). A feature importance was assigned to each of the features positively correlating with atherosclerotic plaque burden, and indeed, this analysis confirmed known risk factors for atherogenesis such as IL-1β and VLDL (Fig. 3.1B) (Ridker et al., 2017; Van der Laan et al., 2009). Further, several sphingomyelin (SM) species were identified via portal vein serum metabolomics that were highly associated with plaque burden in mice (Fig. 3.1C(i)). Interestingly, the feature importance of individual SM species appeared to be higher for sphingolipids containing short fatty acid tails of 14-17 carbons, with SM d18:1/14:0 (S14) displaying the highest feature importance (Fig. 3.1C (i), (ii)). To screen potential metabolites for their inflammatory potential *in vitro*, I selected a set of commercially available metabolites that were associated with aortic plaque progression. To this end, I stimulated bone marrow-derived macrophages (BMDMs) with different concentrations of the metabolites listed in Supplementary Table S1, and initially assessed the cell toxicity of each compound using a CellTiter-Blue® assay (Supplementary Fig. S1A). This assay monitors cellular metabolic capacity based on the ability of viable cells to irreversibly reduce resazurin to its fluorescent end product resorufin. A loss of fluorescence intensity upon treatment with a specific compound, therefore, indicates a reduction in cell viability. As depicted in Supplementary Fig. S1A, none of the compounds tested displayed considerable cytotoxicity. Notably, high concentrations of cholestenone and chenodeoxycholic acid (CDA) even enhanced the metabolic capacity of BMDMs, as evident by an increase in the fluorescence signal. To quickly assess a potential effect of these metabolites on the inflammatory response of macrophages, I determined TNF

concentrations in culture supernatants of stimulated BMDMs (Supplementary Fig. S1B). Treatment of BMDMs with the indicated metabolites did not induce significant TNF release (Supplementary Fig. S1B). Notably, while S14 did not compromise cell viability (Fig. 3.1D), it was the only metabolite to markedly induce TNF release from BMDMs in a concentration-dependent manner (Fig. 3.1E). To ensure the pro-inflammatory response observed was not caused by an endotoxin contamination, I performed a highly sensitive Limulus assay on the S14 preparation, but did not detect significant endotoxin (Fig. 3.1F).

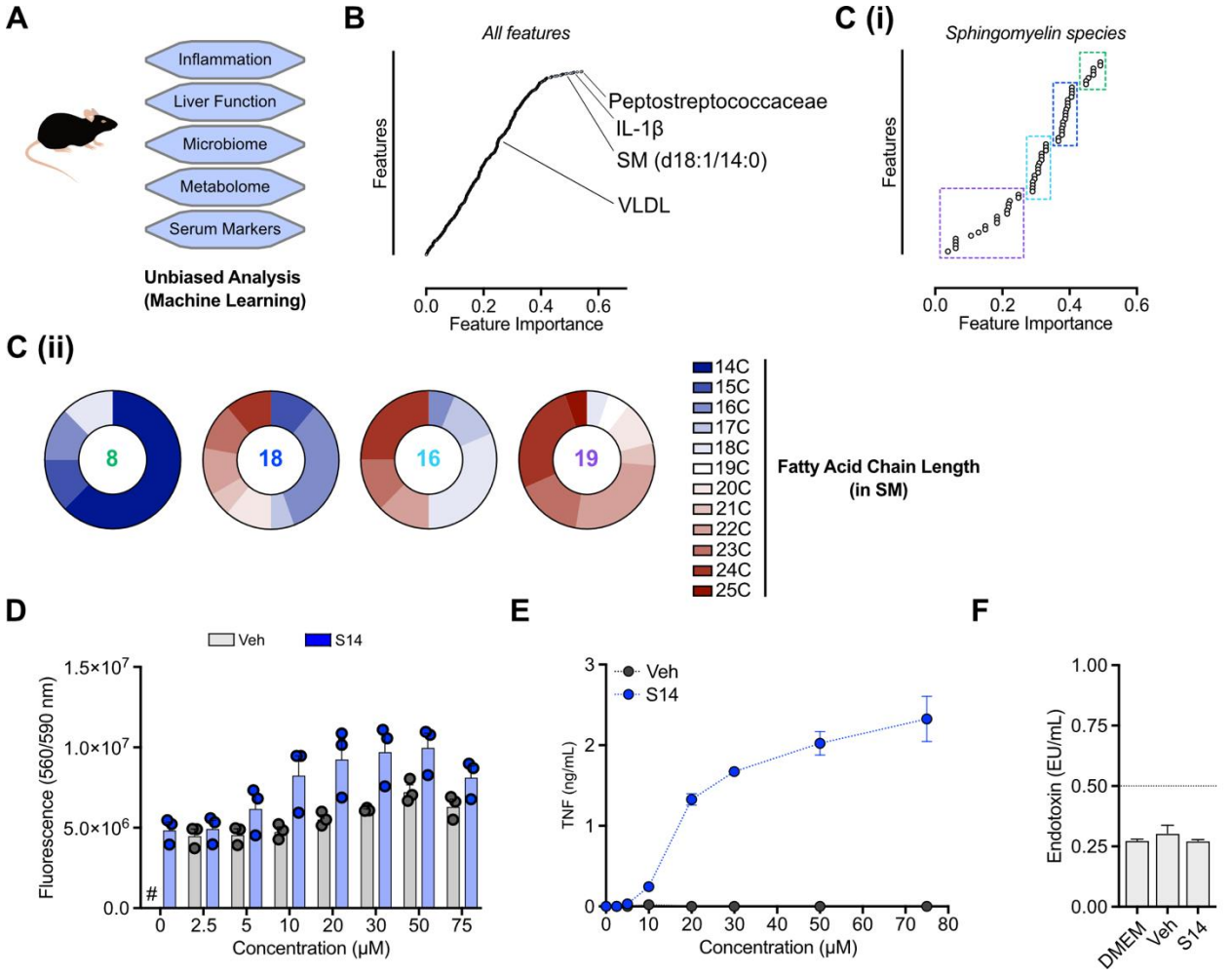

Figure 3.1| Sphingomyelins are associated with atherosclerosis progression in mice
(A) Unbiased analysis of factors influencing aortic root plaque size as a measure of cardiovascular disease progression in mice. (B) Calculated feature importance for all features positively associated with plaque burden with selected features labelled. (C) Analysis of all sphingomyelin species extracted from (B) shown in a separate feature importance graph (i) and manually grouped according to fatty acid chain length (ii), with numbers in the middle of the pie charts indicating the number of individual sphingomyelin species per group. (D, E) WT BMDMs were stimulated for 18 h with indicated concentrations of vehicle control or S14 and (D) cell viability by CellTiter-Blue assay and (E) TNF release were assessed. (F) Conventional DMEM culture medium, vehicle control and S14 were tested for the presence of gram-negative bacterial endotoxin contamination using the Pierce LAL Chromogenic Endotoxin Quantitation Kit. Where applicable, data is presented as mean with SEM of n=3 biological replicates. # indicates no data points (not assessed). (A-C) Raw data was provided by Lenka Dohnalová and Christoph A. Thaiss.

To corroborate that S14 is potentially pro-atherogenic, the data from the previously mentioned unbiased screening approach was re-analyzed. Hereby, only those samples obtained from 159 LDLR KO mice were included, as LDLR KO mice fed a high-fat, high-cholesterol Western-type diet (WD) represent one of the most widely accepted mouse models used in atherosclerosis research. Interestingly, although all mice were genetically identical, the atherosclerotic plaque lesion area in the aortic root varied from 0 to 40 % (Fig. 3.2A). The results from systemic serologic, portal vein metabolomic, and general inflammation parameters from all mice were once again integrated using machine learning analysis (Fig. 3.2B). Overall, this model proved to be reliable as it was highly accurate in predicting plaque size (Fig. 3.2C). To examine factors that potentially contribute to plaque development or are protective in this disease model, the contribution of individual measured features was then evaluated. This analysis, as indicated previously, confirmed widely accepted risk factors for atherosclerosis, such as pro-inflammatory IL-1β (Ridker et al., 2017), which positively correlated with plaque size (Fig. 3.2D). On the other hand, circulating HDL was inversely correlated with plaque size, in line with it being regarded as protective in atherosclerosis (Fig. 3.2E) (Gordon et al., 1989b; Gordon et al., 1977). Notably, within the features derived from portal vein serum metabolomics, several sphingomyelins, including S14, were found highly predictive for plaque burden (Fig. 3.2F, left), aligning with the overall initial data set and confirming our *in vitro* screening data. In fact, S14 was amongst the most important predictive features and significantly correlated with plaque size (Fig. 3.2F, right), suggesting that S14 could indeed be pro-atherogenic.

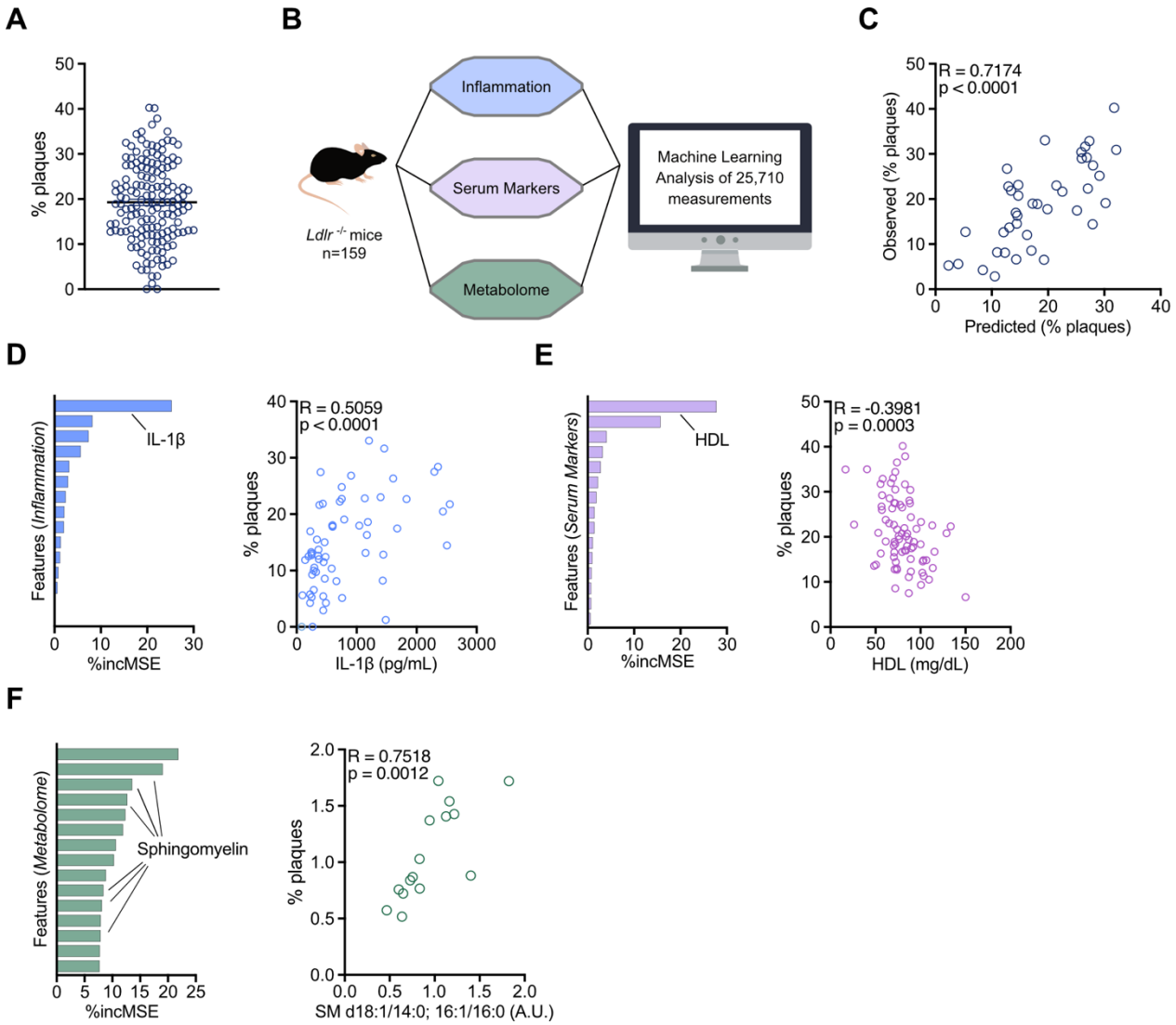

Figure 3.2| Unbiased analysis of factors associated with atherosclerosis progression in mice
(A) LDLR KO mice were fed a 8-week high-fat, high-cholesterol diet and plaque size (normalized lesion area; % plaques) in aortic roots was assessed; n=159. (B) Experimental set up for the unbiased analysis of factors influencing plaque size as a measure of atherosclerosis progression in LDLR KO mice. (C) The model prediction accuracy was analyzed using a test data set, correlating the observed and predicted lesion area; n=40. (D-F) %incMSE variable importance plots showing the 15 most important features per analyzed group as defined in (B), in descending order of importance in the prediction of lesion size in mice. The plots on the right side of each panel display the correlation between a selected individual feature of the respective group (indicated on the x-axis) and the normalized plaque size, for (D) IL-1β; n=61, (E) HDL; n=79 and (F) SM d18:1/14:0, 16:1/16:0; n=15. Correlation data are shown as XY analyses with computation of Pearson correlation coefficients. All raw data in this figure was provided by Lenka Dohnalová and Christoph A. Thaiss.

3.2 Specific sphingolipids activate mouse macrophages

3.2.1 S14 is a potent inducer of pro-inflammatory cytokine release

The unbiased analysis *in vivo* revealed several sphingomyelins to be positively associated with murine plaque development and the initial *in vitro* screen identified S14 to induce TNF release from BMDMs. For that reason, I aimed to further investigate the pro-inflammatory activity of these sphingolipids by stimulating BMDMs with selected sphingomyelins. Structurally, these lipids all contain a zwitterionic phosphocholine head group, a sphingosine and a fatty acid of variable chain length (Fig. 3.3A), requiring them to be coupled to serum albumin for delivery in an aqueous solution. Upon 18 h of stimulation, S14 and, to some degree also sphingomyelin d18:1/16:0 (S16), but not S18, S20 or S26, induced TNF and IL-6 release from BMDMs (Fig. 3.3B).

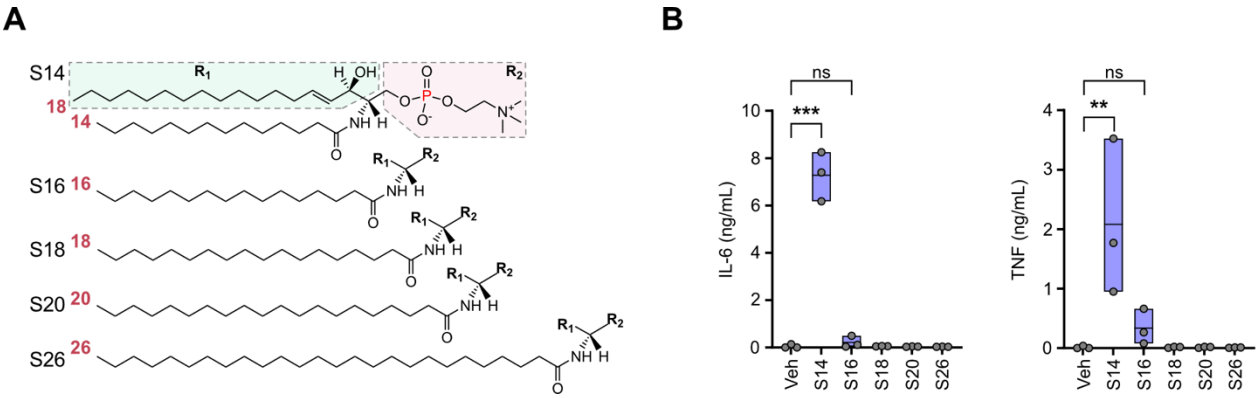

Figure 3.3| Specific sphingomyelins are activating mouse macrophages
(A) Chemical structure of individual sphingomyelin species S14, S16, S18, S20 and S26. The sphingosine chain (R1) and head group (R2) are invariable between these species. (B) Cytokine release measured in cell culture supernatants from WT BMDMs stimulated for 18 h with vehicle control (Veh) or 30 µM sphingomyelin (S) of indicated fatty acid chain length, as indicated in (A). Data is shown as box plots with indicated mean of n=3 biological replicates. P-values adjusted for multiple testing against the control group are presented: *p < 0.05, **p < 0.01, ***p < 0.001.

3.2.2 The S14 gene signature in BMDMs is highly pro-inflammatory

The previous results showed that S14 takes a prominent position in its ability to activate mouse macrophages. Therefore, I next sought to assess S14-mediated gene induction via transcriptomic analysis. Already 3 h after stimulation, S14 significantly induced the

expression of a vast amount of genes amongst which many are known to be highly pro-inflammatory, for example *Il1b*, *Il6*, *Saa3* or *Acod1* (Fig. 3.4A). Indeed, Gene Ontology (GO) analysis of the two hundred most upregulated genes revealed that S14 enhances the expression of genes related to host defense, such as recruitment of immune cells or cellular responses against viruses and bacteria (Fig. 3.4B and 3.4C).

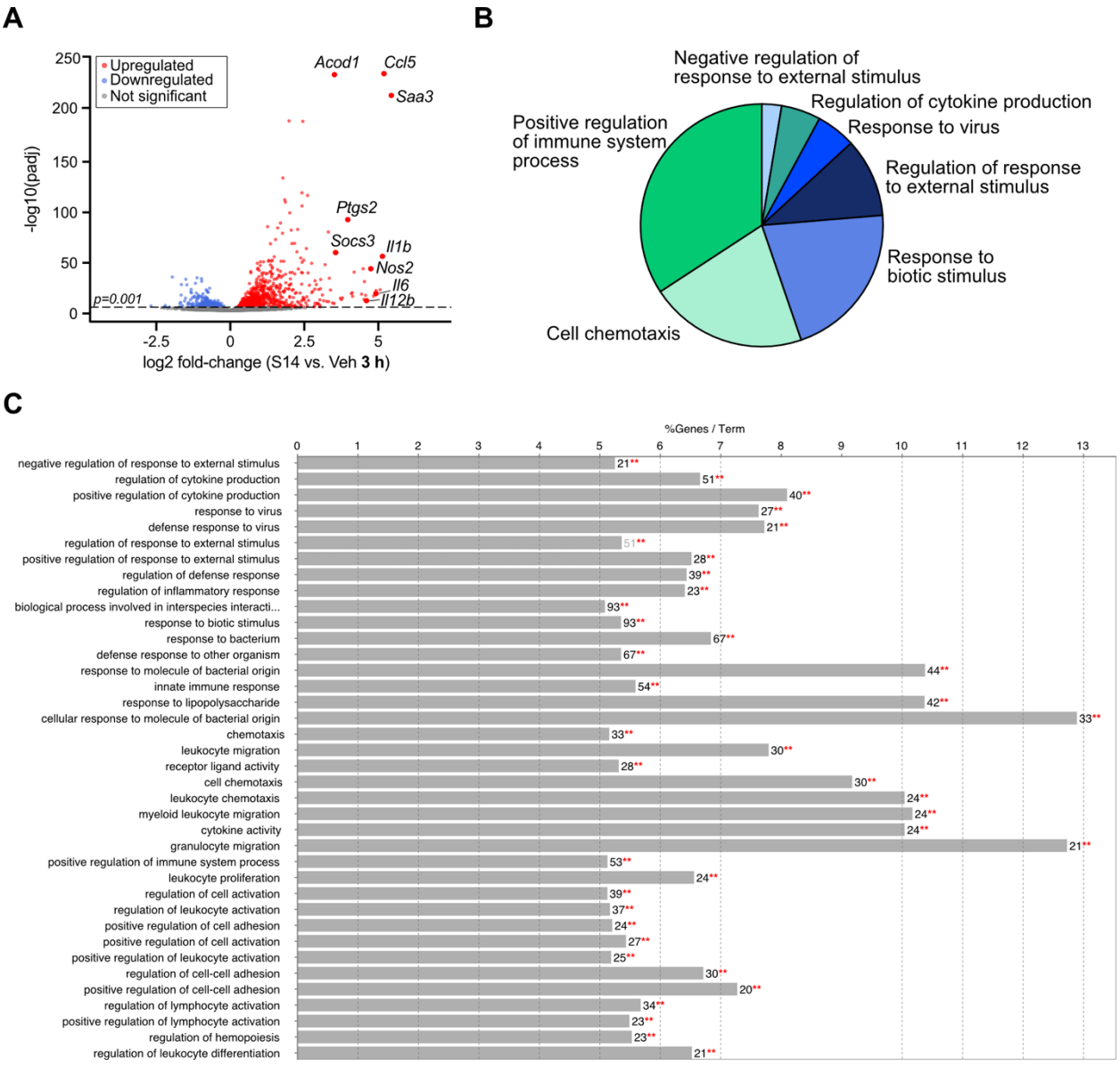

Figure 3.4| S14 induces transcriptional changes in BMDMs
(A) RNA-seq transcriptomic analysis displayed as a volcano plot, showing patterns of gene expression for 3 h S14-treated BMDMs (n=4) relative to vehicle control. Significantly differentially expressed genes (adjusted p <0.001) are indicated in blue (downregulated) or red (upregulated), and selected highly upregulated genes (log2 fold-change >2.5) are highlighted and identified. (B) ClueGO analysis of the top 200 upregulated genes from (A), summarized as an overview chart of functional groups annotated with the major group GO pathway term (p <0.05). (C) Detailed overview of the results shown in (B), annotated with GO pathway terms and the number of corresponding genes associated with the specific term. Double asterisk (**) indicates the significance of the enriched GO term with p <0.01. The percentage of genes associated with a specific term is listed on top of the grid and is represented by the size of the bars.

3.2.3 S14 resembles LPS both functionally and structurally

The transcriptomic analysis of S14-stimulated BMDMs was quite striking, as the observed gene signature was reminiscent of the one expected to be induced by LPS stimulation. Hence, I compared the top thirty genes upregulated by either 3 h stimulation with S14 or LPS. Indeed many of the significantly upregulated genes such as various interleukins and C-C motif chemokine ligands overlapped between the two gene sets (Fig. 3.5A). Interestingly, from a structural perspective, one can also identify certain similarities between S14 and Lipid A, which is the primary immunostimulatory moiety of LPS (Park et al., 2009). Of note, the acyl chains of Lipid A, which bind to the TLR4/MD-2 complex on the cell surface, primarily consist of 14 or 12 carbons (Fig. 3.5B).

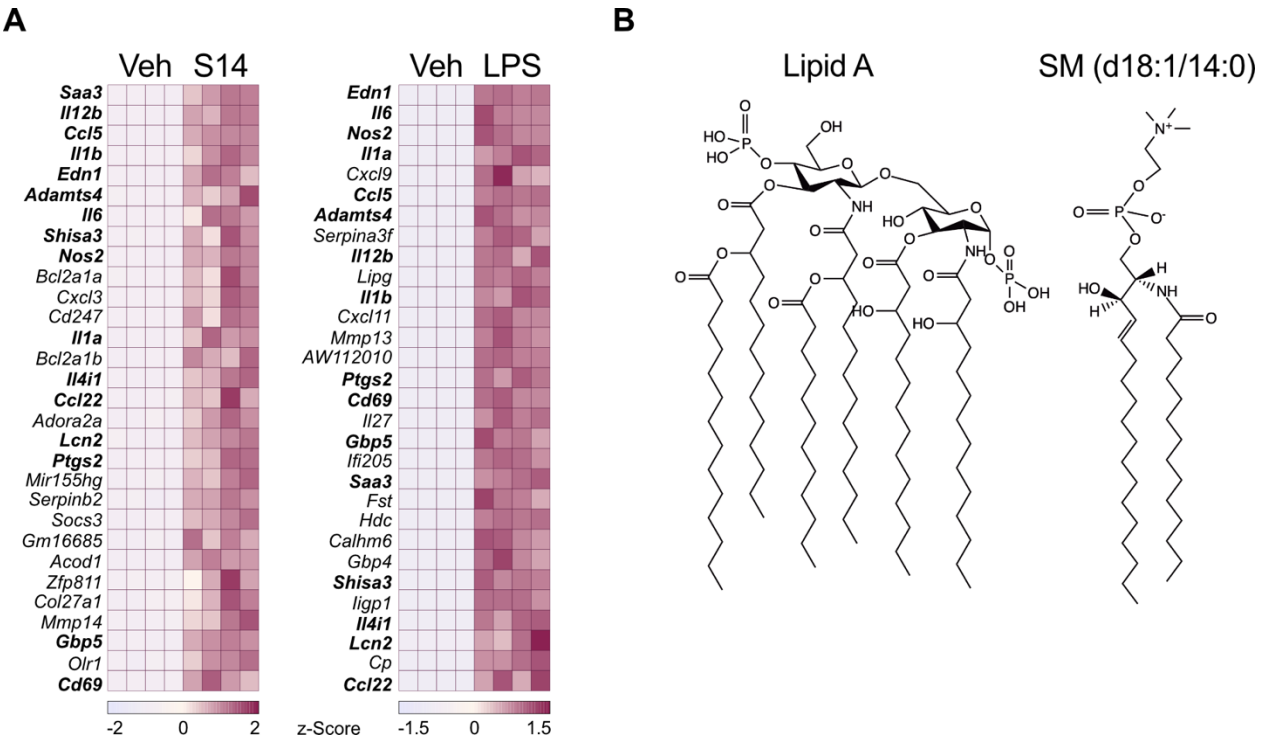

Figure 3.5| S14 and LPS possess functional and structural similarities
(A) Heatmap generated from RNA-seq transcriptomic analysis, displaying gene expression patterns of 3 h S14- and LPS-treated BMDMs (n=4 per condition, each represented in one column), showing the top 30 differentially upregulated genes (adjusted $p < 0.01$) in order of descending log2 fold-change. Genes identified commonly in both conditions are indicated in bold. (B) Chemical structure of the lipid A portion of LPS compared to S14.

3.2.4 Cytokine release from BMDMs by S14 requires TLR4

Based on the structural and functional similarities between Lipid A (LPS) and S14, I speculated that S14 could, just like LPS, also engage the TLR4/MD-2 complex. Pharmacological inhibition of TLR4 using the small-molecule inhibitor TAK-242, which binds to the intracellular domain of TLR4 (Matsunaga et al., 2011), revealed that intact signaling downstream of TLR4 is necessary for IL-6 and TNF release from BMDMs upon S14 treatment (Fig. 3.6A). Using a genetic approach, I then confirmed this TLR4-dependence, by demonstrating that S14 induced cytokine release from WT, but not TLR4 KO BMDMs (Fig. 3.6B).

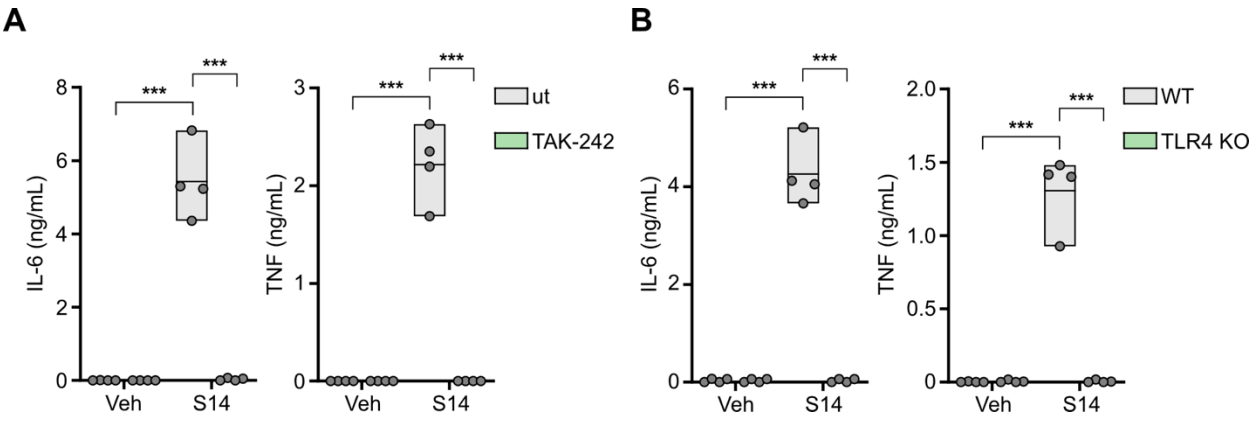

Figure 3.6| Cytokine release from BMDMs induced by S14 is TLR4-dependent
IL-6 and TNF release in cell culture medium from (A) WT BMDMs pre-treated for 30 min with 2 µM TAK-242, prior to adding vehicle or 30 µM S14 for 18 h and (B) WT or TLR4 KO BMDMs stimulated for 18 h with vehicle or 30 µM S14. Data is shown as box plots with indicated mean of n=4 biological replicates and was analyzed by two-way ANOVA with Bonferroni post hoc analysis. P-values adjusted for multiple testing against the control group are presented: *p < 0.05, **p < 0.01, ***p < 0.001.

3.3 S14 renders macrophages to be pro-inflammatory

In a very simplified view, resting macrophages can either polarize towards a pro-resolving phenotype (sometimes also referred to as ‘M2 macrophages’), or become classically activated ‘M1 macrophages’ to support the inflammatory response (Yunna et al., 2020). Specifically, they hereby link the innate with the adaptive immune response through expression of cell surface proteins like MHC-II or co-stimulatory molecules such as CD80, CD86 and CD40 (Mills et al., 2000; Orecchioni et al., 2020). As shown in Fig. 3.7A, 18 h but not 3 h stimulation with S14 significantly increased the expression of CD40, CD80 and

CD86 in WT BMDMs, while the expression in TLR4 KO BMDMs remained unchanged. This pattern was also observed in BMDMs stimulated with LPS. On the other hand, MHC-II expression was decreased in both S14- and LPS-treated WT BMDMs at 18 h (Fig. 3.7A). Next to these important surface markers, classically activated macrophages also express the hallmark protein iNOS intracellularly (Lumeng et al., 2007). Indeed, both 18 h S14 and LPS stimulation significantly induced iNOS expression in BMDMs in a TLR4-dependent manner (Fig. 3.7B). To confirm this observation functionally, I measured nitric oxide concentrations in cell culture supernatants after 18 h stimulation with S14 or LPS. In line with iNOS expression patterns, WT but not TLR4 KO BMDMs released nitric oxide upon S14 and LPS treatment (Fig. 3.7C).

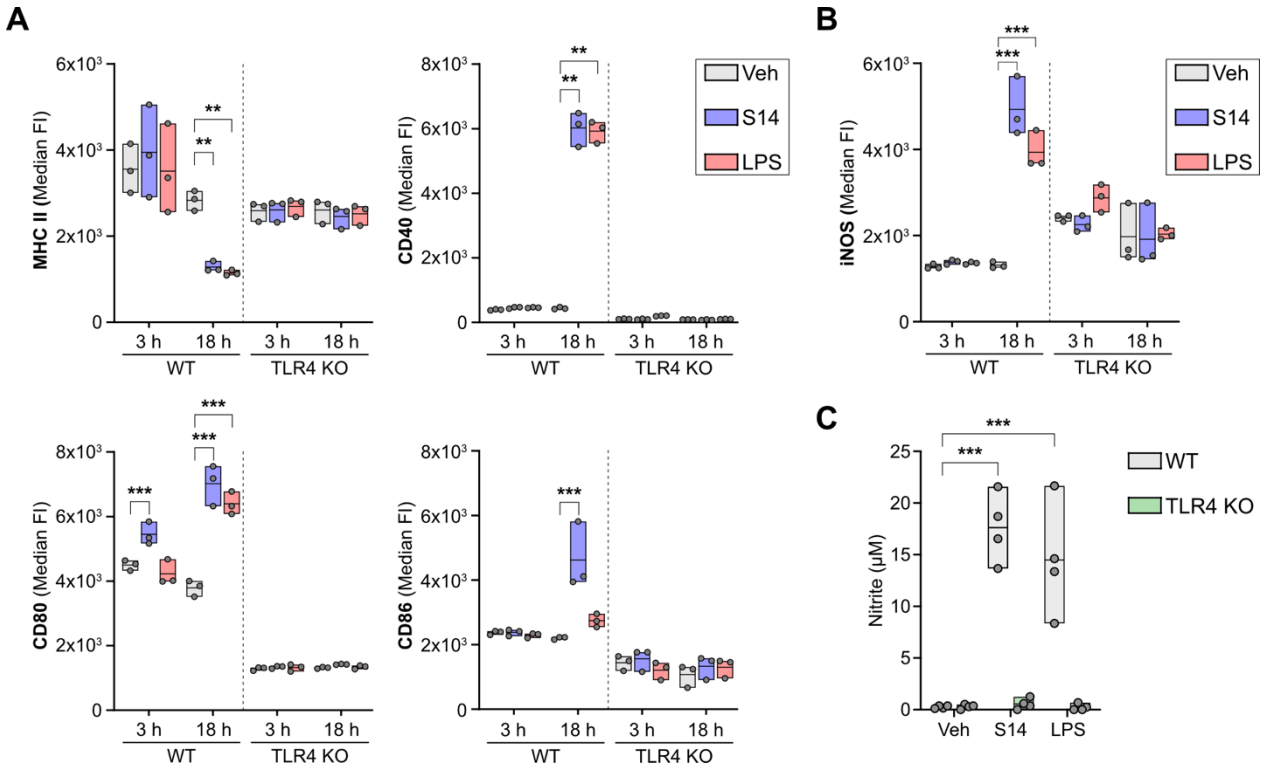

Figure 3.7| S14 upregulates macrophage activation markers in a TLR4-dependent manner
WT or TLR4 KO BMDMs were stimulated for 3 or 18 h with vehicle control, 30 µM S14 or 100 ng/mL LPS before (A) assessing surface expression of indicated co-stimulatory molecules by flow cytometry; n=3 or (B) assessing intracellular expression of iNOS by flow cytometry; n=3. (C) Griess Assay determining nitrite concentrations in culture medium of WT or TLR4 KO BMDMs stimulated for 18 h with vehicle control, 30 µM S14 or 100 ng/mL LPS; n=4. All data, if not stated otherwise, is presented as box plots with indicated mean and individual replicate data points. Data was analyzed by two-way ANOVA with Bonferroni post hoc analysis. P-values adjusted for multiple testing against the control group are presented: *p < 0.05, **p < 0.01, ***p < 0.001.

It is well established that pro-inflammatory macrophages adapt their cellular metabolism upon TLR stimulation to meet their energetic needs required to carry out their function

(Lauterbach et al., 2019). Hence, an extracellular flux analysis of BMDMs stimulated with S14 for 3 h or 18 h was performed. As predicted, BMDMs stimulated for 18 h but not 3 h with S14 (Fig. 3.8A) or LPS+IFNγ (Fig. 3.8B), the latter combination being a prototypical 'M1' macrophage inducer, prompted a drastic decrease in overall oxygen consumption rate (OCR: a measure for oxidative phosphorylation). Concurrently, BMDMs treated with S14 exhibited a significant surge in the measured extracellular acidification rate (ECAR), indicative of an increase in basal glycolysis (Fig. 3.8C). Summarizing these results in an energy map revealed that while a 3 h stimulation with S14 slightly shifted BMDM metabolism more towards an energetic phenotype, 18 h S14 treatment rewired metabolism towards the cells becoming highly dependent on glycolysis (Fig. 3.8D).

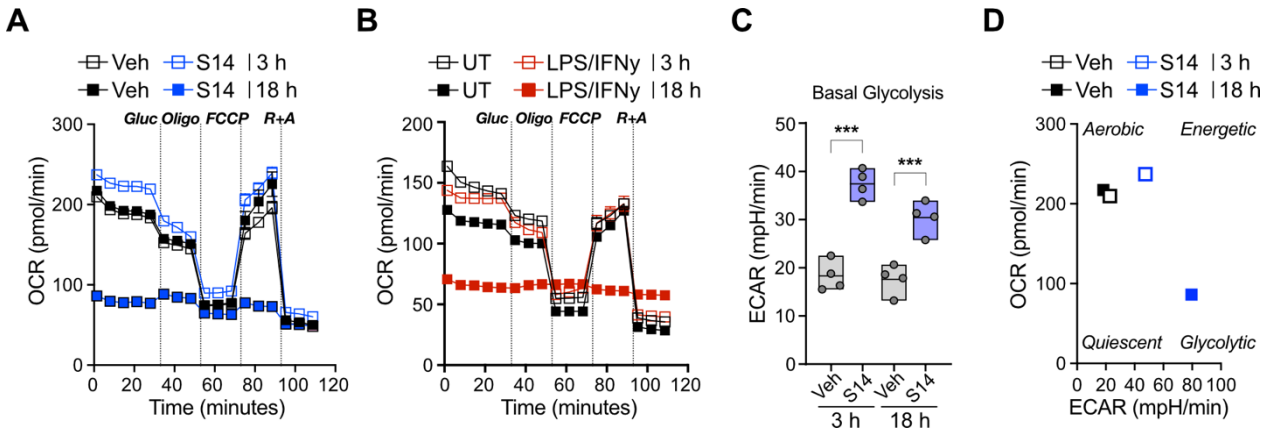

Figure 3.8| S14 rewires macrophage metabolism
Oxygen Consumption Rate (OCR) analyzed by extracellular flux analysis of WT BMDMs stimulated for 3 h or 18 h with (A) vehicle or 30 µM S14 or (B) vehicle or 20 ng/mL LPS in combination and 50 ng/mL recombinant IFNγ. Data is shown as one representative graph of n=4 biological replicates. (C) Extracellular Acidification Rate (ECAR) indicative of glycolysis in WT BMDMs stimulated with vehicle control or 30 µM S14 for 3 or 18 h; n=4. Data is presented as box plots with indicated mean and individual replicate data points. (D) Energy Map summarizing the Extracellular Flux Analysis Data of BMDMs stimulated for 3 or 18 h with vehicle control or 30 µM S14, displaying basal oxygen consumption rate against basal glycolysis; n=4. Where applicable, data was analyzed by one-way ANOVA with Bonferroni post hoc analysis. P-values adjusted for multiple testing against the control group are presented: *p < 0.05, **p < 0.01, ***p < 0.001.

In order to avoid severe tissue damage during a pro-inflammatory response, activation of macrophages usually entails a counter-regulation of this response. TLR4 stimulation with LPS has previously been shown to induce the anti-inflammatory cytokine IL-10, which inhibits the expression of TNF to limit the pro-inflammatory response (Alexander et al., 2021). To investigate, whether S14 employs the same counterregulatory mechanism as LPS, I compared LPS- and S14-induced kinetics of TNF and IL-10 release (Fig. 3.9A). As expected, both LPS and S14 prompted significant TNF release already after 3 h of

stimulation, maintaining or even increasing this release towards later timepoints (Fig. 3.9A, left). Of note, the amount of TNF released by S14 stimulation was greater compared to LPS, especially during early timepoints. The kinetics of IL-10 release were similar to that of TNF, as significant amounts of IL-10 were already detected after 3 h of stimulation (Fig. 3.9A, right). Interestingly, while S14, compared to LPS, was more potent regarding the induction of TNF, counterregulatory IL-10 release from S14-stimulated BMDMs was lower in this experiment. In order to prove that IL-10 indeed serves as a mediator of dampening the inflammatory response, I added recombinant IL-10 to BMDMs before treating them for 18 h with S14 or LPS. Both S14 and LPS induced TNF release, however, this was significantly curbed in presence of IL-10 (Fig. 3.9B). Together, these results show that S14, like LPS, induces a pro-inflammatory response in macrophages that is kept in balance by an anti-inflammatory negative feedback mechanism involving IL-10.

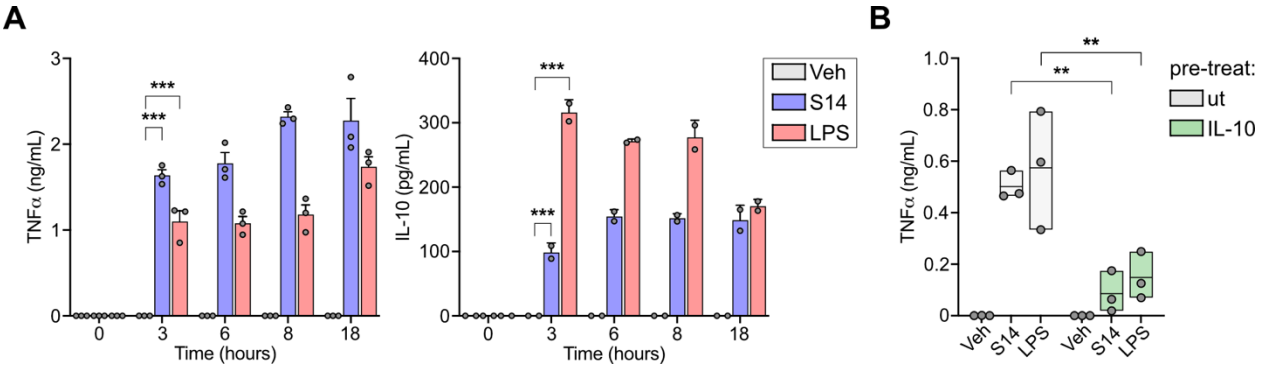

Figure 3.9| IL-10 dampens the S14-induced pro-inflammatory response
(A) TNF and IL-10 release from BMDMs stimulated for the indicated times with vehicle, 30 µM S14 or 100 ng/mL LPS. Data is presented of n=2-3 biological replicates as bar graphs indicating mean with SD. (B) TNF release from BMDMs left untreated or pre-treated with 20 ng/mL IL-10 for 30 min, before adding vehicle, 30 µM S14 or 100 ng/mL LPS for 18 h. Data is presented as box plots with indicated mean and individual replicate data points (n=3). All data was analyzed by two-way ANOVA with Bonferroni post hoc analysis. P-values adjusted for multiple testing against the control are presented: *p < 0.05, **p < 0.01, ***p < 0.001.

3.4 MyD88- and TRIF-dependent signaling are engaged by S14

All of the preceding data led me to reason that if S14 activity requires TLR4, one or both adaptor proteins, MyD88 and TRIF, would be engaged. Both pathways employ different transcription factors, leading to the expression of distinct set of genes (Akira et al., 2001). I treated BMDMs isolated from either WT, MYD88- or TRIF-deficient mice with S14 and detected significantly less TNF release from both MYD88- and TRIF KO BMDMs compared to WT, indicating that both adaptor proteins mediate S14-induced TNF release

(Fig. 3.10A). Since TRIF-dependent signaling principally leads to the transcription of IRF3-regulated genes (Ivashkiv & Donlin, 2014), I compared IFNβ and IP-10 release from WT and IRF3-deficient BMDMs upon S14 and LPS treatment (Fig. 3.10B). Indeed, both LPS as well as S14 prompted IFNβ and IP-10 release from WT BMDMs, which was significantly reduced or even ablated in IRF3-KO BMDMs. However, while IP-10 release was comparable between LPS and S14 stimulation, LPS was more potent than S14 regarding the induction of IFNβ release from WT BMDMs (Fig. 3.10B, left). Direct TLR4 activation leads to the rapid engagement of MAPK and NF-κB signaling cascades downstream of MyD88 and TRIF recruitment (Lancaster et al., 2018). Hence, I assessed the phosphorylation status of NF-κB and JNK upon S14 stimulation, using LPS again as a positive control. Already after 15 min, LPS and S14 prompted phosphorylation of both NF-κB and JNK without significant changes in the total protein expression. These results confirm once again that the cytokine release observed upon S14 stimulation is linked to activation of TLR4 and its downstream signaling events.

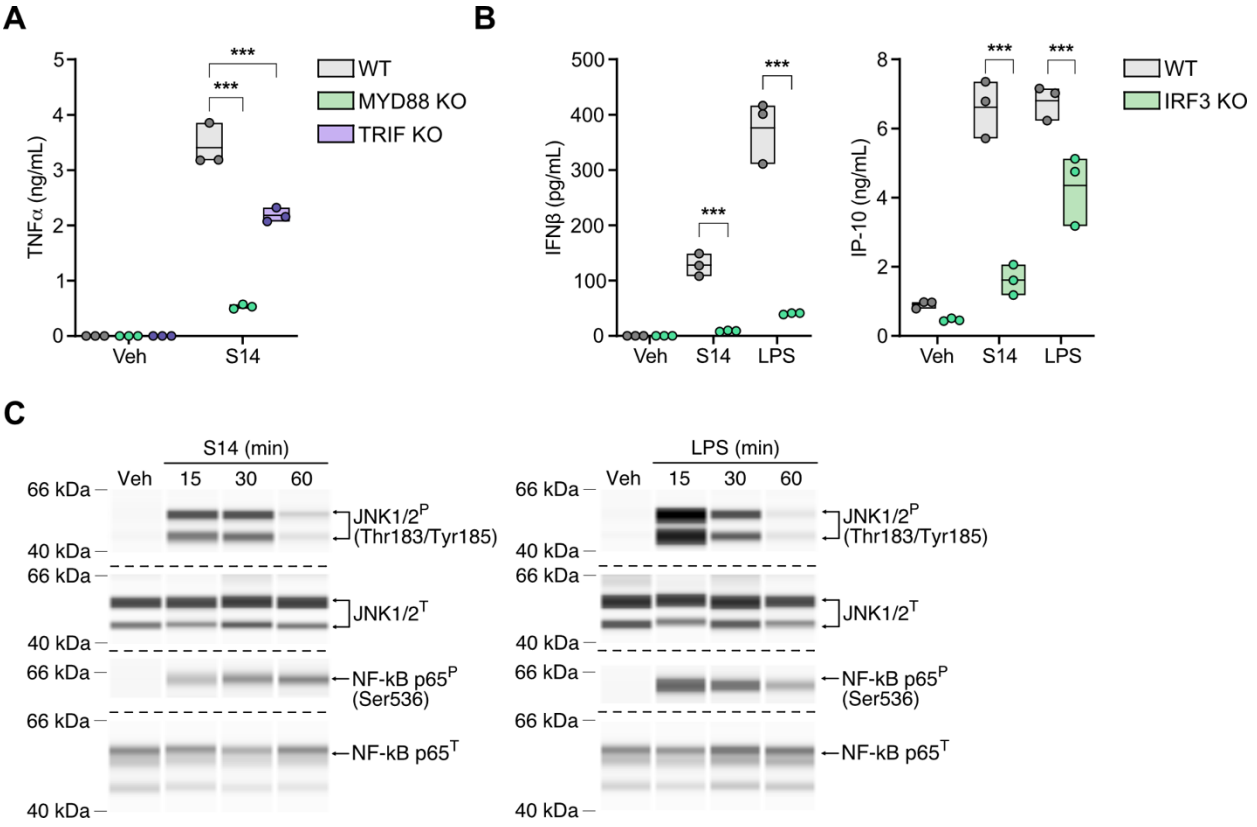

Figure 3.10| MyD88- and TRIF-signaling are activated by S14
(A) TNF release from WT, MYD88 KO or TRIF KO BMDMs stimulated for 18 h with vehicle or 30 µM S14. (B) IFNβ and IP-10 release from WT or IRF3-KO BMDMs treated for 8 h vehicle, 30 µM S14 or 100 ng/mL LPS. Data is presented as box plots with indicated mean and individual replicate data points (n=3).

(C) WT BMDMs were stimulated for the indicated durations with either 30 µM S14 or 100 ng/mL LPS and subsequently assayed for protein levels of phosphorylated and total JNK and NF-κB. One representative Western Blot of n=3 biological replicates is shown. Where applicable (A, B) data was analyzed by two-way ANOVA with Bonferroni post hoc analysis. P-values adjusted for multiple testing against the control group are presented: *p < 0.05, **p < 0.01, ***p < 0.001. Simple western blot (WES) experiments shown in (C), were performed with support from Eike Geissmar.

3.5 The effect of S14 is conserved in human myeloid cells

Having established a TLR4-dependent pro-inflammatory response to S14 in BMDMs, I next sought to validate these findings in human cells, as TLR4/MD-2 activation can have species-specific effects (Ohto et al., 2012; Schroder et al., 2012). Therefore, I isolated monocytes from buffy coats obtained from healthy human donors, and either stimulated them directly, or differentiated them *in vitro* with M-CSF into human monocyte-derived macrophages (hMDMs) before stimulation. Figure 3.11A depicts cytokine release from monocytes stimulated for 18 h with S14 or LPS. Significant IL-6 release from human monocytes was observed using either stimulus, but TNF release only reached significance in case of LPS stimulation (Fig. 3.11A). The same pattern was also observed upon stimulation of hMDMs. Whereas human macrophages released large amounts of IL-6 and TNF upon LPS treatment, and S14 treatment induced IL-6 release comparable to LPS, S14-induced TNF release was undetectable (Fig. 3.11B). However, I could confirm TLR4-dependence in hMDMs using a TLR4-neutralizing antibody, which completely abolished IL-6 release, confirming the results obtained in BMDMs (Fig. 3.11C).

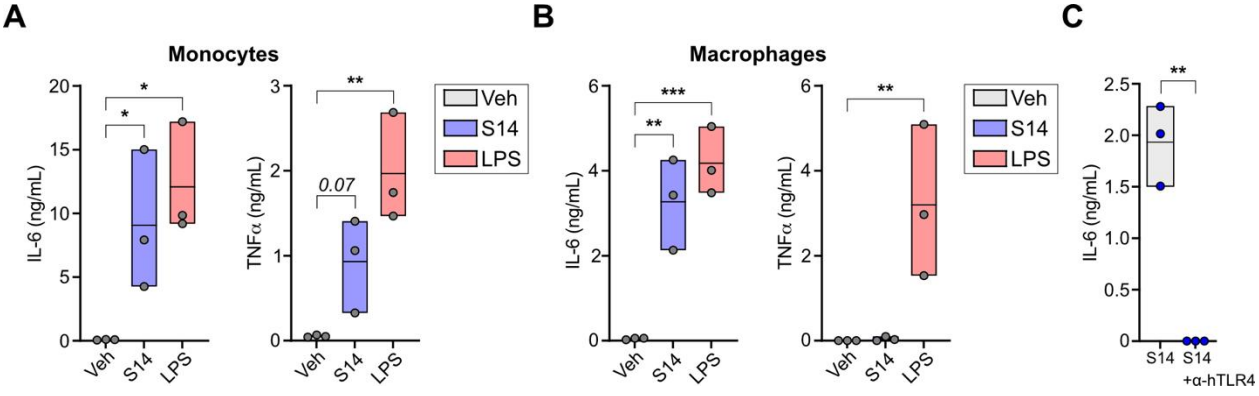

Figure 3.11| S14 activates primary human myeloid cells in a TLR4-dependent manner
IL-6 and TNF release from (A) human monocytes or (B) human M-CSF-differentiated monocyte-derived macrophages (hMDMs), stimulated for 18 h with vehicle, 30 µM S14 or 10 ng/mL LPS. (C) IL-6 release from hMDMs pre-treated with or without anti-hTLR4-IgG neutralizing antibody for 1 h, before stimulating for 18 h with 30 µM S14. All data is presented as box plots with indicated mean and individual replicate data points (n=3). Data was analyzed by one-way ANOVA with Bonferroni post hoc analysis (A, B) or unpaired two-tailed t-test (C).P-values adjusted for multiple testing against the control group are presented: *p < 0.05, **p < 0.01, ***p < 0.001.

I detected substantially lower amounts of TNF released from S14- compared to LPS-treated human monocytes and macrophages. As TNF release from hMDMs was even undetectable, I analyzed gene expression after treatment with S14 or LPS, to determine whether a default in transcription was the underlying reason for this observed discrepancy. As expected, gene expression of *IL6* was significantly increased by both LPS and S14 (Fig. 3.12A, left). Notably, *TNF* gene expression was significantly increased as well, although to less extent by S14 compared to LPS (Fig. 3.12A, right). Given that I previously only investigated cytokine release after 18 h S14 treatment, I next aimed to assess earlier timepoints, as TNF is usually regarded as one of the initial cytokines. Surprisingly, although I could detect TNF release between 3 and 8 h of S14 stimulation, the amounts were insignificant and not nearly comparable with those elicited by LPS (Fig. 3.12B).

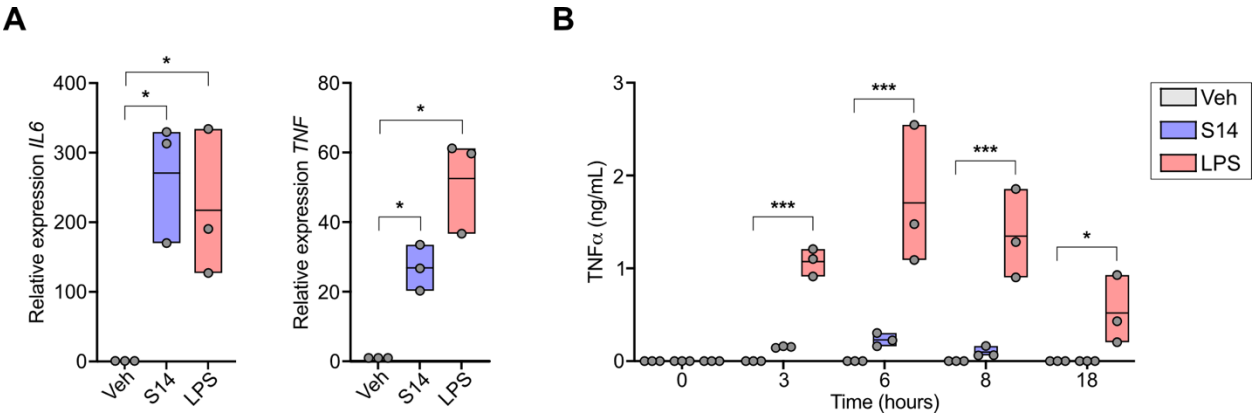

Figure 3.12| Human macrophages exhibit a weak TNF response upon S14 stimulation
(A) Relative gene expression of IL-6 and TNF in hMDMs stimulated for 6 h with vehicle, 30 µM S14 or 10 ng/mL LPS. (B) TNF release from hMDMs stimulated for the indicated times with vehicle, 30 µM S14 or 10 ng/mL LPS. All data is presented as box plots with indicated mean and individual replicate data points (n=3). The data was analyzed by one-way ANOVA (A) or two-way ANOVA (B) with Bonferroni post hoc analysis. P-values adjusted for multiple testing against the control group are presented: *p < 0.05, **p < 0.01, ***p < 0.001.

Next, I analyzed cytokine release from freshly drawn human whole blood, stimulated *ex vivo* with S14. To this end, human whole blood was diluted 1 to 5 in medium containing S14 and incubated it for 8 or 24 h before obtaining the cell-free supernatant and assessing cytokine release (Fig. 3.13A). I detected significant amounts of IL-1β and IL-8 and IL-6 at 8 h as well as MCP-1 and IL-8 after 24 h of stimulation (Fig. 3.13B). Overall, these results confirm that the inflammatory potential of S14 observed in mouse macrophages is conserved in primary human cells.

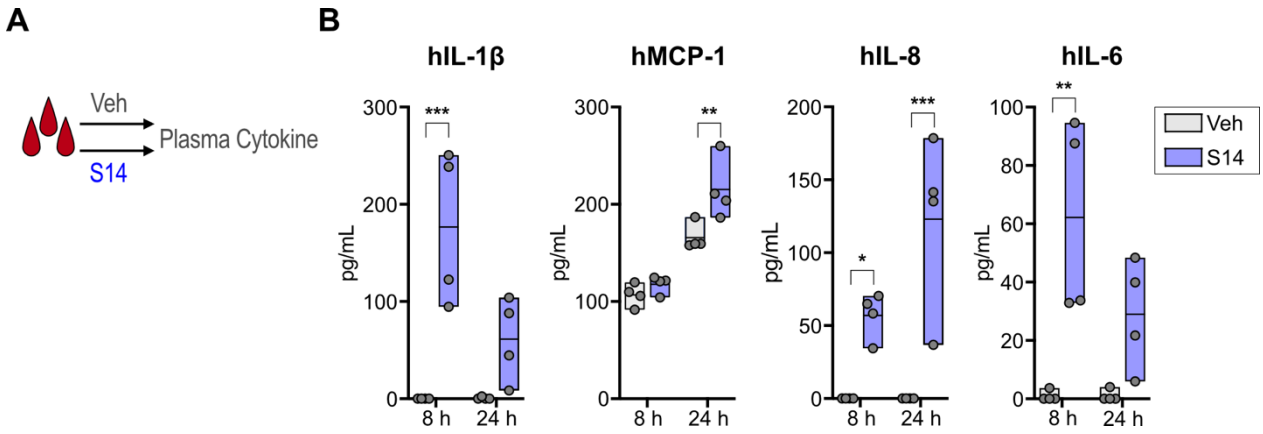

Figure 3.13| Stimulation of human whole blood *ex vivo* induces a pro-inflammatory response
(A) Experimental set up of human whole blood stimulation *ex vivo*. (B) Cytokine release from human whole blood, diluted 1:5 in RPMI containing either vehicle or 30 µM S14 and incubated for 8 or 24 h; n=4. The data was analyzed by two-way ANOVA with Bonferroni post hoc analysis. P-values adjusted for multiple testing against the control group are presented: *p < 0.05, **p < 0.01, ***p < 0.001.

3.6 S14 directly activates the human NLRP3 inflammasome

Activation of the NLRP3 inflammasome has been recognized as an important contributor to metaflammation in context of cardiovascular diseases and obesity (Christ & Latz, 2019; Mori et al., 2011). Given that I measured significant amounts of IL-1β in the whole blood assay, I hypothesized that S14 could prompt assembly and activation of the human NLRP3 inflammasome, resulting in pro-inflammatory IL-1β release. Therefore, I initially assessed the gene expression of important inflammasome components upon S14 treatment in hMDMs, to determine whether efficient “priming” occurs. As shown in Figure 3.14A, S14 indeed induced the transcription of NLRP3, gasdermin D, caspase-1 and IL-1β, while a decrease in ASC transcripts (*PYCARD*) could be noted. To confirm that IL-1β was also expressed on protein level, I performed a western blot analysis of whole cell lysates and detected ample amounts of pro-IL-1β, the immature form of IL-1β (Fig. 3.14B). Finally, I set up another whole blood assay to confirm full engagement of the NLRP3 Inflammasome using the NLRP3-selective inhibitor MCC950 (CRID3) and the caspase-1 inhibitor VX-765 (Fig. 3.14C). S14, similar but less potent compared to LPS, directly induced extracellular IL-1β release fully dependent on both NLRP3 and caspase-1 (Fig. 3.14C), confirming my initial hypothesis.

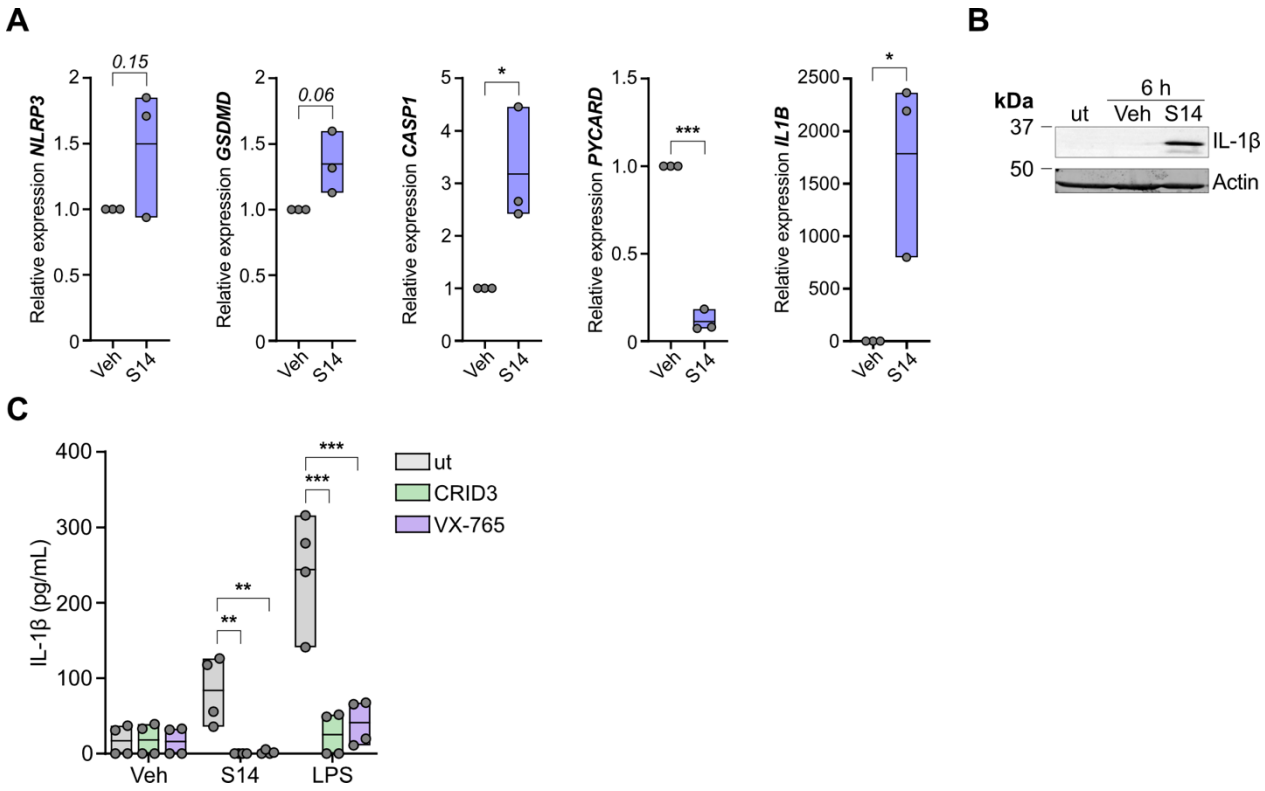

Figure 3.14| S14 leads to human NLRP3 inflammasome activation
(A) Relative gene expression of indicated genes in hMDMs stimulated for 6 h with vehicle or 30 µM S14; n=3. (B) Whole cell lysates of hMDMs left untreated or stimulated for 6 h with vehicle or 30 µM S14 were analyzed via western blotting for the protein expression of IL-1β, using actin as a loading control. One representative blot of n=3 biological replicates is shown. (C) Inflammasome assay: Diluted human whole blood was pre-treated for 15 min with 2.5 µM CRID3 or 8 µM VX-765, before incubating for 8 h with either vehicle, 30 µM S14 or 10 ng/mL LPS; n=4. The data is shown as box plots with indicated mean and individual replicate points and was analyzed either by (A) unpaired two-tailed student's t-test or (B) two-way ANOVA with Bonferroni post hoc analysis. P-values adjusted for multiple testing against the control group are presented: *p < 0.05, **p < 0.01, ***p < 0.001. qPCR analysis was performed with support from Daan Heister (Amsterdam UMC, The Netherlands).

3.7 Ceramides are not pro-inflammatory in macrophages

Based on previous reports about the pro-inflammatory potential of specific ceramide species (Fischer et al., 2007; Gaggini et al., 2022), the question was raised, whether not S14 itself, but one of its catabolites mediates the observed effects. Sphingomyelins are catabolized by sphingomyelinase (SMase) into their direct precursors, ceramides (Marchesini & Hannun, 2004). Inhibition of sphingomyelin hydrolysis using GW4869 and ARC39 to block the neutral or acidic SMase to synthesize ceramide 14:0 (Cer14), did not affect S14-induced TNF and IL-6 release from BMDMs (Fig. 3.15A). Accordingly, while stimulation of BMDMs with either S14 or S16 resulted in the expected amounts of TNF released, their related ceramides, Cer14 and Cer16 failed to induce TNF release from

BMDMs (Fig. 3.15B). Together, these results prove that S14 is in fact a novel bioactive lipid that engages TLR4 signaling.

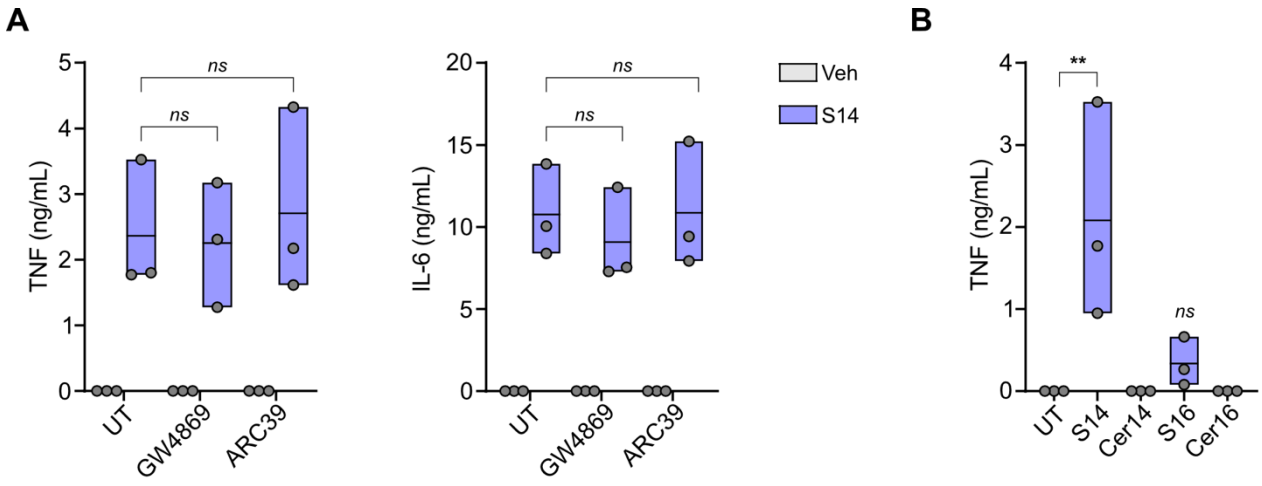

Figure 3.15| TLR4 activation is mediated by S14 but not its catabolites
(A) TNF and IL-6 release from BMDMs pre-treated for 30 min with either 10 µM GW4869 or 5 µM ARC39 to inhibit sphingomyelinase activity, before stimulating for 18 h with vehicle control or 30 µM S14 and assessing cytokine release in supernatants. (B) TNF release from BMDMs incubated for 18 h with vehicle, 30 µM Sphingomyelin (S14 or S16) or 30 µM Ceramide (Cer) of indicated fatty acid chain length (Cer14 or Cer16). The data is shown as box plots with indicated mean and individual replicate points and was analyzed by one-way ANOVA with Bonferroni post hoc analysis. P-values adjusted for multiple testing against the control group are presented: *p < 0.05, **p < 0.01, ***p < 0.001.

3.8 S14 is a ligand for the mouse TLR4/MD-2 complex

3.8.1 S14 binds to the mouse TLR4/MD-2 complex

As many studies have claimed to have identified novel TLR4 agonists, but only few have provided structural considerations, I next sought to determine whether S14 can physically interact with TLR4. Direct TLR4 ligands such as LPS principally bind to MD-2, which associates with the extracellular domain of TLR4, resulting in an inactive heterodimer (TLR4/MD-2) (Park et al., 2009; Park & Lee, 2013). When a ligand binds, the TLR4/MD-2 complex dimerizes to become an active dimer-dimer $(TLR4/MD\text{-}2)_2$. To gain insight into the potential of S14 as well as S16 and their ceramide analogues Cer14 and Cer16 to act as direct TLR4/MD-2 agonists, molecular dynamics (MD) simulations were performed by Jan K. Marzinek and Peter J. Bond. Using the X-ray structure of hexa-acylated LPS and the positioning of its acyl chains in the $(TLR4/MD\text{-}2)_2$-bound state (Park et al., 2009), four 1 µs simulations with three diacylated molecules of either S14, S16, Cer14 or S16 in

complex with MD-2 were performed (Fig. 3.16A). To assess conformational shifts, the TLR4 ectodomains of the sphingolipid-bound systems were aligned to the X-ray structure to determine the RMSD, revealing that the S14-bound system exhibited the least structural divergence (Fig. 3.16B). The same held true for the RMSD calculated for the MD-2 domains, with MD-2 being more stable for sphingolipids than ceramides, with S14 displaying the least structural drift (Fig. 3.16C). Indeed, both S14 and S16 formed more hydrogen bonds compared to ceramides (Fig. 3.16D). Furthermore, considerable salt bridge interactions between TLR4 and S14 (Fig. 3.16E), but to less extent with the other lipids (Supplementary Fig. S2A), were evident. As the F126-containing loop of MD-2 is of particular importance for maintaining the stability of the active $(TLR4/MD\text{-}2)_2$ complex(Lancaster et al., 2018), the stability of the MD-2 loop was analyzed. S14 and S16 were once again more stabilizing than the according ceramides (Fig. 3.16F), but only for S14, F126 adopted an ‘active-like’ conformation in both of the MD-2 protein chains (Fig. 3.16G and Supplementary Fig. S2B). Only in the presence of S14, F126 pointed inside the MD-2 cavity (“closed conformation”), which promotes stability of the receptor complex by not physically disrupting the dimerization interface (Fig. 3.16G and Supplementary Fig. S2B). In line with that, the solvent-accessible surface are (SASA) between S14 and the surrounding protein was largest compared to the other sphingolipids (Fig. 3.16H). Together, the MD simulations indicate that due to the presence of the zwitterionic headgroup, there is favorable binding between sphingomyelins and $(TLR4/MD\text{-}2)_2$ compared to ceramides, and that S14 is potentially more ‘activating’ than S16.

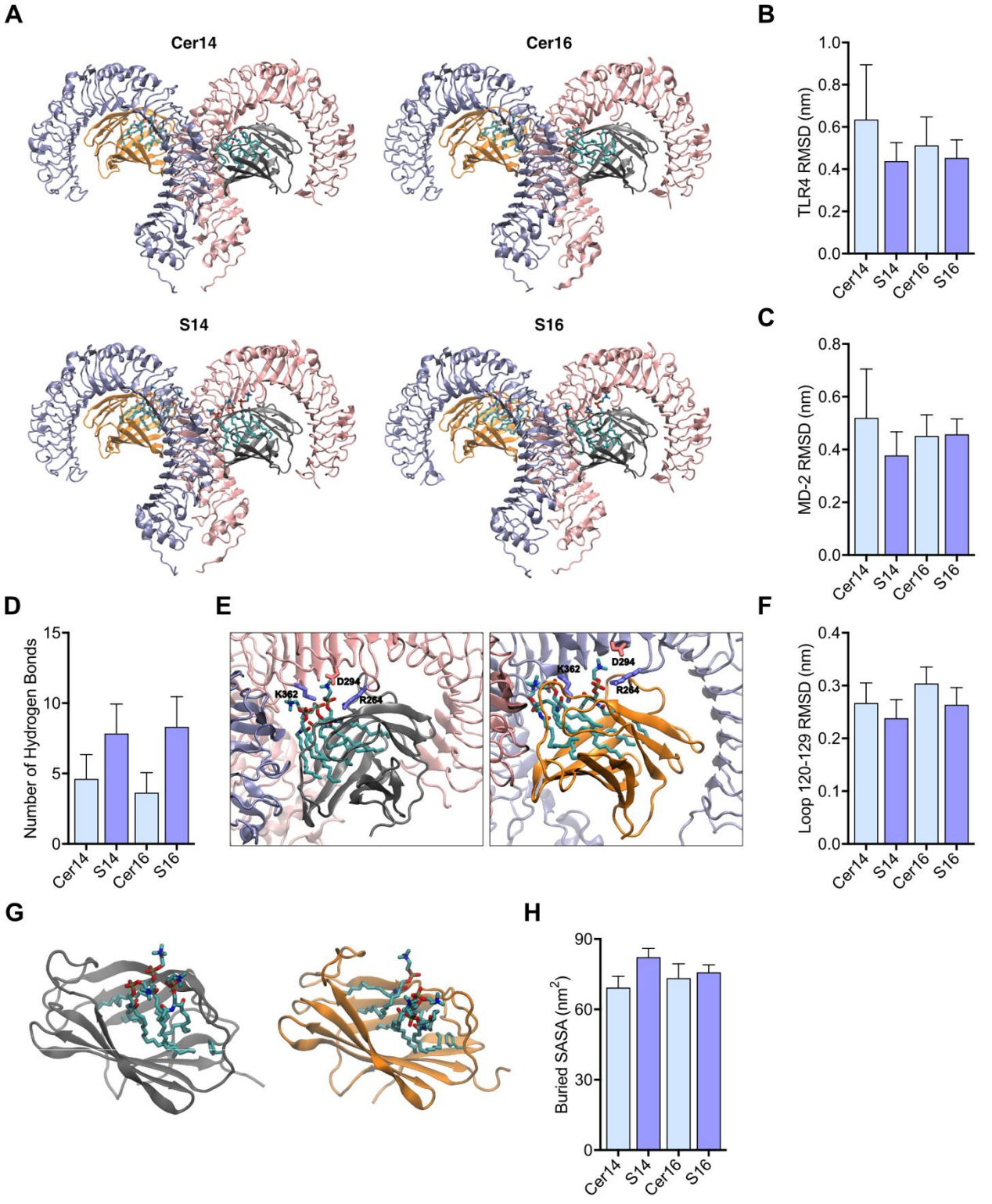

Figure 3.16| MD simulations indicate a potential binding interface between S14 and TLR4/MD-2
MD simulations were ran twice for sphingomyelins and ceramides. Individual protein chains are shown in cartoon and color-coded, whereas sphingolipid and amino acid residues are indicated in CPK licorice format. (A) Initial snapshot of the $(TLR4/MD\text{-}2)_2$ complex bound to the respective sphingolipids. (B-D) Assessment of $(TLR4/MD\text{-}2)_2$ complex stability during simulation when bound to different lipids with (B) backbone RMSD of dimer of TLR4 proteins with respect to X-ray structure, (C) backbone RMSD of each MD-2 protein and (D) number of hydrogen bonds formed between lipid per monomer. (E) Final snapshots of each side of the $(TLR4/MD\text{-}2)_2$ complex, bound to S14. Labelled ionizable amino acid residues observed to make significant hydrogen-bonding interactions with

S14 during each trajectory are shown in licorice format, colored in red or blue for acidic or basic, respectively. (F) Backbone RMSD of each MD-2 loop containing F126 compared to X-ray structure, after first aligning on MD-2. (G) Final snapshot of each MD-2 of the $(TLR4/MD\text{-}2)_2$ complex, bound to S14. (H) Buried SASA between each MD-2/lipid complex and dimer of TLR4 ectodomains. Means and standard deviations for all calculated data were analyzed over the final 200 ns of each trajectory (average of calculated values for each side of the $(TLR4/MD\text{-}2)_2$ complex), and combined from two individual simulation experiments. The data presented in this figure was provided by Jan K. Marzinek and Peter J. Bond.

To corroborate the MD simulations, potential TLR4/MD-2-Sphingolipid complex formation was assessed by Umeharu Ohto in a cell-free system using the purified mouse TLR4/MD-2 proteins. Based on the observations made during the simulations, the purified receptor proteins were incubated with S14 or S16 and the complexes were analyzed via native polyacrylamide-gel electrophoresis (PAGE) mobility shift assay. In line with previous reports (Ohto et al., 2012; Park et al., 2009), the purified extracellular domain of TLR4/MD-2 by itself migrated as a monomer (Fig. 3.17, lane 1 and 11), while the addition of LPS induced an upwards shift of the band, pointing towards dimerization of TLR4/MD-2 (Fig. 3.17, lane 2). Similarly, incubation of purified TLR4/MD-2 with S14 also increased the presence of dimer bands dose-dependently (Fig. 3.17, lanes 3-6). On the other hand, incubation of S16 with TLR4/MD-2 only resulted in a slight shift of the monomer band, but no dimer bands were detected independent of the concentration of S16 (Fig. 3.17, lanes 7-10). In summary, these results point towards a direct interaction between S14 and the TLR4/MD-2 complex, which leads to dimerization and subsequent activation of downstream signaling.

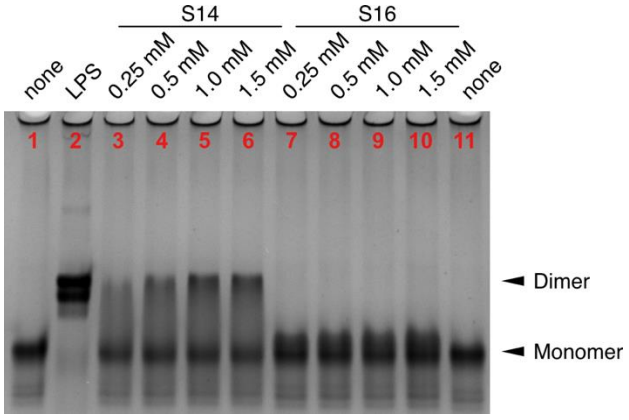

Figure 3.17| S14 binds to mouse TLR4/MD-2 and causes dimerization
Purified extracellular domains of mTLR4/MD-2 (25 µM) were mixed with either Re-LPS (125 µM), S14 or S16 of the indicated concentration, and incubated for 3 h at 37 ºC before subjecting samples to a 12.5 % native PAGE followed by Coomassie Brilliant Blue staining. The data in this figure was provided by Umeharu Ohto.

3.8.2 S14 causes TLR4/MD-2 dimerization and endocytosis

As described above, ligand binding leads to dimerization of the TLR4/MD-2 complex to form the active tetramer $(TLR4/MD\text{-}2)_2$, which is subsequently endocytosed to initiate TLR4 pathway activation. Using two conformation-specific antibodies that recognize different epitopes of TLR4, which allows detection of only monomeric TLR4/MD-2 (clone MTS510), or both monomeric and dimeric TLR4/MD-2 (clone Sa15-21) (Tan et al., 2015b; Zanoni et al., 2011, 2017b), I assessed the proximal events of pathway initiation in BMDMs *in vitro*. The detailed approach for this experiment including the necessary calculations is described in the method section 2.2.7. In short, tracking the loss of MTS510 surface staining allowed comprehension of the TLR4/MD-2 dimerization status. Indeed, in line with the MD simulation data and the cell-free protein-lipid binding experiments, both S14- and LPS-treated BMDMs showed rapid dimerization of TLR4/MD-2, albeit with slightly different kinetics (Fig. 3.18A and 3.18C). Accordingly, subsequent endocytosis of the activated TLR4/MD-2 complex was also observed for both S14- and LPS-treated BMDMs, with similar kinetics compared to the dimerization process (Fig. 3.18B and 3.18C). As expected, and in contrast to S14, S16 only induced insignificant receptor dimerization and endocytosis (Fig. 3.18D).

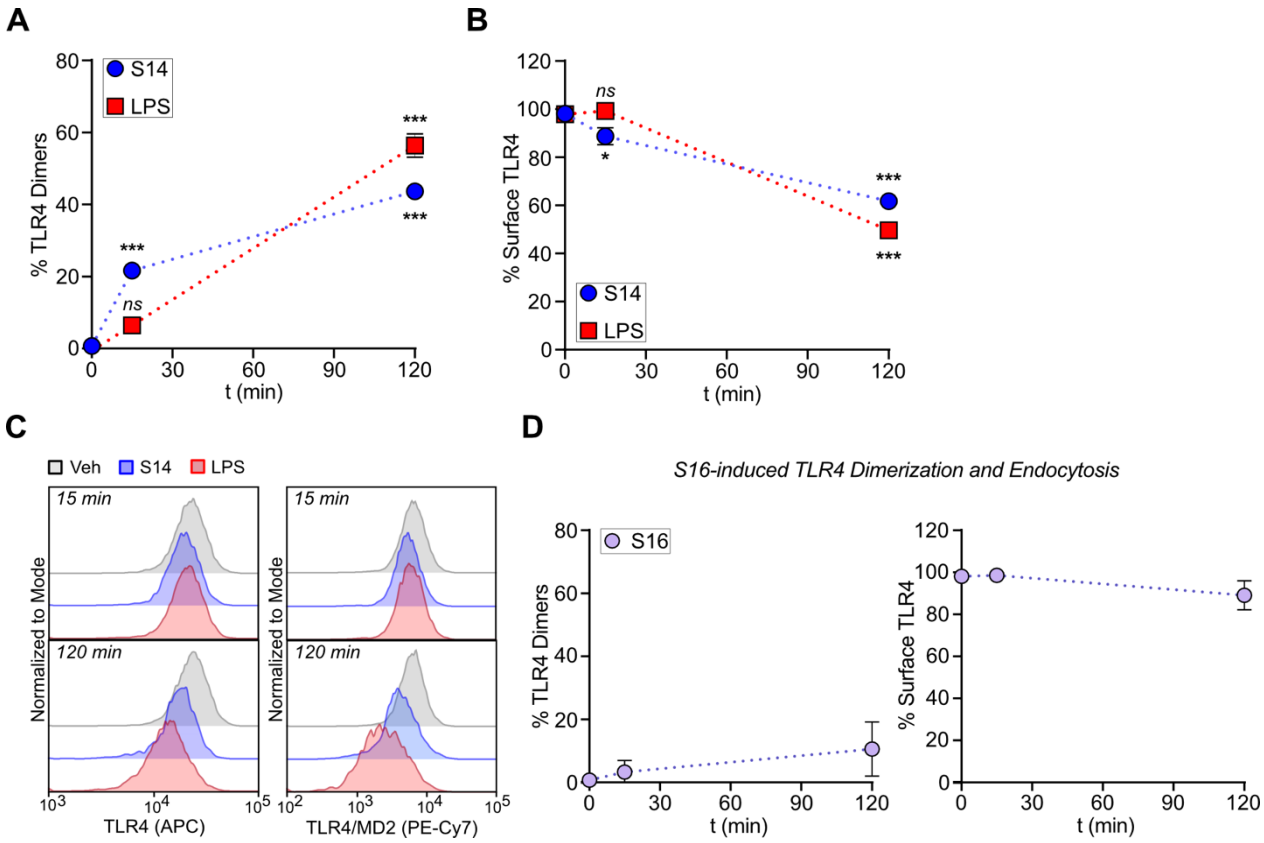

Figure 3.18| S14 elicits ligand-dependent TLR4/MD-2 dimerization and endocytosis
BMDMs were stimulated with 100 ng/mL LPS or 30 µM S14 and (A) TLR4/MD-2 dimerization and (B) TLR4/MD-2 endocytosis were assessed by flow cytometry by tracking surface expression of monomeric and dimeric TLR4/MD-2; SEM of n=3 biological replicates. (C) Histograms showing MFI of surface expression of TLR4/MD-2 assessed with two different antibodies over time, used to calculate the data shown in (A, B). (D) BMDMs were stimulated with 30 µM S16 and TLR4/MD-2 dimerization and endocytosis were assessed by flow cytometry by tracking surface expression of monomeric and dimeric TLR4/MD-2; SEM of n=3 biological replicates. Data was analyzed by two-way ANOVA with Bonferroni post hoc analysis. P-values adjusted for multiple testing are presented: *p < 0.05, **p < 0.01, ***p < 0.001.

3.8.3 MD-2 is required for S14-induced inflammation

Previous literature has shown that TLR4 may be activated in a MD-2-independent manner (Raghavan et al., 2012). Although the MD simulations confirmed a potential interaction between S14 and MD-2, I wanted to address whether MD-2 was, in fact, required for the agonistic activity of S14. To this end, I compared S14-induced IL-8 release from HEK293T cells expressing either human TLR4 alone or in combination with its co-receptor MD-2, using LPS as a positive control. Considerable IL-8 release upon LPS- and S14 stimulation was only found when MD-2 was expressed in addition to TLR4 (Fig. 3.19A). Having established this MD-2 dependence, I next sought to determine, whether S14 binds to the same hydrophobic pocket in MD-2 as LPS. The lipid A analogue Eritoran (E5564) is a

competitive LPS antagonist that binds to this specific pocket in MD-2 and thereby prevents $(TLR4/MD\text{-}2)_2$ complex formation and activation (Mullarkey et al., 2003). Indeed, treatment of BMDMs with LPS and also S14 in the presence of E5564 completely abolished IL-6 release (Fig. 3.19B). These results further strengthen the notion that S14 can directly engage TLR4/MD-2 in a manner similar to LPS.

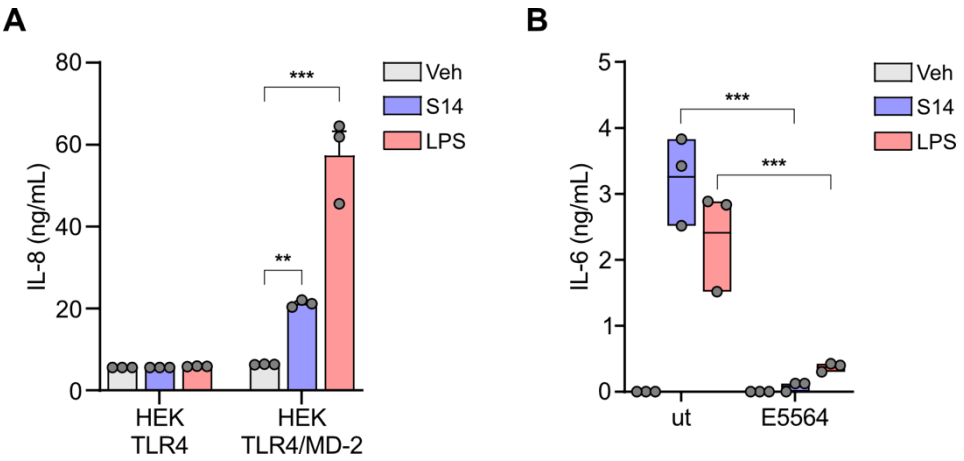

Figure 3.19| The S14-induced cytokine response is MD-2-dependent
(A) HEK293T cells expressing either human TLR4 alone or both human TLR4 and MD-2 were stimulated for 18 h with vehicle, 30 µM S14 or 10 ng/mL LPS before analyzing IL-8; n=3 shown as mean with SEM. (B) Cytokine release from WT BMDMs, pre-incubated for 1 h with or without 1.25 µg/mL E5564, followed by 18 h treatment with either vehicle control, 30 µM S14 or 100 ng/mL LPS. Data is shown as box plots with indicated mean of n=3 biological replicates. MD Data was analyzed by two-way ANOVA with Bonferroni post hoc analysis. P-values adjusted for multiple testing are presented: *p < 0.05, **p < 0.01, ***p < 0.001.

3.9 S14 and LPS are competitive TLR4 agonists

Having established that both LPS and S14 are agonists for TLR4, I asked whether both lipids could compete for receptor binding or would potentially act synergistically. To this end, I cross-titrated S14 and LPS, stimulating BMDMs with S14 for 15 min, before further adding LPS and incubating for 18 h and measuring TNF release. Without LPS addition and at a low concentration of LPS (0.2 ng/mL), S14 induced comparable TNF release in a dose-dependent manner, starting at a minimum concentration of 5 µM (Fig. 3.20A). Treatment of BMDMs with 1 ng/mL LPS, without S14, induced TNF at a magnitude similar to 20 µM S14 alone, while addition of 1 ng/mL LPS to cells pre-treated with 0.15 to 10 µM did not alter TNF release compared to the condition in which no S14 was added. Interestingly, no synergistic effect for the cells pre-treated with 20 or 40 µM S14 followed by addition of 1 ng/mL LPS was observed, while TNF release comparable to the condition

without any LPS added could be noted (Fig. 3.20A). Strikingly, 5, 25 and 50 ng/mL LPS addition to S14 pre-treated cells induced very comparable TNF release patterns, seemingly LPS “taking over” and governing the cytokine response, as TNF levels did not significantly change with either combination treatment (Fig. 3.20A). Next, I aimed to shed light on a role for S16, potentially as a partial receptor agonist also competing with S14, or maybe even inhibiting its inflammatory potential. I set up a similar experiment as displayed in panel A, pre-treating cells with 40 μM S16 for 15 min before adding increasing concentrations of S14. Of note, while S16 on its own was not enough to induce considerable TNF release from BMDMs, it shifted the concentration titration curve of S14 (without S16 pre-treatment) slightly to the left, making a synergistic effect obvious at S14 concentrations of 2.5 to 20 μM, but not at 40 μM (Fig. 3.20B).

Furthermore, I wanted to investigate a potential interplay between S14 and LPS in hMDMs, bearing in mind its potential physiological relevance. Making use of the fact that 18 h stimulation of hMDMs with S14 does not lead to measurable TNF release, I initially stimulated hMDMs with S14 for 18 h, before adding LPS for further 3 h. As expected, S14 did not elicit TNF release from hMDMs by itself, independent of the concentration used, whereas LPS treatment (no S14) induced significant TNF release (Fig. 3.20C). However, S14 pre-treatment dose-dependently negated the LPS-induced TNF release to near undetectable levels at high concentrations of S14 (Fig. 3.20C). In summary, the data supports a competitive interplay between endogenous S14 and LPS, which might be physiologically relevant in context of bacterial infections.

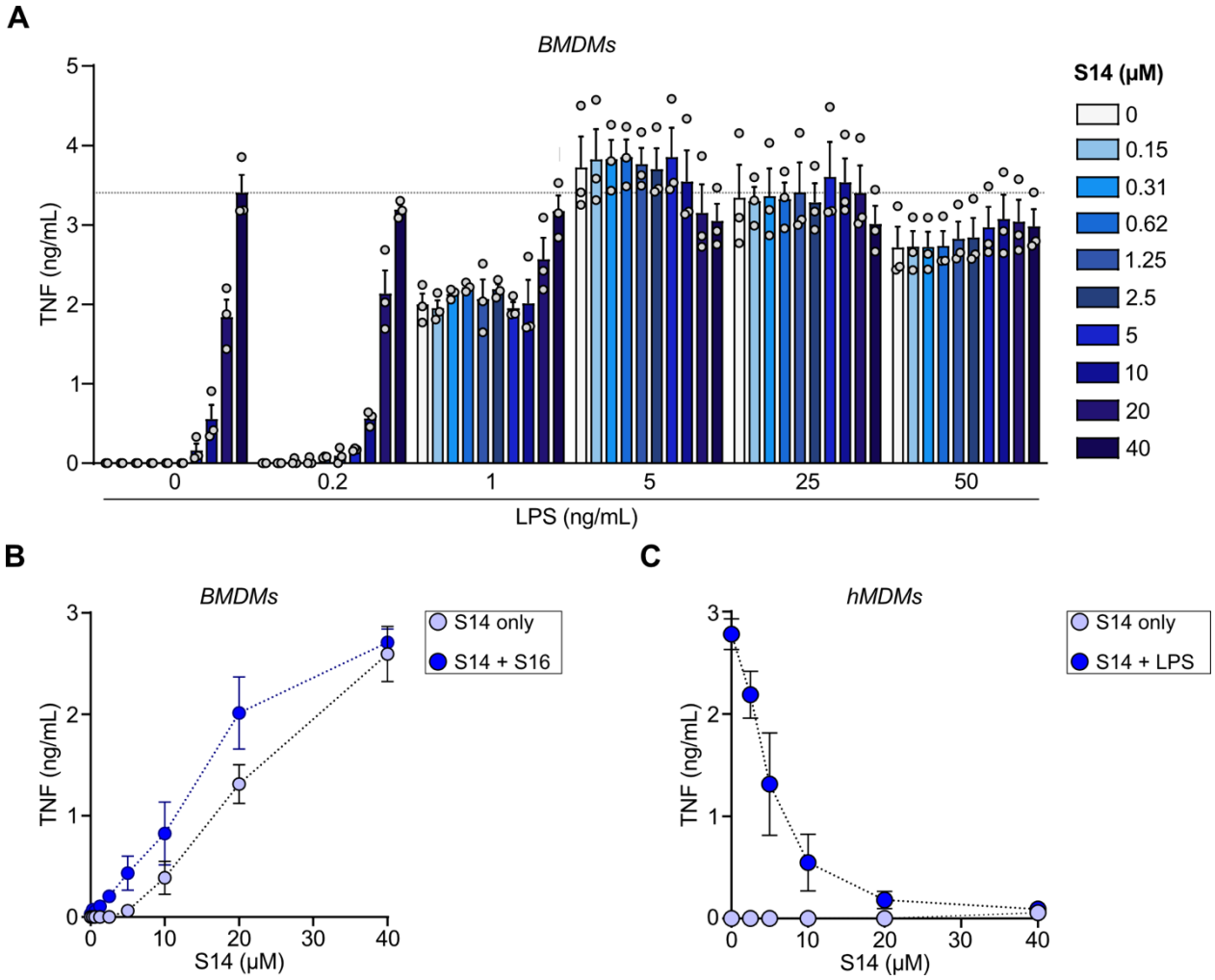

Figure 3.20| LPS and S14 competitively activate TLR4/MD-2
(A) TNF release from BMDMs, pre-treated for 15 min with the indicated concentration of S14, before adding increasing concentrations of LPS and incubating together for 18 h. (B) TNF release from BMDMs, pre-incubated for 15 min with 40 µM S16, before adding the indicated concentration of S14 and incubating together for 18 h. (C) M-CSF differentiated hMDMs were incubated for 18 h with different concentrations of S14, before adding 10 ng/mL LPS to the cells and incubating for further 3 h and assessing TNF release. All data is presented as mean with SEM of n=3 (A, C) or n=5 (B) biological replicates.

3.10 S14 does not induce acute peritonitis in mice

As S14 was initially identified to be predictive for atherosclerotic plaque burden in mice, and having thoroughly analyzed its pro-inflammatory capacity *in vitro,* I sought to determine whether these findings also translate into an acute inflammatory response *in vivo*. Hence, I attempted to induce acute peritonitis by intraperitoneal injection of S14, which is a commonly used mouse model when studying LPS (Lewis et al., 2016). As expected, 3 h after LPS injection, both TNF and IL-6 were detected systemically in the blood (Fig. 3.21A) and locally in the peritoneal lavage fluid (Fig. 3.21B). However, I did

not detect cytokine release post-S14 injection (Fig. 3.21A/B). In addition, the leukocyte populations in the peritoneal exudate of mice were investigated via flow cytometry. While LPS injection led to increased recruitment of $CD19^+$ B cells, $CD3^+$ T cells, $NK.1.1^+$ NK cells and $CD11c^+$ dendritic cells (DCs) into the peritoneum, the percentage of $Ly6G^+$ neutrophils and $Ly6C^+$ monocytes decreased (Fig. 3.21C). On the other hand, injection of S14 did not affect most of the leukocyte populations, although an influx of NK cells, DCs and monocytes could be noted (Fig. 3.21C). Overall, while S14 injection appeared to have a slight effect, it did not induce acute inflammation to the extent that LPS does.

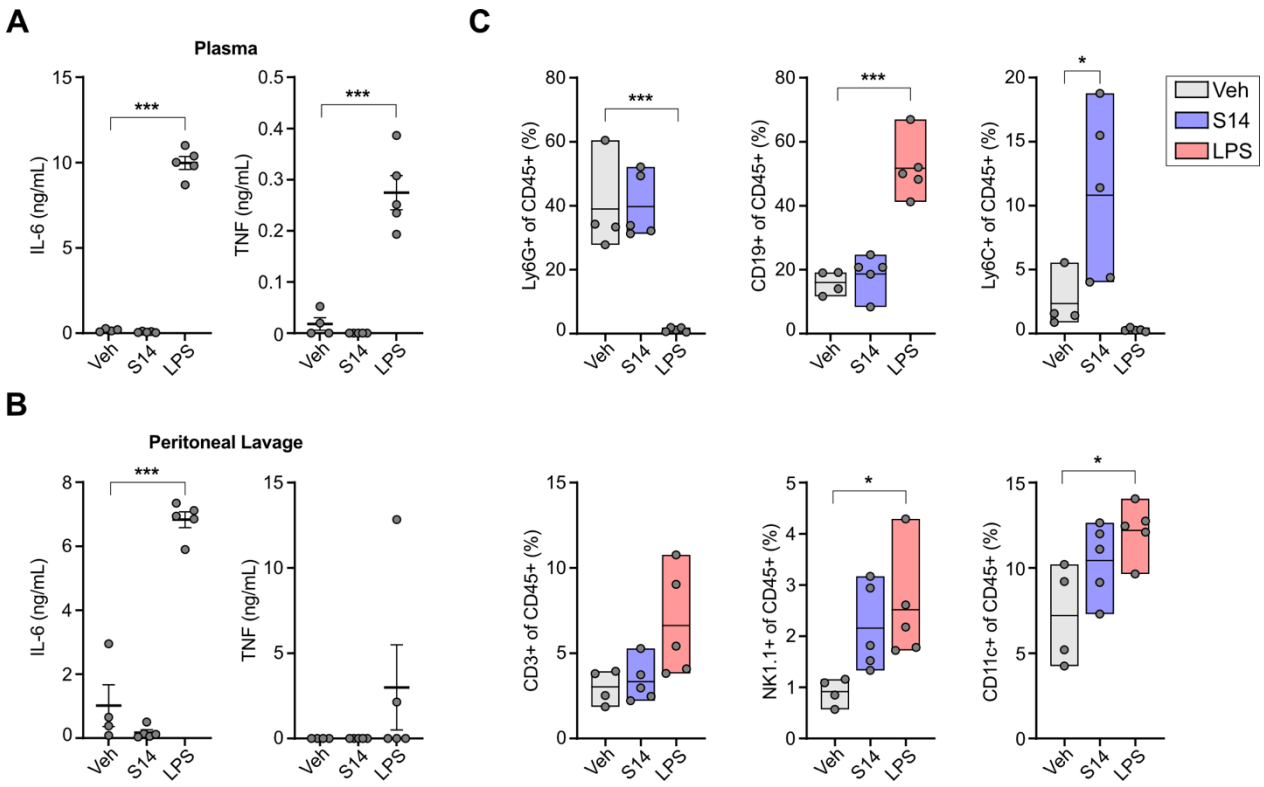

Figure 3.21| S14, unlike LPS, does not induce acute peritonitis *in vivo*
Male WT C57BL/6 mice (n=4-5 per group) were intraperitoneally injected with 5 mg/kg bodyweight of LPS, S14 or vehicle control. After 3 h, blood and peritoneal lavage fluid were collected. Cytokines in (A) systemic plasma and (B) peritoneal lavage fluid were assessed. (C) Cells in the peritoneal lavage fluid were analyzed by flow cytometry and populations are shown as the amount (%) of $CD45^+$ immune cells. Data is shown as (A, B) mean with SEM or (C) box plots with indicated mean of n=4-5 biological replicates. All data was analyzed by one-way ANOVA with Bonferroni post hoc analysis. P-values adjusted for multiple testing are presented: *p < 0.05, **p < 0.01, ***p < 0.001. Live animal handling was carried out by Kyra de Goede and Eelco Keuning.

3.11 Macrophage cholesterol efflux is altered by S14

While I did not observe a direct acute inflammatory effect of S14 in the peritonitis model, I set out to understand how S14 could potentially contribute to systemic low-grade inflammation and plaque progression in atherosclerosis, beyond rewiring macrophages to become pro-inflammatory. The net flux of cholesterol is an essential process for vessel wall macrophages and excess deposition and storage of cholesterol results in the formation of foamy macrophages (Ouimet & Marcel, 2012). Therefore, I investigated the effect of S14 on cholesterol efflux from macrophages *in vitro*. I set up an optimized efflux assay, which is described in detail in section 2.2.9, but in short, BMDMs were loaded overnight with BODIPY-Cholesterol, then stimulated for 18 h before assessing the efflux of externally loaded cholesterol (Fig. 3.22A). Almost 40 % of cholesterol efflux was observed from untreated cells, whereas S14 treatment nearly reduced the efflux by half, indicating retention of cholesterol (Fig. 3.22B). Interestingly, S16 and LPS both reduced cholesterol efflux as well, however, not reaching significance (Fig. 3.22B). Based on these results, I wanted to investigate the TLR4-dependence and stimulated WT and TLR4 KO BMDMs with S14 in the efflux assay. As observed previously, cholesterol efflux from WT cells was drastically reduced by S14 treatment, whereas this effect of S14 was considerably reduced in the TLR4 KO cells (Fig. 3.22C).

Studies have shown that an impaired mitochondrial function negatively affects cholesterol efflux from macrophages (Allen & Graham, 2012). Since I could demonstrate both a rewired macrophage metabolism and reduced cholesterol efflux upon S14 stimulation, I hypothesized that rescue of the mitochondrial function could also rescue the reduction in cholesterol efflux. Thus, I pre-treated cholesterol-loaded macrophages with the PDK inhibitor KPLH1130 in combination with IL-10, which has previously been shown to rescue macrophage OXPHOS after LPS stimulation (Dowling et al., 2021; Min et al., 2019). Upon stimulation with S14, BMDMs that were not pre-treated, exhibited the expected reduction in cholesterol efflux, whereas pre-treatment rescued, and even enhanced, overall cholesterol efflux capacity (Fig. 3.22D).

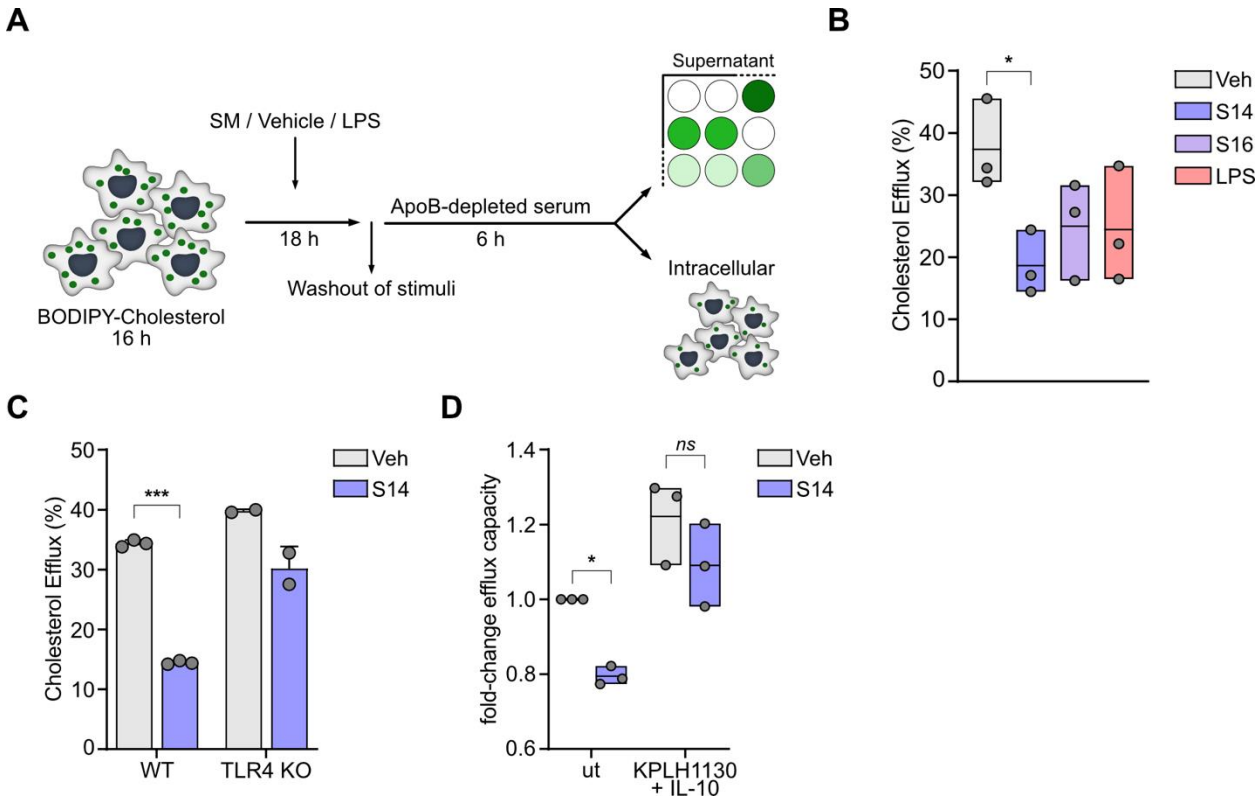

Figure 3.22| S14 reduces the macrophage cholesterol efflux capacity *in vitro*
(A) Simplified overview of the experimental set up to assess cholesterol efflux capacity *in vitro*. (B) Percent efflux of externally loaded cholesterol from WT BMDMs after 12 h stimulation with vehicle, 30 µM S14, 30 µM S16 or 100 ng/mL LPS; n=3 biological replicates. (C) Percent efflux of externally loaded cholesterol from WT or TLR4-KO BMDMs after 12 h stimulation with vehicle or 30 µM S14; n=2-3 biological replicates. (D) Fold-change in efflux capacity from WT BMDMs after 30 min pre-treatment with medium only or 5 µM KPLH1130 together with 20 ng/mL IL-10 followed by stimulation with vehicle or 30 µM S14 for 12 h; n=3. All data was analyzed by one-way ANOVA with Bonferroni post hoc analysis. P-values adjusted for multiple testing are presented: *p < 0.05, **p < 0.01, ***p < 0.001.

3.12 Dietary changes affect circulating S14 concentrations

3.12.1 S14 concentrations are associated with obesity and T2D

In the initial unbiased approach, S14 was identified as a factor associated with disease severity in a diet-induced mouse model of atherosclerosis, and the *in vitro* data showed that S14 can activate murine and human TLR4/MD-2. To confirm a physiological relevance, I therefore assessed whether circulating S14 concentrations were affected by a dietary intervention in healthy human volunteers. I analyzed serum samples collected as part of the DESIRE study (ClinicalTrials.gov ID: NCT02628301), in which healthy volunteers received a hypercaloric diet (HCD) for 30 days, followed by a low-caloric diet

(LCD) for another 30 days (Emanuel et al., 2020). Indeed, consumption of a HCD led to an increase in blood S14 concentration, which decreased significantly after participants had lowered their caloric intake (Fig. 3.23A, left). In the original study, Emanuel *et al*. observed diet-dependent changes in body weight and body fat, which prompted me to additionally analyze serum adipokines (Emanuel et al., 2020). I found that the concentrations of both resistin (Fig. 3.23A, middle) and adiponectin (Fig. 3.23A, right) principally aligned with the pattern observed for the diet-induced changes in S14 concentration. Given that human resistin is primarily released from circulating myeloid cells and is regarded to be pro-inflammatory (Kaser et al., 2003; Steppan et al., 2001), I sought to determine whether S14 could modulate resistin release. Stimulation of human whole blood *ex vivo* for 24 h with S14 indeed led to a significant increase in resistin concentration (Fig. 3.23B). Therefore, I reasoned that S14 can stimulate *de novo* synthesis of resistin, which potentially contributes to the inflammatory response *in vivo*.

Overnutrition, which often leads to obesity and insulin resistance, augments the development of type 2 diabetes (T2D) (Kahn & Flier, 2000). To evaluate S14 concentrations in context of T2D, lipidomics analysis was performed on plasma samples obtained from the FAIR study (ClinicalTrials.gov ID: NCT05295160). In this study, overweight and obese patients diagnosed with T2D were exposed to a very-low-caloric diet (VLCD) until a weight loss of 15 kg was achieved and insulin sensitivity was restored. Plasma lipidomics analysis revealed that the overall sphingomyelin pool was significantly reduced following the dietary intervention (Fig. 3.23C, left). Furthermore, circulating S14 concentrations in both female and male participants were substantially reduced at study endpoint (Fig. 3.23C, right), corroborating the data described in the previous section.

Finally, I sought to verify the predictions made in the atherosclerotic mouse model and place it in context of human cardiovascular disease. To this end, lipidomics analysis was performed on plasma samples of the 300-OB study (ter Horst et al., 2020), to assess whether presence of carotid plaques in obese individuals coincides with higher blood S14 concentrations. Indeed, circulating S14 concentrations were significantly higher in male, but surprisingly not female, participants with carotid plaques compared to those with no carotid plaques (Fig. 3.23D). As approximately 30 % of circulating sphingomyelin is

associated with HDL (Hammad et al., 2010), and the purely beneficial properties of HDL have been challenged (Yan et al., 2014), I compared both the total amount of S14 and HDL-associated S14 in serum of healthy volunteers and patients with coronary artery disease (CAD). The analysis revealed that the S14 concentration in blood was higher in CAD patients, and that the amount of S14 extracted from HDL particles was also significantly higher for CAD patients compared to healthy volunteers (Fig. 3.23E). Taken together, these results indicate that systemic S14 concentrations are affected by our diet, and that they are, as predicted, indeed associated with cardiovascular disease.

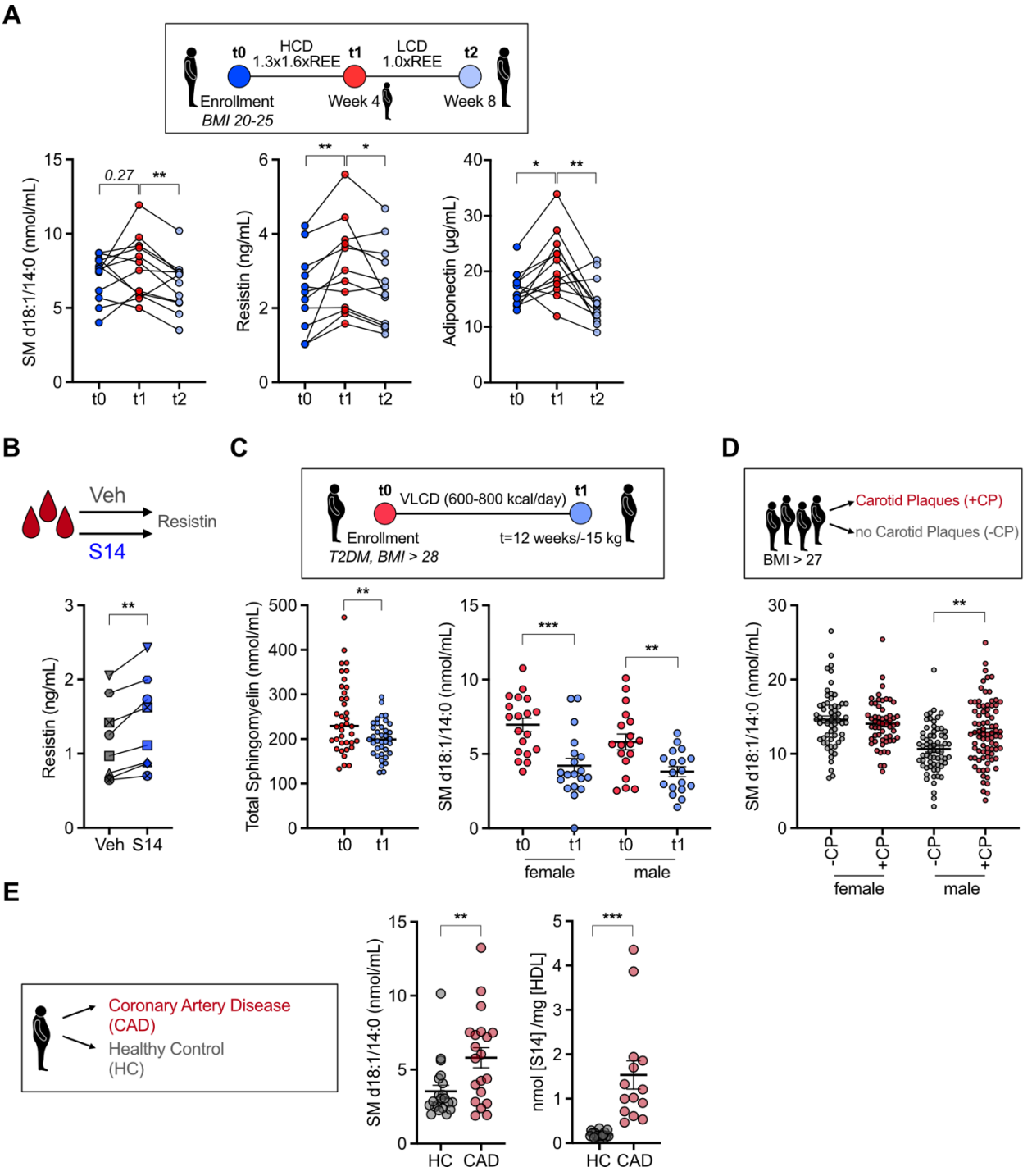

Figure 3.23| Circulating S14 concentrations are elevated in obese individuals and CVD patients
(A) As participants of the DESIRE study, healthy male volunteers (n=12) followed a 4-week hypercaloric diet (HCD), followed by a low-caloric diet (LCD) for further 4 weeks. Serum samples obtained from different timepoints during the study were analyzed via lipidomics to determine S14 concentrations and serum resistin and adiponectin were measured. (B) Resistin release was determined in *ex vivo* stimulated human whole blood from healthy human volunteers (n=8). Freshly drawn blood was diluted 1:5 in RPMI containing either vehicle or 30 µM S14 and incubated for 24 h before obtaining diluted plasma for adipokine analysis. (C) Lipidomic analysis of total sphingomyelin (left graph) and S14 concentrations (right graph) in serum samples from participants of the FAIR study cohort (n=37). In short, type 2 diabetes patients were exposed to a very low-caloric diet (VLCD) for 12 weeks, or until a reduction of 15 kg body weight were achieved.

(D) Plasma samples of participants of the 300-OB study cohort, grouped according to carotid plaque (CP) presence, were analyzed via lipidomics to determine circulating S14 concentrations; left to right: n=59/56/66/81. (E) Plasma samples obtained from healthy volunteers (HC) or patients with coronary artery disease (CAD) were analyzed via lipidomics to assess the overall S14 concentration (right graph); n=21 (HC) and n=20 (CAD), as well as the amount of S14 associated with HDL (left graph); n=21 (HC) and n=14 (CAD). All individual biological replicates are indicated, and where applicable, presented including a line at mean with SEM. Data was analyzed by paired two-tailed student's t-test (A-C) or one-way ANOVA with Bonferroni post hoc analysis. P-values adjusted for multiple testing are presented: *$p < 0.05$, **$p < 0.01$, ***$p < 0.001$. Acquisition of samples analyzed and presented in this figure was organized by the respective clinical study leaders as described in section 2.2.2. Lipidomic analyses of samples were performed by (A, C) Jelena Zurkovic, (D) Arslan Hamid and Mohamed Yaghmour and (E) Philip Wollnitzke.

3.12.2 White adipose tissue is a reservoir for S14 in mice

Previous studies and the data collected in this study demonstrate that TLR4 activation is associated with obesity-mediated inflammation and the development of related diseases (Moser et al., 2018; Saberi et al., 2009). Consistent with earlier reports, linking obesity to increased white adipose tissue (WAT) sphingomyelin in mice (Turner et al., 2013), I found that LDLR KO mice fed a 4-week high-fat diet (HFD) compared to normal chow diet (CD) accumulated significantly more S14 in both subcutaneous and visceral WAT (Fig. 3.24A, left). Notably however, the molar ratio of S14 to other sphingomyelins was significantly higher in visceral compared to subcutaneous adipose tissue in HFD-fed mice (Fig. 3.24A, right). This falls in line with the notion that especially visceral adipose tissue contributes to inflammation in obesity and diabetes (Fontana et al., 2007). Speculating that adipocytes are a S14 reservoir, I chronically stimulated mature 3T3-L1 adipocytes with insulin, which is a widely accepted model of obesity-induced insulin resistance (Ruiz-Ojeda et al., 2016; Thomson et al., 1997), and indeed observed a trend towards elevated intracellular S14 levels (Fig. 3.24B). Therefore, it is likely that particularly the visceral white adipose tissue contributes to an increase in both WAT-associated and circulating S14 in context of overnutrition and chronic inflammation.

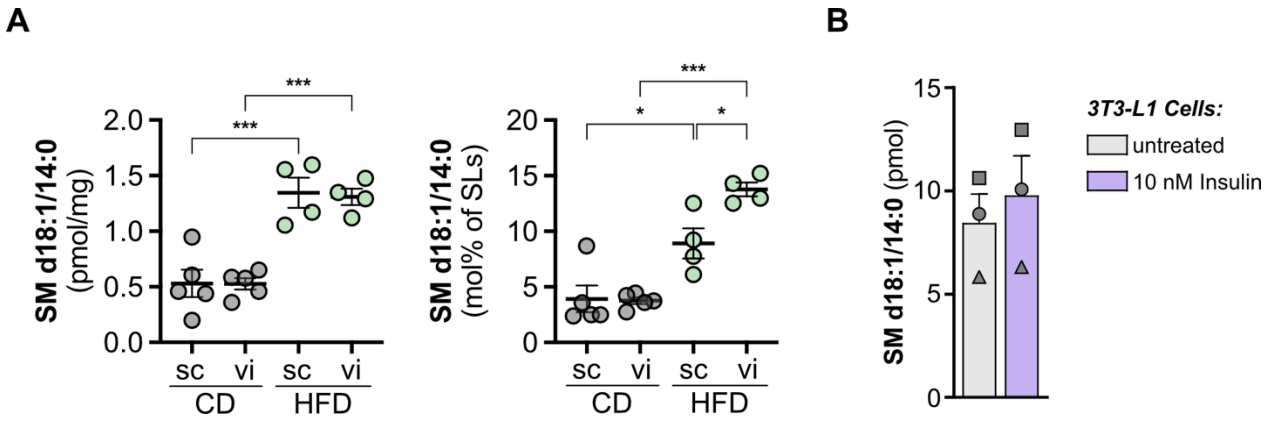

Figure 3.24| Increased S14 concentrations in obesity are potentially derived from adipose tissue
(A) Female LDLR KO mice were exposed to either a chow diet (CD) or high-fat diet for 4 weeks. Subcutaneous (sc) and visceral (vi) white adipose tissue were collected and prepared for lipidomic analysis of S14 concentration; n=4-5. (B) Fully differentiated 3T3-L1 adipocytes were exposed for 12 h to 10 nM Insulin in presence of high glucose as a model of insulin resistance. Intracellular S14 concentrations were determined by lipidomic analysis; n=3. All individual biological replicates are indicated and presented as mean with SEM. Data was analyzed by (A) one-way ANOVA with Bonferroni post hoc analysis, or (B) paired two-tailed students t-test. P-values adjusted for multiple testing are presented: *p < 0.05, **p < 0.01, ***p < 0.001. The *in vivo* experiment presented in (A) was registered and performed by Christabel Mennicken and Maximilian Rothe. Isolation of lipids was performed by myself and the lipidomic analysis subsequently performed by Jelena Zurkovic.

3.13 Age potentially influences sphingolipid homeostasis

The general concept and the molecular mechanisms underlying metaflammation can also be found in ageing. The term '*inflammaging*' was introduced to describe the sterile, chronic low-grade inflammation that occurs during ageing, and that contributes to common age-related diseases (Ferrucci & Fabbri, 2018). Several studies have described age-related dysfunctions in adipose tissue and low-grade systemic inflammation (Findeisen et al., 2011; Stout et al., 2017). Due to the similarities between metaflammation and inflammaging, I reasoned that the latter could potentially also be associated with an altered sphingolipid profile, specifically regarding S14. To interrogate the effect of age on sphingomyelin concentrations, I analyzed the abundance of the lipids S14, S16, S18 and S26 in epididymal WAT (eWAT) and serum of young (age: 8 weeks) and old (age: 70-75 weeks) WT mice. I found that the eWAT concentration of none of the sphingomyelin species was affected by age, and S26 was even undetectable (Fig. 3.25A). However, the total eWAT mass was not assessed, and the absolute amount of S14 could, therefore, differ between young and old mice. On the other hand, significantly more S14 and also S18 was detected in serum of old mice, while S16 and S26 concentrations were not affected (Fig. 3.25B). Taken together, these results indicate that S14 potentially

contributes to low-grade inflammation during ageing. However, to verify the data, the total adipose tissue mass and systemic cytokines as well as adipokines such as resistin should be analyzed in future studies.

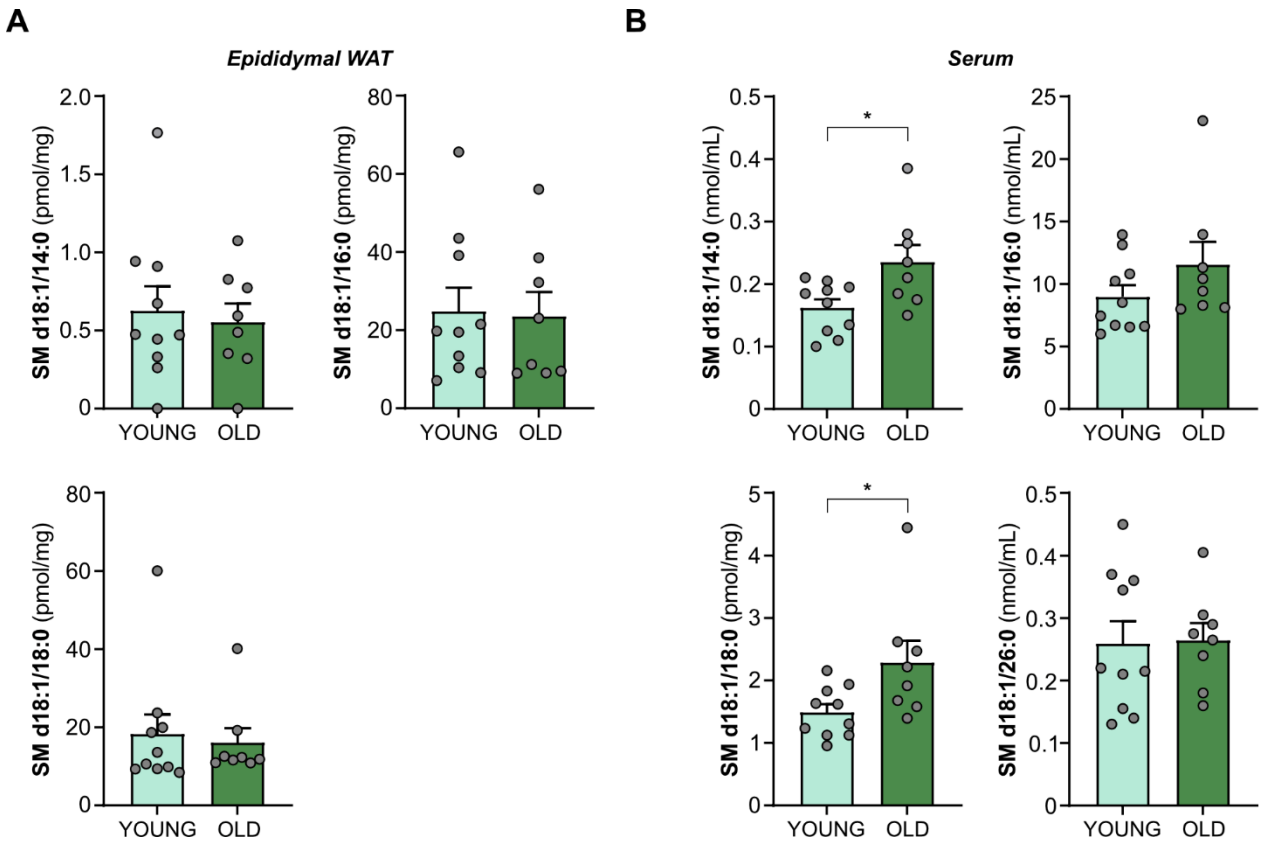

Figure 3.25| Potential association between age and S14 concentrations
(A) Epididymal (visceral) white adipose tissue (WAT) and (B) serum from young (ca. 8 weeks; n=10) and old (70-75 weeks; n=8) WT mice was collected and analyzed by lipidomics. Sphingolipids shown are S14, S16, S18 and S26 (undetectable in WAT). All individual biological replicates are indicated and presented as mean with SEM. Data was analyzed by unpaired two-tailed students t-test (B). P-values are presented: *p < 0.05, **p < 0.01, ***p < 0.001. Sample acquisition and processing was performed by Maximilian Rothe and myself, whereas lipidomic analysis was performed by Jelena Zurkovic.

4 DISCUSSION

4.1 Unbiased analysis of factors influencing atherogenesis in mice

A western-type diet (WD) leads to chronic low-grade inflammation (‘metaflammation’) alongside long-term alterations in the innate immune cell compartment (Christ et al., 2018). The immediate underlying mechanisms controlling metaflammation and the development of disease are not yet fully understood. Here, I utilized a data set from an unbiased analysis that was previously generated in our group, to identify novel non-genetic factors that link WD consumption to the progression of murine atherosclerosis. Such factor(s) could potentially also hold an implication for other clinically relevant conditions within the context of metaflammation. Integration of all measured features from mice of various genetic backgrounds revealed, that amongst the factors positively associated with atherosclerosis progression, were many sphingomyelin species (Fig. 3.1C). This result was not very surprising, because sphingomyelin and other sphingolipids have previously been implicated in the pathogenesis of atherosclerosis based on their abundance in human atherosclerotic plaques and their association with markers of plaque instability (Edsfeldt et al., 2016; Jiang et al., 2000). Proposed mechanisms include the modulation of endothelial function (Lai et al., 2022), plaque growth (Edsfeldt et al., 2016) and an altered lipoprotein metabolism (Iqbal et al., 2017). Interestingly, closer analysis of the sphingomyelin species detected in the screening approach suggest a link between the length of the fatty acid chain of the sphingomyelin and its assigned feature importance. The sphingomyelin species with 14 or 16 carbon fatty acids appeared to be highly predictive for disease progression, while longer chain sphingomyelins appeared to be weaker risk factors (Fig. 3.1C). These observations were compelling due to the fact that most existing studies have focused on sphingomyelins as an entity, rather than investigating individual species. Sphingolipids, both as a family and its individual species, have previously been shown to exert pro-inflammatory effects (MacEyka & Spiegel, 2014). Amongst the selected portal vein metabolites (chosen based on their commercial availability) that were tested for their pro-inflammatory potential *in vitro*, sphingomyelin d18:1/14:0 (S14) was the only one that dose-dependently induced TNF release from mouse BMDMs (Fig. 3.1E). A more refined bioinformatic analysis of this unbiased screen,

including only the data generated from samples of mice on a LDLR-deficient background (due to its relevance as a prototypical atherosclerosis mouse model), confirmed the highly predictive nature of sphingomyelins, and specifically of S14. The abundance of S14 in portal vein serum was positively correlated to the plaque area in the aortic root, and thereby to disease severity. The robustness of the machine learning analysis was confirmed by both the model prediction accuracy as well as by identification of known risk and protective factors such as IL-1β (Ridker et al., 2017) and HDL (Gordon et al., 1989b; Gordon et al., 1977; MacMahon et al., 2007), respectively, indicating a reliable and powerful prediction for plaque progression in mice (Fig 3.2B-F).

One of the initial objectives of this thesis was to use the machine learning data from the unbiased screen in mice to identify and investigate non-genetic metabolites that influence cardiovascular disease progression. While the analysis confirmed known risk factors, it also led to the identification of the endogenous lipid S14, which proved to be strongly activating in mouse macrophages *in vitro*. Together, these results rationalized the more in-depth investigation of S14, to corroborate its potential role as a contributing factor to metaflammation.

4.2 S14 exhibits strong pro-inflammatory effects *in vitro*

4.2.1 Effect of S14 in mouse macrophages

Sphingomyelins, as mentioned before, are a heterogenous group of lipids and several studies have reported that their individual functions are determined by their acyl chain composition (Park & Park, 2015). My data confirmed this notion in that S14, and to less extent also S16, but not sphingomyelins of longer acyl chain length, exerted pro-inflammatory effects on BMDMs (Fig. 3.3B). However, caution must be applied when generalizing ‘long acyl chain’ sphingomyelins, as only selected lipids could be tested based on their availability. Nevertheless, the data extracted from the *in vivo* screen corresponded to the data generated *in vitro*. S14 had a distinct effect on mouse macrophages, while longer acyl chain sphingomyelins were less activating, and therefore, are probably less likely to influence disease progression *in vivo*. It is important to take into account that the data generated *in vitro* could potentially be influenced by a reduction in

solubility, especially for the long acyl chain sphingomyelins, which is a factor that was not reconfirmed prior to stimulation of cells, and should, therefore, be determined in future studies.

To my knowledge, no study to date has investigated the effect of treating macrophages, or any other cell type, with S14. Nevertheless, previous studies have reported on the effects of ceramides, the direct precursors of sphingomyelin, and dietary milk sphingomyelin stimulation, although with conflicting results (Fischer et al., 2007; Norris & Blesso, 2017). These findings might be explained, in part, by the specific sphingolipid species and its concentration used, or the cell type being stimulated. In addition, milk sphingomyelin is a complex mixture of sphingomyelins containing different sphingoid backbones and variable acyl chains, potentially negating each other's effects. However, the transcriptomic analysis of BMDMs stimulated with S14, which was performed within the scope of this thesis, strongly corroborated the cytokine release data (Fig. 3.4). The S14-induced gene signature was noticeably similar to LPS, including an upregulation in the expression of genes such as *Il6*, *Il1b*, *Saa3* and *Nos2,* that are commonly associated with inflammatory responses (Fig. 3.5A). Next to this striking functional resemblance, certain structural similarities between S14 and the Lipid A moiety of LPS, namely the acyl chains and the zwitterionic phosphocholine head group of the sphingolipid, were found.

Investigation into the TLR4 dependence using both a pharmacological and genetic approach confirmed that S14, like LPS, requires intact TLR4 signaling (Fig. 3.6). Interestingly, it has previously been proposed that TLR4 signaling is elicited in epithelial cells by addition of exogenous short acyl chain ceramides (Fischer et al., 2007). However, in the present study, two approaches were utilized, namely sphingomyelinase inhibition as well as direct ceramide stimulation, to excluded that ceramides are the active signaling components that drive inflammation (Fig. 3.15). My investigation not only proved that S14-mediated inflammation was TLR4-dependent, but also showed that S14 strongly engaged both MyD88 and TRIF-dependent signaling downstream of TLR4 activation (Fig. 3.10). In terms of functional output, the marked dependence on TLR4 was evident by efficient cytokine release from BMDMs as well as by the upregulation of co-stimulatory molecules that aid to initiate the adaptive immune response. These findings were further supported

by the fact that S14-stimulated macrophages adapted their metabolic flux to meet their high energetic demand. A shift towards glycolysis at the expense of overall oxidative phosphorylation was noted in S14-treated BMDMs (Fig. 3.8). These results may partially be explained by the upregulation of nitric oxide, a concept that has been described in literature, and that was confirmed here (Van den Bossche et al., 2016). Another interesting finding was that S14 induced an intrinsic counter-regulatory mechanism via expression of anti-inflammatory IL-10, which is known to be regulated downstream of TLR4 (Sanin et al., 2015). Indeed, expression of IL-10 has been regarded as being protective against chronic inflammation observed in atherosclerosis (Caligiuri et al., 2003; Mallat et al., 1999). Overall, the results obtained here (Fig. 3.7 – 9), fall in line with the pro-inflammatory macrophage phenotype that other studies have assigned to BMDMs upon TLR4 activation. In a simplified view, this is sometimes referred to as an ‘M1’ or classically activated macrophage phenotype.

4.2.2 Effect of S14 in human myeloid cells

In order to verify that the pro-inflammatory effects of S14 were conserved in human myeloid cells, a series of experiments was performed in freshly drawn whole blood, or using $CD14^+$-selected blood monocytes and M-CSF-differentiated monocyte-derived macrophages (hMDMs). Although S14 had a largely similar effect in human immune cells, some surprising observations were made. While LPS, as expected, strongly induced IL-6 and TNF release from both *in vitro* stimulated monocytes and macrophages, S14 treatment only lead to significant TLR4-dependent release of IL-6 from both cell types. TNF release on the other hand, although statistically not significant, was solely observed from S14-stimulated monocytes but not monocyte-derived macrophages (Fig. 3.11). These findings were rather unexpected, as literature suggests that hMDMs generally secrete more mature TNF protein than isolated monocytes (MacKenzie et al., 2002). Therefore, S14 either affects gene transcription, the post-transcriptional control mechanism, or the trafficking machinery of mature TNF, via a mechanism that specifically occurs in hMDMs. Further investigation of these possibilities revealed that the absence of TNF release from human macrophages could not be explained by inefficient transcription of TNF, as *TNF* gene expression was significantly induced by both LPS and S14 in human

macrophages. Moreover, it was ruled out that the initial observations made at 24 h post-stimulation were due to a shift in cytokine release kinetics. While TNF release from macrophages indeed peaked already at earlier timepoints (6 to 8 h) after LPS stimulation, extracellular TNF following S14 treatment was either undetectable or only present in minimal amounts (Fig. 3.12).

The discrepancy between functional IL-6 release as opposed to drastically reduced TNF release from hMDMs after S14 treatment, presents an intriguing finding. Both cytokines are, amongst others, controlled by the common transcription factor NF-κB downstream of TLR4 activation. However, release of mature IL-6 and TNF may be regulated differentially, as evident in LPS-activated vascular smooth muscle cells (Lee et al., 2016). My investigation shows that a defect in transcription of either cytokine could be excluded, indicating that S14 likely affects either protein translation or the trafficking of mature TNF, but not IL-6. Most cytokines employ a rather specific intracellular trafficking and release machinery. In fact, soluble cytokines such as IL-6 and transmembrane cytokines like TNF are distinctly sorted at the trans-Golgi network for further transport to the cell surface (Murray & Stow, 2014). Thus, it is feasible that S14 interferes specifically with the transport of mature TNF, but not IL-6. Further experiments to confirm sufficient protein expression and handling might facilitate a deeper understanding of this S14-mediated effect, and its potential physiological consequences. The release of pro-inflammatory cytokines such as IL-6 and TNF from macrophages is known to play a vital role in context of various metabolic diseases (Yao et al., 2022). However, whether human macrophages *in vivo* respond similar to *in vitro* generated macrophages, as well as the extent to which specific cytokines released from macrophages upon activation by S14 contribute to disease, remains uncertain.

Although hMDMs appeared to respond slightly different compared to mouse macrophages and human monocytes, further experiments corroborated the pro-inflammatory nature of S14 in human cells. My results showed that in freshly drawn, *ex vivo* stimulated human whole blood, S14 elicits the release of various pro-inflammatory cytokines like MCP-1 and IL-1β (Fig. 3.13B). Although the origin of these cytokines was not determined, it is likely that they are released from monocytes, T-cells and/or granulocytes, as the latter comprise a large portion of immune cells found in peripheral blood. Another striking finding in this

context was that S14, like LPS, directly activated the human NLRP3 inflammasome independent of classical inflammasome stimuli (Fig. 3.14). S14 stimulation of whole blood was sufficient to induce IL-1β release, presumably by monocytes. These results are consistent with earlier studies, demonstrating a species-specific TLR4-dependent alternative NLRP3 inflammasome activation in human monocytes (described in detail in section 1.2.3.2) (Gaidt et al., 2016). To confirm this hypothesis, the dependency on caspase-8 and RIPK1 should be assessed using both whole blood and isolated human monocytes. Inflammation driven by engagement of the TLR4-NLRP3 axis has been associated with several metabolic diseases such as diabetes or atherosclerosis. Therefore, it is probable that the promiscuous activation of the human NLRP3 inflammasome by S14 can fuel metaflammation.

4.3 S14 is an endogenous ligand for the TLR4/MD-2 complex

The concept of sterile inflammation, whereby inflammation is triggered in the absence of microbial agents, has been widely acknowledged in context of various pathologies. Hereby, endogenous molecules are purportedly sensed by pattern-recognition receptors such as TLR4 (Chen & Nuñez, 2010). Over the years, several novel TLR4 agonists have been proposed, including proteins released from damaged or dying cells, as well as long-chain saturated fatty acids (lcSFAs) such as palmitate (Kim et al., 2013; Rocha et al., 2016). For a long time, fatty acids seemed to provide an appealing link between nutrient excess and inflammation, such as it is observed in obesity. However, recent evidence refutes the prevailing idea that lcSFAs are direct TLR4 agonists. It instead shows that TLR4-dependent priming and rewiring of cellular metabolism regulate lcSFA-induced inflammation (Lancaster et al., 2018). These contradicting findings epitomize the general problem that to date, most studies have either not considered potential endotoxin contaminations in their preparations, or more importantly, have failed to provide structural evidence upon introduction of novel TLR4 ligands.

In the present study I gathered convincing evidence for S14-induced inflammation in mouse and human myeloid cells that was highly dependent on TLR4. Based on my initial objectives, experiments were performed to investigate the mechanism underlying S14-

mediated inflammation in more detail. Utilizing a line of complementary experimental approaches, I was able to show that S14 is in fact a novel endogenous TLR4 agonist that directly interacts with the TLR4/MD-2 complex. The MD simulations, which were similar to those performed by Lancaster *et al*. for lcSFAs (Lancaster et al., 2018), albeit with a contrasting outcome, demonstrated that S14 can effectively interact with the TLR4/MD-2 receptor complex. S16 however, appeared to be less potently activating, and the respective ceramides failed to productively engage the receptor complex completely. The simulation results were corroborated by a native PAGE mobility shift assay, which revealed that S14 induced binding to, and dimerization of TLR4/MD-2 (Figs. 3.16 – 17). One plausible explanation for the uniqueness of S14 might be that it comprises essential structural aspects that make it fitting to directly interact with TLR4/MD-2. Although molecules such as neoseptin-3, which is structurally highly disparate from the prototypical TLR4 ligand LPS, have been shown to be able to engage TLR4 (Wang et al., 2016), it appears that the structural similarity between S14 and LPS is of importance in this case. Firstly, S14 possesses a zwitterionic headgroup that is absent in ceramides, but is important for receptor binding. Secondly, the acyl chains present in S14 potentially mimic the acyl chains of lipid A. Of note, five out of the six acyl chains in lipid A from *E.coli* consist of 14 carbons (C14). Many of the natural lipid A variants or synthetic mimetics also contain C14 acyl chains (Zamyatina & Heine, 2020), and a recent study suggests that C14 microbial ornithine lipids also possess the potential of activating TLR4 (Pizzuto et al., 2022). Lastly, I confirmed that S14 in fact requires MD-2, and occupies the same hydrophobic binding pocket as LPS (Fig. 3.19). Although I did not test a dependence on CD14, further experiments using a CD14 neutralizing antibody, or BMDMs isolated from CD14-deficient mice, should be performed. Nonetheless, these findings were substantiated by analysis of receptor engagement via flow cytometry, which is a validated method to assess ligand-induced TLR4/MD-2 dimerization and endocytosis (Zanoni et al., 2011, 2017b). S14 stimulation, just like LPS, led to a fast dimerization of the TLR4/MD-2 complex and its subsequent endocytosis. S16 on the other hand, as expected, only induced very weak receptor dimerization and endocytosis (Fig. 3.18). These results are contrary to the findings by Lancaster *et al.* regarding TLR4-dependent inflammation by lcSFAs (Lancaster et al., 2018), and, therefore, once again reiterate that the mechanism of TLR4 activation of S14 is not comparable to indirect TLR4 “activators” such as

palmitate. In addition, the evidence collected likely excludes the possibility of S14 merely functioning via the modulation of lipid rafts. Numerous studies have indicated that lipid rafts, small membrane microdomains rich in sphingolipids, cholesterol and proteins like CD14 and TLRs, guide receptor dimerization and signaling output (Ruysschaert & Lonez, 2015; Wong et al., 2009). It is possible however, that S14, next to directly binding TLR4, also affects the composition of lipid rafts, which in turn may facilitate or enhance TLR4 activation. Altogether, it can conceivably be suggested that S14 not only activates the immediate stereotypic signaling downstream of TLR4, but does so by directly interacting with the TLR4/MD-2 complex.

This conclusion is strongly supported by observations made by Su *et al.* in a recent study, in which they provide compelling evidence that C12 and C16 sulfatides, bind to mouse TLR4/MD-2, causing a potent pro-inflammatory response (Su et al., 2021). Sulfatides are also a class of endogenous sphingolipids, and differ from sphingomyelins only in the structure of their head group. However, while sulfatides were found to be TLR4-activating in mouse macrophages, they had antagonistic properties in human macrophages (Su et al., 2021). This species-specific effect was not apparent in my experiments, and, thus, does not appear to apply for S14. Although my investigation provides robust evidence, further structural analyses are required to develop a full picture of the specific binding interface between TLR4/MD-2 and S14. For example, by introducing site-specific mutations within essential residues of TLR4 and MD-2, and subsequently analyzing the responsiveness of mutant cells to S14, potential interaction sites could be confirmed.

4.4 S14 and LPS are potential competitive TLR4 agonists

Previous literature suggests that TLR4 has evolved to specifically detect its main ligand LPS and bind it with high affinity (Park & Lee, 2013). My data supports this concept, revealing that although S14 may be able to engage TLR4/MD-2, LPS is, in fact, structurally more adapt to do so. In this study competitive stimulation experiments were performed in BMDMs and hMDMs using a series of cross-titrations between S14 and LPS, or S14 and S16, to determine the exact role of the latter (Fig. 3.20). The data obtained from BMDM cultures demonstrated that short pre-treatment with the highest concentration of S14 was

dominating the cytokine response at the minimal receptor activating concentration of LPS (1 ng/mL). LPS on the other hand, as expected, dominated TNF release from BMDMs at higher concentrations tested (≧ 5 ng/mL) without showing a synergistic effect with S14, supporting the notion that LPS has a higher affinity towards TLR4. Pre-treatment of BMDMs with S16, followed by addition of S14, revealed, that while S16 on its own was not sufficient to induce cytokine release, it amplified the cytokine response elicited by S14. These data align to some extent with the dose-response curve obtained for full agonists in a receptor-reserve model (Buchwald, 2020), and are physiologically quite feasible considering that the plasma pool of sphingolipids *in vivo* includes various different sub-species. The experimental set-up was adjusted for hMDMs by stimulating for an extended time with S14 before adding LPS. Here, I was able to show that S14 dose-dependently mediated protection of LPS-induced inflammation by reducing TNF release from hMDMs. This piece of data might either be explained by increasing receptor occupation by S14, or by development of receptor tolerance such as it is also observed during a two-dose LPS administration *in vivo* and *in vitro*. To test this, a follow-up experiment should examine the abundance of inactive TLR4 receptors on the cell surface as well as analyze intracellular TLR4 protein expression. Overall, a relevant implication of these findings could be the possibility that S14, in certain pathophysiological situations, has a protective effect. In fact, several studies have proposed a so-called “obesity paradox” based on the observation that obese patients have a better overall survival rate than normal-weight counterparts during sepsis (Robinson et al., 2020; Yeo et al., 2023). Given the role of TLR4 in obesity, it might be conceivable that endogenous diet-induced TLR4 activators such as S14 contribute to this phenomenon by “priming” TLR4. In another study, human resistin, which is usually regarded as pro-inflammatory, was shown to compete with LPS for binding to TLR4 (Tarkowski et al., 2010). A consecutive investigation supported these findings by demonstrating that resistin protects from endotoxic shock via interference with the LPS-TLR4 interaction (Jang et al., 2017). Thus, the results of the present work might indeed be relevant in context of the association between low-grade inflammatory disease and the outcome of secondary infections.

4.5 Physiological relevance of S14 as an endogenous TLR ligand

The present work sought to identify novel pro-inflammatory metabolites with potential physiological implications for metaflammation-associated diseases such as obesity and atherosclerosis. I demonstrated that S14 drives inflammation *in vitro* via direct activation of TLR4, and it is well established that TLR4 activation plays an important role in many of the non-communicable diseases that have become a major health threat (Molteni et al., 2016). As a proof-of-concept, the effect of S14 was studied in mice, with an experimental set-up similar to that described for LPS-induced endotoxemia. However, compared to LPS, i.p. injection of S14 did not lead to measurable cytokine release in the peritoneum or circulation. Moreover, flow cytometry analysis of immune cells in the peritoneal lavage fluid revealed that there was merely a trend towards changes in the cell population distribution for S14 (for example influx of monocytes, NK cells and DCs), while significant alterations were observed after LPS injection (Fig. 3.21). However, it is important to note that the concentrations of LPS and S14 used in this approach cannot be compared. It has long been acknowledged that mice are less sensitive to LPS (Warren et al., 2010). Consequently, a very high dose of LPS is required to induce a sickness response in mice compared to humans. Besides, the administration of S14 was limited by two factors preventing the use of a higher dose:

- The amount of carrier protein (in this case mouse serum albumin) that can be injected into mice without causing adverse effects
- The volume of stimulus that can be injected into mice i.p.

Administration of a higher dose of S14 might in fact yield the desired proof-of-concept. While the amount of LPS injected into mice was by far higher compared to the dose applied in *in vitro* cell culture experiments, the current study was limited to utilize a concentration of S14 that was comparable to its *in vitro* dose. Hence, it cannot be concluded with certainty that S14 does not activate TLR4 *in vivo*, as there were too many factors that might have influenced this rather unexpected outcome.

Although I was not able to provide direct evidence for a S14-induced acute inflammatory response in mice, further investigations into different human study cohorts supported the prevailing hypothesis that S14 is, in fact, a plausible link between a Western-style diet and

TLR4-mediated metaflammation. Prior studies, as well as my data, show that S14, compared to other sphingomyelins such as S16 or S18, is sparse under homeostatic conditions (Turner et al., 2013). Indeed, it is rather feasible that S14 is only induced under certain pathological circumstances, to prevent continuous TLR4 activation. In coherence with this theory, the adipose tissue concentration of S14 has previously been reported to be significantly increased during obesity in both mice and humans (Turner et al., 2013; Turpin et al., 2014). Moreover, it has been shown that HDL-associated sphingomyelin is decreased upon weight loss in overweight and obese individuals (Martínez-Ramírez et al., 2016). In support of these data, I could demonstrate that plasma S14 concentrations are affected by dietary interventions in both healthy, obese and T2D human volunteers (Fig. 3.23A, C). Consumption of a high-caloric diet was associated with higher circulating S14 concentrations, whereas limiting caloric intake was not only beneficial in reducing weight and insulin sensitivity (parameters determined within the scope of the respective clinical studies), it concurrently decreased plasma S14 concentrations. I was also able to establish a link between resistin and S14, which might be another factor that contributes to inflammation. S14 was able to induce resistin release from blood leukocytes stimulated *ex vivo*. Resistin, as described before, has been associated with systemic inflammation, particularly during obesity, potentially via a mechanism involving activation of TLR4 signaling (Tarkowski et al., 2010).

On another note, it is crucial to mention that not all sphingomyelin species detected in the clinical study samples were affected by the dietary interventions, confirming once again the importance of considering sphingolipid species individually instead of as an entity. Although it may seem an appealing idea, it can be excluded with high certainty that the plasma sphingomyelin is directly derived from the diet, as sphingolipids need to be catabolized in the gut before entering the circulation (Norris & Blesso, 2017). However, it is possible that a diet rich in sphingomyelin precursors contributes to an increased sphingomyelin *de novo* synthesis. One striking observation I made was that the average S14 concentration measured in obese individuals compared to the minimum dose required to induce an inflammatory response *in vitro*. Although most *in vitro* experiments were performed with a slightly higher concentration to illustrate certain effects more clearly, these results were reassuring in that they confirmed a physiological relevance of

the dose range used. Importantly, it must be noted altogether that direct causality cannot be unambiguously established based on the data discussed above.

Given the results obtained from the analysis of the clinical specimens, and based on previous reports describing an elevated expression of S14 in the white adipose tissue (WAT) of obese mice and humans, it is appealing to speculate that the WAT is a major source for S14. Indeed, interrogating this question confirmed prior studies (Turner et al., 2013; Turpin et al., 2014), demonstrating that the concentration of S14 was higher in subcutaneous and visceral WAT of high-fat diet (HFD)-fed mice compared to normal CD-fed mice (Fig. 3.24A). Of note, visceral WAT, as opposed to subcutaneous WAT, has been proposed to play an essential role during inflammation in obesity and diabetes (Chait & den Hartigh, 2020). Interestingly, while the concentration of S14 did not differ between WAT types, the molar ratio of S14 to other sphingolipids was elevated in visceral compared to subcutaneous WAT of HFD-fed mice. However, whether the molar ratio of specific sphingolipids is of importance, remains to be elucidated. It could furthermore be argued that the contribution of visceral WAT to inflammation is merely dependent on its location and the fact that the amount of visceral WAT, and therefore the absolute amount of S14, is higher compared to subcutaneous WAT. Regardless, these results support the hypothesis that the measured S14 is WAT-derived, potentially contributing to adipose tissue inflammation and activation of immune cells in the periphery. In fact, a recent study by Turpin *et al.* demonstrated that elevated expression of the enzyme CerS6, which is specifically responsible for the synthesis of Cer14 and Cer16, the direct precursors of S14 and S16, correlates with obesity in both mice and humans (Turpin et al., 2014). Deletion of CerS6 protects mice from diet-induced obesity, and genetic ablation of sphingomyelin synthase (SMS) increases glucose tolerance and insulin sensitivity in HFD-fed mice, although these results cannot directly be attributed to a lack of S14 due to the universal nature of the SMS (Meikle & Summers, 2017; Turpin et al., 2014).

To support the hypothesis that increased S14 release occurs from white adipocytes in obesity, this study analyzed terminally differentiated 3T3-L1 adipocytes exposed to high glucose and insulin. The results indicated a trend towards elevated S14 synthesis in insulin-resistant adipocytes (Fig. 3.24B), confirming previous literature describing that

mature 3T3-L1 cells exposed to high glucose produce more precursor short-chain fatty acids such as C8, C10 and C14 (Roberts et al., 2009). Nevertheless, further experiments would need to be performed showing that:

- 3T3-L1 adipocytes produce *significantly* more S14 (potentially by optimizing the experimental set-up)
- 3T3-L1 adipocytes release S14 into the culture medium
- Primary adipocytes (mouse and human) behave like 3T3-L1 adipocytes

It is important to provide evidence for the second point mentioned above, to prove that S14 enters the circulation and can act on TLR4 exposed on the surface of cells. Future studies should thus include tracing experiments using either labeled sphingomyelin precursors, or labeled glucose. This idea seems feasible based on results obtained by Roberts *et al.*, showing that 3T3-L1 cells clearly utilize ^{13}C glucose for the de novo synthesis of myristic acid (Roberts et al., 2009). This approach would not only allow for discrimination of newly synthesized S14, but would also enable tracing of released S14 into the cell culture medium.

A strong relationship between obesity and atherosclerosis has been reported in literature (Grundy, 2004). The unbiased analysis of non-genetic factors contributing to disease burden in the atherosclerotic mouse model and the data obtained from the diet-associated clinical intervention studies prompted the hypothesis that circulating S14 is associated with cardiovascular disease. Indeed, my data confirmed that S14 directly affects macrophage cholesterol efflux *in vitro*, which might have important implications in light of macrophage foam cells being main drivers of atherosclerosis progression. Although sphingomyelins have been associated with reduced reverse cholesterol transport and cardiovascular disease risk (Jensen et al., 2022; Martínez-Beamonte et al., 2013), a link to individual sphingolipids such as S14, has not been established yet. Indeed, this study found that plasma S14 concentrations in plasma are higher in CAD patients, and are associated with presence of carotid plaques in obese individuals (Fig. 3.23D, E). Once again, not all sphingomyelin species exhibited a similar pattern compared to S14 (data not shown), which further supports the notion that only certain sphingolipid species contribute to inflammation. One unanticipated finding was that S14 concentrations differed only significantly amongst male, but not female participants of the 300-OB cohort.

However, research into the original publication on this cohort corroborated these findings, as the authors found specific sex-associated differences. In their investigation, they observed that the presence of metabolic syndrome was associated with hyper-responsive circulating immune cells only in male participants of the cohort (ter Horst et al., 2020).

Another unexpected finding was that within the CAD patient cohort, patients exhibited an S14 accumulation on HDL particles compared to their healthy counterparts. Although HDL has long been considered to be atheroprotective (Navab et al., 2011), recent studies have challenged the concept of HDL only being the “good” cholesterol (Yan et al., 2014). It is indeed intriguing to speculate that the composition of HDL particles plays a role in this theory. To further substantiate the data presented here, one should examine the amount of HDL present in these patients, as well as include an analysis of LDL particles, as only 30 % of circulating sphingomyelin are actually associated with HDL (Iqbal et al., 2017). In light of S14 being differentially associated with lipoprotein particles that originate from the liver, it would be highly interesting to study the liver as a potential hub for S14 handling, or potentially even *de novo* synthesis. In summary, my results are highly indicative of S14 contributing to metaflammation in context of cardiovascular disease via activation of TLR4 in peripheral immune cells.

Finally, this study also provided evidence that S14 may be considered as a contributing pro-inflammatory factor in the context of ageing. Although I only found a significantly elevated S14 concentration in plasma but not epididymal adipose tissue (eWAT) of aged mice, it appears feasible that S14 potentially plays a role in the process of ‘inflammaging’, which is conceptually certainly similar to metaflammation (Fig. 3.25). However, since the experiment performed was only preliminary, important parameters were not assessed. Firstly, it has to be taken into account that young mice are generally more lean than old mice (Von Bank et al., 2021). The eWAT mass was visually considerably higher in all old mice (this data was not recorded), indicating that the absolute amount of S14 would theoretically be higher in old compared to young mice. Secondly, no other inflammatory parameters such as cytokines and chemokines were measured. It would, therefore, surely be intriguing to study S14 in context of ageing and other metaflammation-associated disorders (e.g. neuro-inflammation) using appropriate controls and analysis parameters.

4.6 Concluding Remarks

The development of obesity-related diseases is centrally rooted in a continuous state of chronic, low-grade inflammation. While nutrient excess and TLR4 signaling are known to play an important role in context of metaflammation, the exact proximal triggers remain unknown. In this thesis, I not only identified an endogenous lipid, S14, that is positively associated with obesity, type 2 diabetes and cardiovascular disease in mice and humans, but also uncovered the potential mechanism by which it can fuel disease progression.

I could show that S14 directly engages the TLR4/MD-2 receptor complex in macrophages, leading to its dimerization and subsequent activation. S14 induced a potent pro-inflammatory response in macrophages, similar to the prototypical TLR4 ligand LPS, including an immediate activation of the human NLRP3 inflammasome.

While homeostatic S14 concentrations were comparatively low, I found both adipose tissue and systemic S14 concentrations to be increased in obesity. These results point towards TLR4 having evolved not only as a highly specific sensor of infection, but also for excess energy intake. Together, my results provide a rationale for the development of therapeutic interventions, to potentially curb inflammation in context of prevalent lifestyle-associated diseases.

5 ABSTRACT

Metaflammation, the chronic low-grade inflammation originating from metabolic organs such as adipose tissue and liver, is associated with many prevalent non-communicable diseases such as obesity, type 2 diabetes and atherosclerosis. Although we have developed a profound knowledge on the underlying disease mechanisms, the immediate triggers of metaflammation remain obscure. Here, an unbiased discovery approach was utilized to identify non-genetic factors that influence diet-induced atherosclerosis progression in mice. Integration of various parameters including thousands of host- and microbe-derived features not only confirmed well-known pro- and anti-atherogenic factors, but identified the endogenous lipid sphingomyelin d18:1/14:0 (S14) as highly associated with disease severity. *In vitro*, S14 was shown to activate pro-inflammatory innate immune signaling in macrophages in a manner that was fully dependent on TLR4 and MD-2. Molecular dynamic simulations, biochemical and cell-based analyses confirmed a direct interaction of S14 with TLR4/MD-2, promoting the formation of active TLR4/MD-2 dimers that subsequently mediated both MyD88- and TRIF-dependent signaling downstream of TLR4. Interventional studies in mice and humans confirmed the machine-learning predictions and previous literature, demonstrating that S14 concentrations are altered by dietary changes, and that an increase in S14 is associated with markers of cardiovascular disease and obesity. Collectively, the findings presented in this thesis propose a novel, host-derived TLR4 ligand of inducible nature that potentially fuels metaflammation secondary to contemporary Western-type lifestyle habits.

6 LIST OF FIGURES AND TABLES

TABLE **TITLE**

7 APPENDIX

7.1 Supplementary Figures and Tables

A

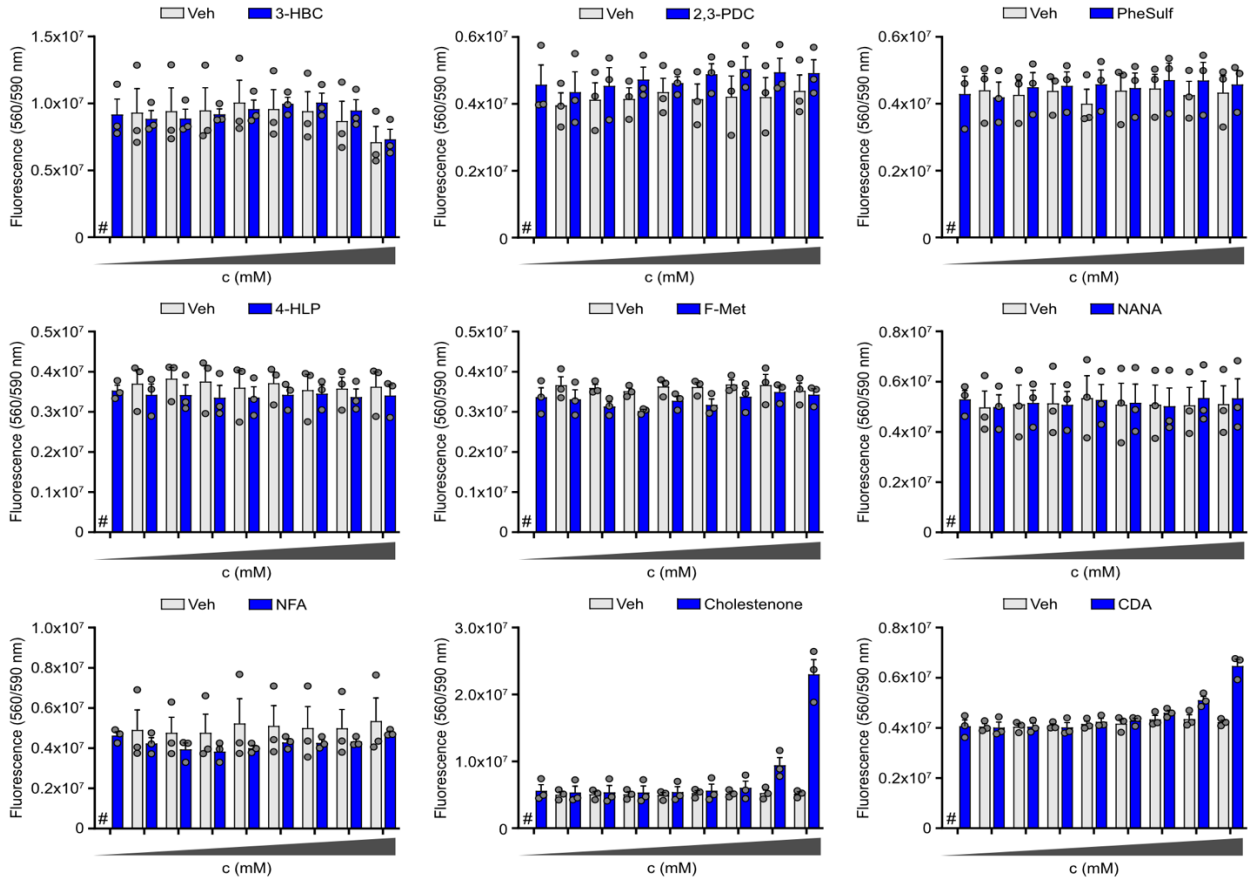

B

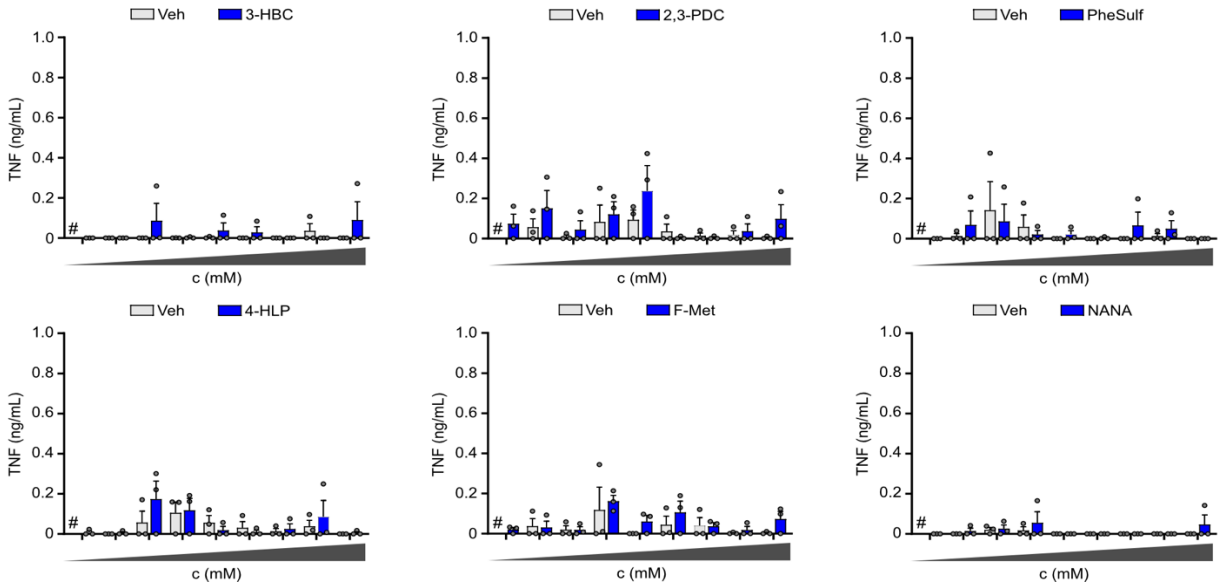

B (continued)

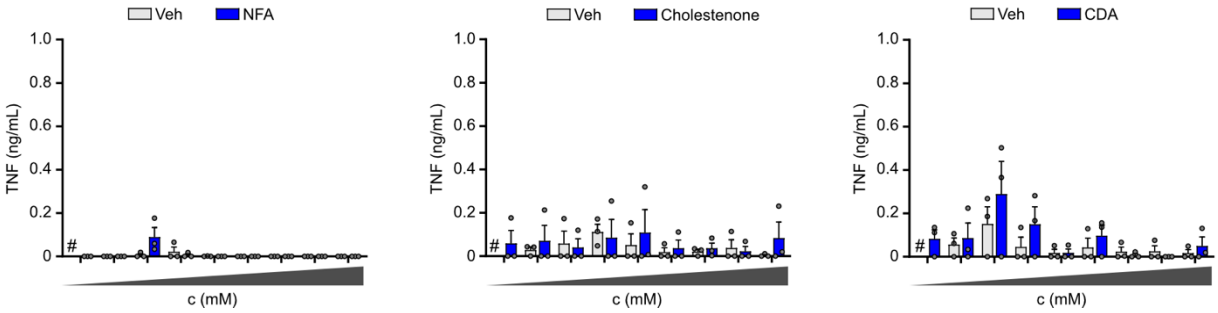

Figure S1| Effect of selected portal vein metabolites on macrophages
(A) CTB Viability Assay and (B) TNF release from WT BMDMs stimulated for 18 h with different concentrations (listed in Table S1) of the following compounds or their respective vehicle as controls: 3-Hydroxybutyrylcarnitine (3-HBC), Pyridine-2,3-dicarboxylic acid (2,3-PDC), phenol sulfate (PheSulf), 4-Hydrdxy-L-proline (4-HLP), N-Formylmethionine (F-Met), N-Acetylneuraminate (NANA), Nudifloramide (NFA), Cholestenone, Chenodeoxycholate (CDA). All data is shown as bar graphs with mean and SEM of n=3 biological replicates that are each indicated. Experiments shown in this figure were performed together with Eike Geissmar.

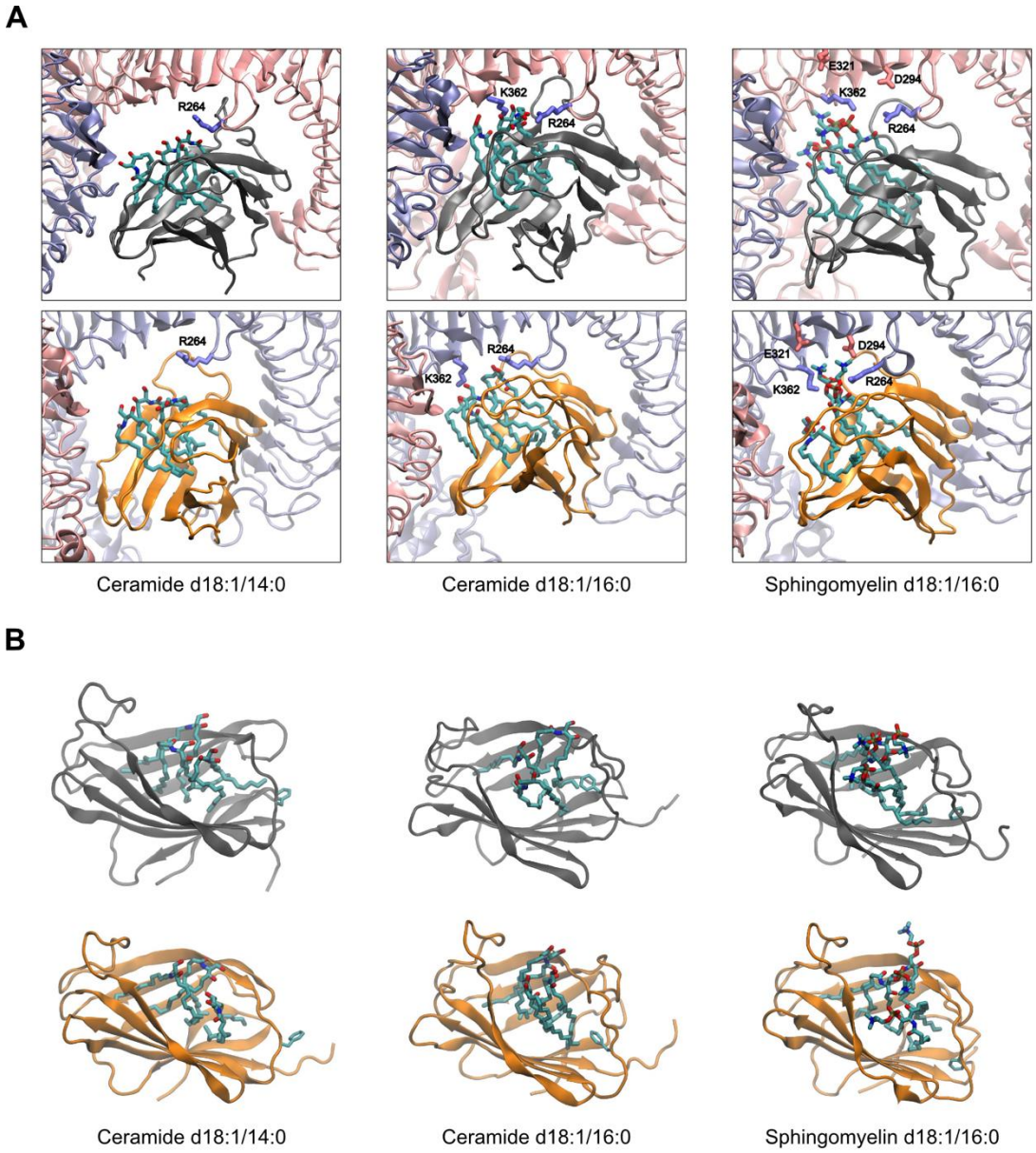

Figure S2| MD simulations investigating an interaction of selected sphingolipids and TLR4/MD-2
Individual protein chains are shown in cartoon and color-coded, whereas sphingolipid and amino acid residues are indicated in CPK licorice format. (A) Final snapshots of each side of the $(TLR4/MD\text{-}2)_2$ complex, bound to the indicated ceramide or sphingomyelin. Labelled ionizable amino acid residues observed to make significant hydrogen-bonding interactions with the respective sphingolipid during each trajectory are shown in licorice format, colored in red or blue for acidic or basic, respectively. (B) Final snapshot of each MD-2 of the $(TLR4/MD\text{-}2)_2$ complex, bound to the indicated ceramide or sphingomyelin. The data presented in this figure were provided by Jan K. Marzinek and Peter J. Bond.

Table S1: Concentrations of selected portal vein metabolites tested *in vitro*

Compound	Vehicle	Unit	Concentrations (ascending order)
3-HBC	DMSO	µM	0, 0.01, 0.03, 0.1, 0.3, 1, 3, 10, 30
2,3-PDC	H_2O	µM	0, 0.0013, 0.0064, 0.032, 0.16, 0.8, 4, 20, 100
PheSulf	DMSO	µM	0, 0.0013, 0.0064, 0.032, 0.16, 0.8, 4, 20, 100
4-HLP	H_2O	µM	0, 0.0013, 0.0064, 0.032, 0.16, 0.8, 4, 20, 100
F-Met	H_2O	µM	0, 0.0013, 0.0064, 0.032, 0.16, 0.8, 4, 20, 100
NANA	DMSO	µM	0, 0.0013, 0.0064, 0.032, 0.16, 0.8, 4, 20, 100
NFA	DMSO	µM	0, 0.0013, 0.0064, 0.032, 0.16, 0.8, 4, 20, 100
Cholestenone	EtOH	µM	0, 0.0013, 0.0064, 0.032, 0.16, 0.8, 4, 20, 100
CDA	EtOH	µM	0, 0.0013, 0.0064, 0.032, 0.16, 0.8, 4, 20, 100

7.2 Reprint Permission

Some of the figures and methods presented in this thesis have been prepared for publication and have been deposited on the preprint server Research Square under a CC Y 4.0 license. The preprint is accessible at: https://doi.org/10.21203/rs.3.rs-2792338/v1.

8 REFERENCES

Agha, M., & Agha, R. (2017). The rising prevalence of obesity: part A: impact on public health. *International Journal of Surgery: Oncology*, *2*(7), 17. https://doi.org/10.1097/IJ9.0000000000000017

Ahmed, B., Sultana, R., & Greene, M. W. (2021). Adipose tissue and insulin resistance in obese. *Biomedicine and Pharmacotherapy*, *137*. https://doi.org/10.1016/J.BIOPHA.2021.111315

Akira, S., Takeda, K., & Kaisho, T. (2001). Toll-like receptors: Critical proteins linking innate and acquired immunity. *Nature Immunology*, *2*(8), 675–680. https://doi.org/10.1038/90609

Akira, S., Uematsu, S., & Takeuchi, O. (2006). Pathogen recognition and innate immunity. *Cell*, *124*(4), 783–801. https://doi.org/10.1016/J.CELL.2006.02.015

Alberts, B., Johnson, A., Lewis, J., Raff, M., Roberts, K., & Walter, P. (2002). *Innate Immunity*. https://www.ncbi.nlm.nih.gov/books/NBK26846/

Alexander, A. F., Kelsey, I., Forbes, H., & Miller-Jensen, K. (2021). Single-cell secretion analysis reveals a dual role for IL-10 in restraining and resolving the TLR4-induced inflammatory response. *Cell Reports*, *36*(12). https://doi.org/10.1016/J.CELREP.2021.109728

Allen, A. M., & Graham, A. (2012). Mitochondrial function is involved in regulation of cholesterol efflux to apolipoprotein (apo)A-I from murine RAW 264.7 macrophages. *Lipids in Health and Disease*, *11*. https://doi.org/10.1186/1476-511X-11-169

Barton, G. M. (2008). A calculated response: control of inflammation by the innate immune system. *The Journal of Clinical Investigation*, *118*(2), 413–420. https://doi.org/10.1172/JCI34431

Bauernfeind, F. G., Horvath, G., Stutz, A., Alnemri, E. S., MacDonald, K., Speert, D., Fernandes-Alnemri, T., Wu, J., Monks, B. G., Fitzgerald, K. A., Hornung, V., & Latz, E. (2009). Cutting Edge: NF-κB Activating Pattern Recognition and Cytokine Receptors License NLRP3 Inflammasome Activation by Regulating NLRP3 Expression. *The Journal of Immunology*, *183*(2), 787–791. https://doi.org/10.4049/JIMMUNOL.0901363

Bekkering, S., Quintin, J., Joosten, L. A. B., Van Der Meer, J. W. M., Netea, M. G., & Riksen, N. P. (2014). Oxidized low-density lipoprotein induces long-term proinflammatory cytokine production and foam cell formation via epigenetic reprogramming of monocytes. *Arteriosclerosis, Thrombosis, and Vascular Biology*, *34*(8), 1731–1738. https://doi.org/10.1161/ATVBAHA.114.303887

Bentzon, J. F., Otsuka, F., Virmani, R., & Falk, E. (2014). Mechanisms of plaque formation and rupture. *Circulation Research*, *114*(12), 1852–1866. https://doi.org/10.1161/CIRCRESAHA.114.302721

Bindea, G., Galon, J., & Mlecnik, B. (2013). CluePedia Cytoscape plugin: Pathway insights using integrated experimental and in silico data. *Bioinformatics*, *29*(5), 661–663. https://doi.org/10.1093/BIOINFORMATICS/BTT019

Bindea, G., Mlecnik, B., Hackl, H., Charoentong, P., Tosolini, M., Kirilovsky, A., Fridman, W. H., Pagès, F., Trajanoski, Z., & Galon, J. (2009). ClueGO: A Cytoscape plug-in to decipher functionally grouped gene ontology and pathway annotation networks. *Bioinformatics*, *25*(8), 1091–1093. https://doi.org/10.1093/BIOINFORMATICS/BTP101

Boutens, L., & Stienstra, R. (2016). Adipose tissue macrophages: going off track during obesity. *Diabetologia*, *59*(5), 879–894. https://doi.org/10.1007/S00125-016-3904-9

Brady, R. O., Kanfer, J. N., Mock, M. B., & Fredrickson, D. S. (1966). The metabolism of sphingomyelin. II. Evidence of an enzymatic deficiency in Niemann-Pick diseae. *Proceedings of the National Academy of Sciences of the United States of America*, *55*(2), 366–369. https://doi.org/10.1073/PNAS.55.2.366

Broz, P., & Dixit, V. M. (2016). Inflammasomes: Mechanism of assembly, regulation and signalling. *Nature Reviews Immunology*, *16*(7), 407–420. https://doi.org/10.1038/NRI.2016.58

Broz, P., & Monack, D. M. (2013). Newly described pattern recognition receptors team up against intracellular pathogens. *Nature Reviews Immunology*, *13*(8), 551–565. https://doi.org/10.1038/NRI3479

Buchwald, P. (2020). A single unified model for fitting simple to complex receptor response data. *Scientific Reports*, *10*(1). https://doi.org/10.1038/S41598-020-70220-W

Caligiuri, G., Rudling, M., Ollivier, V., Jacob, M. P., Michel, J. B., Hansson, G. K., & Nicoletti, A. (2003). Interleukin-10 Deficiency Increases Atherosclerosis, Thrombosis, and Low-density Lipoproteins in Apolipoprotein E Knockout Mice. *Molecular Medicine*, *9*(1–2), 10. https://doi.org/10.1007/bf03402102

Camont, L., Chapman, M. J., & Kontush, A. (2011). Biological activities of HDL subpopulations and their relevance to cardiovascular disease. *Trends in Molecular Medicine*, *17*(10), 594–603. https://doi.org/10.1016/J.MOLMED.2011.05.013

Chait, A., & den Hartigh, L. J. (2020). Adipose Tissue Distribution, Inflammation and Its Metabolic Consequences, Including Diabetes and Cardiovascular Disease. *Frontiers in Cardiovascular Medicine*, *7*. https://doi.org/10.3389/FCVM.2020.00022

Chaplin, D. D. (2010). Overview of the immune response. *Journal of Allergy and Clinical Immunology*, *125*(2 SUPPL. 2). https://doi.org/10.1016/J.JACI.2009.12.980

Charles A Janeway, J., Travers, P., Walport, M., & Shlomchik, M. J. (2001). Immunobiology. *Immunobiology*, *14102*, 1–10. https://www.ncbi.nlm.nih.gov/books/NBK10757/

Chen, G. Y., & Nuñez, G. (2010). Sterile inflammation: Sensing and reacting to damage. *Nature Reviews Immunology*, *10*(12), 826–837. https://doi.org/10.1038/NRI2873

Christ, A., Günther, P., Lauterbach, M. A. R., Duewell, P., Biswas, D., Pelka, K., Scholz, C. J., Oosting, M., Haendler, K., Baßler, K., Klee, K., Schulte-Schrepping, J., Ulas, T., Moorlag, S. J. C. F. M., Kumar, V., Park, M. H., Joosten, L. A. B., Groh, L. A., Riksen, N. P., … Latz, E. (2018). Western Diet Triggers NLRP3-Dependent Innate Immune Reprogramming. *Cell*, *172*(1–2), 162-175.e14. https://doi.org/10.1016/J.CELL.2017.12.013

Christ, A., & Latz, E. (2019). The Western lifestyle has lasting effects on metaflammation. *Nature Reviews Immunology*, *19*(5), 267–268. https://doi.org/10.1038/S41577-019-0156-1

Cordero, M. D., Alcocer-Gómez, E., & Ryffel, B. (2018). Gain of function mutation and inflammasome driven diseases in human and mouse models. *Journal of Autoimmunity*, *91*, 13–22. https://doi.org/10.1016/J.JAUT.2018.03.002

Creagh, E. M., & O'Neill, L. A. J. (2006). TLRs, NLRs and RLRs: a trinity of pathogen sensors that co-operate in innate immunity. *Trends in Immunology*, *27*(8), 352–357. https://doi.org/10.1016/J.IT.2006.06.003

Crowther, M. A. (2005). Pathogenesis of atherosclerosis. *Hematology / the Education Program of the American Society of Hematology. American Society of Hematology. Education Program*, 436–441. https://doi.org/10.1182/ASHEDUCATION-2005.1.436

Dang, E. V., Lei, S., Radkov, A., Volk, R. F., Zaro, B. W., & Madhani, H. D. (2022). Secreted fungal virulence effector triggers allergic inflammation via TLR4. *Nature*, *608*(7921), 161–167. https://doi.org/10.1038/S41586-022-05005-4

Dinarello, C. A., & Fantuzzi, G. (2003). Interleukin-18 and host defense against infection. *Journal of Infectious Diseases*, *187*(SUPPL. 2). https://doi.org/10.1086/374751

Dobin, A., Davis, C. A., Schlesinger, F., Drenkow, J., Zaleski, C., Jha, S., Batut, P., Chaisson, M., & Gingeras, T. R. (2013). STAR: Ultrafast universal RNA-seq aligner. *Bioinformatics*, *29*(1), 15–21. https://doi.org/10.1093/BIOINFORMATICS/BTS635

Dowling, J. K., Afzal, R., Gearing, L. J., Cervantes-Silva, M. P., Annett, S., Davis, G. M., De Santi, C., Assmann, N., Dettmer, K., Gough, D. J., Bantug, G. R., Hamid, F. I., Nally, F. K., Duffy, C. P., Gorman, A. L., Liddicoat, A. M., Lavelle, E. C., Hess, C., Oefner, P. J., … McCoy, C. E. (2021). Mitochondrial arginase-2 is essential for IL-10 metabolic reprogramming of inflammatory macrophages. *Nature Communications*, *12*(1). https://doi.org/10.1038/S41467-021-21617-2

Duewell, P., Kono, H., Rayner, K. J., Sirois, C. M., Vladimer, G., Bauernfeind, F. G., Abela, G. S., Franchi, L., Nũez, G., Schnurr, M., Espevik, T., Lien, E., Fitzgerald, K. A., Rock, K. L., Moore, K. J., Wright, S. D., Hornung, V., & Latz, E. (2010). NLRP3 inflammasomes are required for atherogenesis and activated by cholesterol crystals. *Nature*, *464*(7293), 1357–1361. https://doi.org/10.1038/NATURE08938

Edsfeldt, A., Dunér, P., Stahlman, M., Mollet, I. G., Asciutto, G., Grufman, H., Nitulescu, M., Persson, A. F., Fisher, R. M., Melander, O., Orho-Melander, M., Borén, J., Nilsson, J., & Gonçalves, I. (2016). Sphingolipids contribute to human atherosclerotic plaque inflammation. *Arteriosclerosis, Thrombosis, and Vascular Biology*, *36*(6), 1132–1140. https://doi.org/10.1161/ATVBAHA.116.305675

Egger, G., & Dixon, J. (2011). Non-nutrient causes of low-grade, systemic inflammation: Support for a “canary in the mineshaft” view of obesity in chronic disease. *Obesity Reviews*, *12*(5), 339–345. https://doi.org/10.1111/J.1467-789X.2010.00795.X

Ehses, J. A., Meier, D. T., Wueest, S., Rytka, J., Boller, S., Wielinga, P. Y., Schraenen, A., Lemaire, K., Debray, S., Van Lommel, L., Pospisilik, J. A., Tschopp, O., Schultze, S. M., Malipiero, U., Esterbauer, H., Ellingsgaard, H., Rütti, S., Schuit, F. C., Lutz, T. A., … Donath, M. Y. (2010). Toll-like receptor 2-deficient mice are protected from insulin resistance and beta cell dysfunction induced by a high-fat diet. *Diabetologia*, *53*(8), 1795–1806. https://doi.org/10.1007/S00125-010-1747-3

Elinav, E., Strowig, T., Henao-Mejia, J., & Flavell, R. A. (2011). Regulation of the Antimicrobial Response by NLR Proteins. *Immunity*, *34*(5), 665–679. https://doi.org/10.1016/J.IMMUNI.2011.05.007

Emanuel, A. L., Meijer, R. I., Woerdeman, J., Van Raalte, D. H., Diamant, M., Kramer, M. H. H., Serlie, M. J., Eringa, E. C., & Serné, E. H. (2020). Effects of a Hypercaloric and Hypocaloric Diet on Insulin-Induced Microvascular Recruitment, Glucose Uptake, and Lipolysis in Healthy Lean Men. *Arteriosclerosis, Thrombosis, and Vascular Biology*, *40*(7), 1695–1704. https://doi.org/10.1161/ATVBAHA.120.314129

Epstein, F. H., Fuster, V., Badimon, L., Badimon, J. J., & Chesebro, J. H. (1992). The Pathogenesis of Coronary Artery Disease and the Acute Coronary Syndromes. *New*

England Journal of Medicine, *326*(5), 310–318. https://doi.org/10.1056/NEJM199201303260506

Essmann, U., Perera, L., Berkowitz, M. L., Darden, T., Lee, H., & Pedersen, L. G. (1995). A smooth particle mesh Ewald method. *The Journal of Chemical Physics*, *103*(19), 8577–8593. https://doi.org/10.1063/1.470117

Eyerich, S., Eyerich, K., Traidl-Hoffmann, C., & Biedermann, T. (2018). Cutaneous Barriers and Skin Immunity: Differentiating A Connected Network. *Trends in Immunology*, *39*(4), 315–327. https://doi.org/10.1016/J.IT.2018.02.004

Fang, H., Wu, Y., Huang, X., Wang, W., Ang, B., Cao, X., & Wan, T. (2011). Toll-like receptor 4 (TLR4) is essential for Hsp70-like protein 1 (HSP70L1) to activate dendritic cells and induce Th1 response. *Journal of Biological Chemistry*, *286*(35), 30393–30400. https://doi.org/10.1074/JBC.M111.266528

Fanucchi, S., Domínguez-Andrés, J., Joosten, L. A. B., Netea, M. G., & Mhlanga, M. M. (2021). The Intersection of Epigenetics and Metabolism in Trained Immunity. *Immunity*, *54*(1), 32–43. https://doi.org/10.1016/J.IMMUNI.2020.10.011

Ferrucci, L., & Fabbri, E. (2018). Inflammageing: chronic inflammation in ageing, cardiovascular disease, and frailty. *Nature Reviews Cardiology*, *15*(9), 505–522. https://doi.org/10.1038/S41569-018-0064-2

Findeisen, H. M., Pearson, K. J., Gizard, F., Zhao, Y., Qing, H., Jones, K. L., Cohn, D., Heywood, E. B., de Cabo, R., & Bruemmer, D. (2011). Oxidative stress accumulates in adipose tissue during aging and inhibits adipogenesis. *PLoS ONE*, *6*(4). https://doi.org/10.1371/JOURNAL.PONE.0018532

Fischer, H., Ellström, P., Ekström, K., Gustafsson, L., Gustafsson, M., & Svanborg, C. (2007). Ceramide as a TLR4 agonist; a putative signalling intermediate between sphingolipid receptors for microbial ligands and TLR4. *Cellular Microbiology*, *9*(5), 1239–1251. https://doi.org/10.1111/J.1462-5822.2006.00867.X

Foell, D., Wittkowski, H., Kessel, C., Lüken, A., Weinhage, T., Varga, G., Vogl, T., Wirth, T., Viemann, D., Björk, P., Van Zoelen, M. A. D., Gohar, F., Srikrishna, G., Kraft, M., & Roth, J. (2013). Proinflammatory S100A12 can activate human monocytes via toll-like receptor 4. *American Journal of Respiratory and Critical Care Medicine*, *187*(12), 1324–1334. https://doi.org/10.1164/RCCM.201209-1602OC

Fontana, L., Eagon, J. C., Trujillo, M. E., Scherer, P. E., & Klein, S. (2007). Visceral fat adipokine secretion is associated with systemic inflammation in obese humans. *Diabetes*, *56*(4), 1010–1013. https://doi.org/10.2337/DB06-1656

Frostegård, J. (2013). Immunity, atherosclerosis and cardiovascular disease. *BMC Medicine*, *11*(1). https://doi.org/10.1186/1741-7015-11-117

Gaggini, M., Ndreu, R., Michelucci, E., Rocchiccioli, S., & Vassalle, C. (2022). Ceramides as Mediators of Oxidative Stress and Inflammation in Cardiometabolic Disease. *International Journal of Molecular Sciences*, *23*(5). https://doi.org/10.3390/IJMS23052719

Gaidt, M. M., Ebert, T. S., Chauhan, D., Schmidt, T., Schmid-Burgk, J. L., Rapino, F., Robertson, A. A. B., Cooper, M. A., Graf, T., & Hornung, V. (2016). Human Monocytes Engage an Alternative Inflammasome Pathway. *Immunity*, *44*(4), 833–846. https://doi.org/10.1016/J.IMMUNI.2016.01.012

Gaidt, M. M., & Hornung, V. (2017). Alternative inflammasome activation enables IL-1β release from living cells. *Current Opinion in Immunology*, *44*, 7–13. https://doi.org/10.1016/J.COI.2016.10.007

Gault, C. R., Obeid, L. M., & Hannun, Y. A. (2010). An overview of sphingolipid metabolism: From synthesis to breakdown. *Advances in Experimental Medicine and Biology*, *688*, 1–23. https://doi.org/10.1007/978-1-4419-6741-1_1

Gay, N. J., Symmons, M. F., Gangloff, M., & Bryant, C. E. (2014). Assembly and localization of Toll-like receptor signalling complexes. *Nature Reviews Immunology*, *14*(8), 546–558. https://doi.org/10.1038/NRI3713

Gordon, D. J., Probstfield, J. L., Garrison, R. J., Neaton, J. D., Castelli, W. P., Knoke, J. D., Jacobs, D. R., Bangdiwala, S., & Tyroler, H. A. (1989a). High-density lipoprotein cholesterol and cardiovascular disease. Four prospective American studies. *Circulation*, *79*(1), 8–15. https://doi.org/10.1161/01.CIR.79.1.8

Gordon, D. J., Probstfield, J. L., Garrison, R. J., Neaton, J. D., Castelli, W. P., Knoke, J. D., Jacobs, D. R., Bangdiwala, S., & Tyroler, H. A. (1989b). High-density lipoprotein cholesterol and cardiovascular disease. Four prospective American studies. *Circulation*, *79*(1), 8–15. https://doi.org/10.1161/01.CIR.79.1.8

Gordon, T., Castelli, W. P., Hjortland, M. C., Kannel, W. B., & Dawber, T. R. (1977). High density lipoprotein as a protective factor against coronary heart disease. The Framingham study. *The American Journal of Medicine*, *62*(5), 707–714. https://doi.org/10.1016/0002-9343(77)90874-9

Green, C. D., Maceyka, M., Cowart, L. A., & Spiegel, S. (2021). Sphingolipids in metabolic disease: The good, the bad, and the unknown. *Cell Metabolism*, *33*(7), 1293–1306. https://doi.org/10.1016/J.CMET.2021.06.006

Gritsenko, A., Green, J. P., Brough, D., & Lopez-Castejon, G. (2020). Mechanisms of NLRP3 priming in inflammaging and age related diseases. *Cytokine and Growth Factor Reviews*, *55*, 15–25. https://doi.org/10.1016/J.CYTOGFR.2020.08.003

Grundy, S. M. (2004). Obesity, metabolic syndrome, and cardiovascular disease. *Journal of Clinical Endocrinology and Metabolism*, *89*(6), 2595–2600. https://doi.org/10.1210/JC.2004-0372

Haase, J., Weyer, U., Immig, K., Klöting, N., Blüher, M., Eilers, J., Bechmann, I., & Gericke, M. (2014). Local proliferation of macrophages in adipose tissue during obesity-induced inflammation. *Diabetologia*, *57*(3), 562–571. https://doi.org/10.1007/S00125-013-3139-Y

Hahn, B. H., Grossman, J., Ansell, B. J., Skaggs, B. J., & McMahon, M. (2008). Altered lipoprotein metabolism in chronic inflammatory states: Proinflammatory high-density lipoprotein and accelerated atherosclerosis in systemic lupus erythematosus and rheumatoid arthritis. *Arthritis Research and Therapy*, *10*(4). https://doi.org/10.1186/AR2471

Hammad, S. M., Pierce, J. S., Soodavar, F., Smith, K. J., Al Gadban, M. M., Rembiesa, B., Klein, R. L., Hannun, Y. A., Bielawski, J., & Bielawska, A. (2010). Blood sphingolipidomics in healthy humans: impact of sample collection methodology. *Journal of Lipid Research*, *51*(10), 3074–3087. https://doi.org/10.1194/JLR.D008532

Hannun, Y. A., & Obeid, L. M. (2018). Sphingolipids and their metabolism in physiology and disease. *Nature Reviews Molecular Cell Biology*, *19*(3), 175–191. https://doi.org/10.1038/NRM.2017.107

Hansson, G. K., & Hermansson, A. (2011). The immune system in atherosclerosis. *Nature Immunology*, *12*(3), 204–212. https://doi.org/10.1038/NI.2001

He, W. T., Wan, H., Hu, L., Chen, P., Wang, X., Huang, Z., Yang, Z. H., Zhong, C. Q., & Han, J. (2015). Gasdermin D is an executor of pyroptosis and required for

interleukin-1β secretion. *Cell Research*, *25*(12), 1285–1298. https://doi.org/10.1038/CR.2015.139

Hegele, R. A. (2009). Plasma lipoproteins: Genetic influences and clinical implications. *Nature Reviews Genetics*, *10*(2), 109–121. https://doi.org/10.1038/NRG2481

Hersoug, L. G., Møller, P., & Loft, S. (2018). Role of microbiota-derived lipopolysaccharide in adipose tissue inflammation, adipocyte size and pyroptosis during obesity. *Nutrition Research Reviews*, *31*(2), 153–163. https://doi.org/10.1017/S0954422417000269

Hildebrandt, X., Ibrahim, M., & Peltzer, N. (2023). Cell death and inflammation during obesity: "Know my methods, WAT(son)." *Cell Death and Differentiation*, *30*(2), 279–292. https://doi.org/10.1038/S41418-022-01062-4

Hosseini, Z., Whiting, S. J., & Vatanparast, H. (2016). Current evidence on the association of the metabolic syndrome and dietary patterns in a global perspective. *Nutrition Research Reviews*, *29*(2), 152–162. https://doi.org/10.1017/S095442241600007X

Hotamisligil, G. S. (2006). Inflammation and metabolic disorders. *Nature*, *444*(7121), 860–867. https://doi.org/10.1038/NATURE05485

Hotamisligil, G. S. (2017a). Inflammation, metaflammation and immunometabolic disorders. *Nature*, *542*(7640), 177–185. https://doi.org/10.1038/NATURE21363

Hotamisligil, G. S. (2017b). Inflammation, metaflammation and immunometabolic disorders. *Nature*, *542*(7640), 177–185. https://doi.org/10.1038/NATURE21363

Huang, J., Rauscher, S., Nawrocki, G., Ran, T., Feig, M., De Groot, B. L., Grubmüller, H., & MacKerell, A. D. (2016). CHARMM36m: An improved force field for folded and intrinsically disordered proteins. *Nature Methods*, *14*(1), 71–73. https://doi.org/10.1038/NMETH.4067

Humphrey, W., Dalke, A., & Schulten, K. (1996). VMD: Visual molecular dynamics. *Journal of Molecular Graphics*, *14*(1), 33–38. https://doi.org/10.1016/0263-7855(96)00018-5

Ihaka, R., & Gentleman, R. (1996). R: A Language for Data Analysis and Graphics. *Journal of Computational and Graphical Statistics*, *5*(3), 299–314. https://doi.org/10.1080/10618600.1996.10474713

Im, S. S., Park, H. Y., Shon, J. C., Chung, I. S., Cho, H. C., Liu, K. H., & Song, D. K. (2019). Plasma sphingomyelins increase in pre-diabetic Korean men with abdominal obesity. *PLoS ONE*, *14*(3). https://doi.org/10.1371/JOURNAL.PONE.0213285

Iqbal, J., Walsh, M. T., Hammad, S. M., & Hussain, M. M. (2017). Sphingolipids and Lipoproteins in Health and Metabolic Disorders. *Trends in Endocrinology and Metabolism*, *28*(7), 506–518. https://doi.org/10.1016/J.TEM.2017.03.005

Isambert, N., Fumoleau, P., Paul, C., Ferrand, C., Zanetta, S., Bauer, J., Ragot, K., Lizard, G., Jeannin, J. F., & Bardou, M. (2013). Phase I study of OM-174, a lipid A analogue, with assessment of immunological response, in patients with refractory solid tumors. *BMC Cancer*, *13*. https://doi.org/10.1186/1471-2407-13-172

Ivashkiv, L. B., & Donlin, L. T. (2014). Regulation of type i interferon responses. *Nature Reviews Immunology*, *14*(1), 36–49. https://doi.org/10.1038/NRI3581

Iwasaki, A., & Medzhitov, R. (2015). Control of adaptive immunity by the innate immune system. *Nature Immunology*, *16*(4), 343–353. https://doi.org/10.1038/NI.3123

Jang, J. C., Li, J., Gambini, L., Batugedara, H. M., Sati, S., Lazar, M. A., Fan, L., Pellecchia, M., & Nair, M. G. (2017). Human resistin protects against endotoxic

shock by blocking LPS–TLR4 interaction. *Proceedings of the National Academy of Sciences of the United States of America*, *114*(48), E10399–E10408. https://doi.org/10.1073/PNAS.1716015114

Jensen, P. N., Fretts, A. M., Hoofnagle, A. N., McKnight, B., Howard, B. V., Umans, J. G., Sitlani, C. M., Siscovick, D. S., King, I. B., Sotoodehnia, N., & Lemaitre, R. N. (2022). Circulating ceramides and sphingomyelins and the risk of incident cardiovascular disease among people with diabetes: the strong heart study. *Cardiovascular Diabetology*, *21*(1). https://doi.org/10.1186/S12933-022-01596-4

Jiang, X. C., Paultre, F., Pearson, T. A., Reed, R. G., Francis, C. K., Lin, M., Berglund, L., & Tall, A. R. (2000). Plasma sphingomyelin level as a risk factor for coronary artery disease. *Arteriosclerosis, Thrombosis, and Vascular Biology*, *20*(12), 2614–2618. https://doi.org/10.1161/01.ATV.20.12.2614

Jo, S., Kim, T., Iyer, V. G., & Im, W. (2008). CHARMM-GUI: A web-based graphical user interface for CHARMM. *Journal of Computational Chemistry*, *29*(11), 1859–1865. https://doi.org/10.1002/JCC.20945

Jonasson, L., Holm, J., Skalli, O., Bondjers, G., & Hansson, G. K. (1986). Regional accumulations of T cells, macrophages, and smooth muscle cells in the human atherosclerotic plaque. *Arteriosclerosis*, *6*(2), 131–138. https://doi.org/10.1161/01.ATV.6.2.131

Jorgensen, W. L., Chandrasekhar, J., Madura, J. D., Impey, R. W., & Klein, M. L. (1983). Comparison of simple potential functions for simulating liquid water. *The Journal of Chemical Physics*, *79*(2), 926–935. https://doi.org/10.1063/1.445869

Kahn, B. B., & Flier, J. S. (2000). Obesity and insulin resistance. *Journal of Clinical Investigation*, *106*(4), 473–481. https://doi.org/10.1172/JCI10842

Kaser, S., Kaser, A., Sandhofer, A., Ebenbichler, C. F., Tilg, H., & Patsch, J. R. (2003). Resistin messenger-RNA expression is increased by proinflammatory cytokines in vitro. *Biochemical and Biophysical Research Communications*, *309*(2), 286–290. https://doi.org/10.1016/J.BBRC.2003.07.003

Kawasaki, T., & Kawai, T. (2014). Toll-like receptor signaling pathways. *Frontiers in Immunology*, *5*(SEP). https://doi.org/10.3389/FIMMU.2014.00461

Khan, S., Chan, Y. T., Revelo, X. S., & Winer, D. A. (2020). The Immune Landscape of Visceral Adipose Tissue During Obesity and Aging. *Frontiers in Endocrinology*, *11*. https://doi.org/10.3389/FENDO.2020.00267

Khera, A. V., & Rader, D. J. (2010). Future therapeutic directions in reverse cholesterol transport. *Current Atherosclerosis Reports*, *12*(1), 73–81. https://doi.org/10.1007/S11883-009-0080-0

Kikas, P., Chalikias, G., & Tziakas, D. (2018). Cardiovascular implications of sphingomyelin presence in biological membranes. *European Cardiology Review* , *13*(1), 42–45. https://doi.org/10.15420/ECR.2017:20:3

Kim, S., Young Kim, S., Pribis, J. P., Lotze, M., Mollen, K. P., Shapiro, R., Loughran, P., Scott, M. J., & Billiar, T. R. (2013). Signaling of high mobility group box 1 (HMGB1) through toll-like receptor 4 in macrophages requires CD14. *Molecular Medicine*, *19*(1), 88–98. https://doi.org/10.2119/MOLMED.2012.00306

Kochumon, S., Wilson, A., Chandy, B., Shenouda, S., Tuomilehto, J., Sindhu, S., & Ahmad, R. (2018). Palmitate Activates CCL4 Expression in Human Monocytic Cells via TLR4/MyD88 Dependent Activation of NF-κB/MAPK/ PI3K Signaling Systems. *Cellular Physiology and Biochemistry*, *46*(3), 953–964. https://doi.org/10.1159/000488824

Kumar, H., Kawai, T., & Akira, S. (2011). Pathogen recognition by the innate immune system. *International Reviews of Immunology*, *30*(1), 16–34. https://doi.org/10.3109/08830185.2010.529976

Lai, Y., Tian, Y., You, X., Du, J., & Huang, J. (2022). Effects of sphingolipid metabolism disorders on endothelial cells. *Lipids in Health and Disease*, *21*(1). https://doi.org/10.1186/S12944-022-01701-2

Lancaster, G. I., Langley, K. G., Berglund, N. A., Kammoun, H. L., Reibe, S., Estevez, E., Weir, J., Mellett, N. A., Pernes, G., Conway, J. R. W., Lee, M. K. S., Timpson, P., Murphy, A. J., Masters, S. L., Gerondakis, S., Bartonicek, N., Kaczorowski, D. C., Dinger, M. E., Meikle, P. J., … Febbraio, M. A. (2018). Evidence that TLR4 Is Not a Receptor for Saturated Fatty Acids but Mediates Lipid-Induced Inflammation by Reprogramming Macrophage Metabolism. *Cell Metabolism*, *27*(5), 1096-1110.e5. https://doi.org/10.1016/J.CMET.2018.03.014

Latz, E., Xiao, T. S., & Stutz, A. (2013). Activation and regulation of the inflammasomes. *Nature Reviews Immunology*, *13*(6), 397–411. https://doi.org/10.1038/NRI3452

Lauterbach, M. A., Hanke, J. E., Serefidou, M., Mangan, M. S. J., Kolbe, C. C., Hess, T., Rothe, M., Kaiser, R., Hoss, F., Gehlen, J., Engels, G., Kreutzenbeck, M., Schmidt, S. V., Christ, A., Imhof, A., Hiller, K., & Latz, E. (2019). Toll-like Receptor Signaling Rewires Macrophage Metabolism and Promotes Histone Acetylation via ATP-Citrate Lyase. *Immunity*, *51*(6), 997-1011.e7. https://doi.org/10.1016/J.IMMUNI.2019.11.009

Lebovitz, H. E. (2001). Insulin resistance: Definition and consequences. *Experimental and Clinical Endocrinology and Diabetes*, *109*(SUPPL. 2). https://doi.org/10.1055/S-2001-18576

Lee, G. L., Wu, J. Y., Tsai, C. S., Lin, C. Y., Tsai, Y. T., Lin, C. S., Wang, Y. F., Yet, S. F., Hsu, Y. J., & Kuo, C. C. (2016). TLR4-activated MAPK-IL-6 axis regulates vascular smooth muscle cell function. *International Journal of Molecular Sciences*, *17*(9). https://doi.org/10.3390/IJMS17091394

Lemaitre, B., Nicolas, E., Michaut, L., Reichhart, J. M., & Hoffmann, J. A. (1996). The dorsoventral regulatory gene cassette spatzle/Toll/Cactus controls the potent antifungal response in Drosophila adults. *Cell*, *86*(6), 973–983. https://doi.org/10.1016/S0092-8674(00)80172-5

Lewis, A. J., Seymour, C. W., & Rosengart, M. R. (2016). Current Murine Models of Sepsis. *Surgical Infections*, *17*(4), 385–393. https://doi.org/10.1089/SUR.2016.021

Lewis, G. F., & Rader, D. J. (2005). New insights into the regulation of HDL metabolism and reverse cholesterol transport. *Circulation Research*, *96*(12), 1221–1232. https://doi.org/10.1161/01.RES.0000170946.56981.5C

Li, D., & Wu, M. (2021). Pattern recognition receptors in health and diseases. *Signal Transduction and Targeted Therapy*, *6*(1). https://doi.org/10.1038/S41392-021-00687-0

Li, Y., Yun, K., & Mu, R. (2020). A review on the biology and properties of adipose tissue macrophages involved in adipose tissue physiological and pathophysiological processes. *Lipids in Health and Disease*, *19*(1). https://doi.org/10.1186/S12944-020-01342-3

Liu, X., Zhang, Z., Ruan, J., Pan, Y., Magupalli, V. G., Wu, H., & Lieberman, J. (2016). Inflammasome-activated gasdermin D causes pyroptosis by forming membrane pores. *Nature*, *535*(7610), 153–158. https://doi.org/10.1038/NATURE18629

Lumeng, C. N., Bodzin, J. L., & Saltiel, A. R. (2007). Obesity induces a phenotypic switch in adipose tissue macrophage polarization. *Journal of Clinical Investigation*, *117*(1), 175–184. https://doi.org/10.1172/JCI29881

MacEyka, M., & Spiegel, S. (2014). Sphingolipid metabolites in inflammatory disease. *Nature*, *510*(7503), 58–67. https://doi.org/10.1038/NATURE13475

MacKenzie, S., Fernàndez-Troy, N., & Espel, E. (2002). Post-transcriptional regulation of TNF-α during in vitro differentiation of human monocytes/macrophages in primary culture. *Journal of Leukocyte Biology*, *71*(6), 1026–1032. https://doi.org/10.1189/JLB.71.6.1026

MacLeod, M. K. L., McKee, A. S., David, A., Wang, J., Mason, R., Kappler, J. W., & Marrack, P. (2011). Vaccine adjuvants aluminum and monophosphoryl lipid A provide distinct signals to generate protective cytotoxic memory CD8 T cells. *Proceedings of the National Academy of Sciences of the United States of America*, *108*(19), 7914–7919. https://doi.org/10.1073/PNAS.1104588108

MacMahon, S., Duffy, S., Rodgers, A., Tominaga, S., Chambless, L., De Backer, G., De Bacquer, D., Kornitzer, M., Whincup, P., Wannamethee, S. G., Morris, R., Wald, N., Morris, J., Law, M., Knuiman, M., Bartholomew, H., Davey Smith, G., Sweetnam, P., Elwood, P., … Whitlock, G. (2007). Blood cholesterol and vascular mortality by age, sex, and blood pressure: A meta-analysis of individual data from 61 prospective studies with 55 000 vascular deaths. *The Lancet*, *370*(9602), 1829–1839. https://doi.org/10.1016/S0140-6736(07)61778-4

Maeshima, N., & Fernandez, R. C. (2013). Recognition of lipid A variants by the TLR4-MD-2 receptor complex. *Frontiers in Cellular and Infection Microbiology*, *4*(FEB). https://doi.org/10.3389/FCIMB.2013.00003

Mallat, Z., Besnard, S., Duriez, M., Deleuze, V., Emmanuel, F., Bureau, M. F., Soubrier, F., Esposito, B., Duez, H., Fievet, C., Staels, B., Duverger, N., Scherman, D., & Tedgui, A. (1999). Protective role of interleukin-10 in atherosclerosis. *Circulation Research*, *85*(8). https://doi.org/10.1161/01.RES.85.8.E17

Mangan, M. S. J., Olhava, E. J., Roush, W. R., Seidel, H. M., Glick, G. D., & Latz, E. (2018). Targeting the NLRP3 inflammasome in inflammatory diseases. *Nature Reviews Drug Discovery*, *17*(8), 588–606. https://doi.org/10.1038/NRD.2018.97

Marchesini, N., & Hannun, Y. A. (2004). Acid and neutral sphingomyelinases: Roles and mechanisms of regulation. *Biochemistry and Cell Biology*, *82*(1), 27–44. https://doi.org/10.1139/O03-091

Martínez-Beamonte, R., Lou-Bonafonte, J. M., Martínez-Gracia, M. V., & Osada, J. (2013). Sphingomyelin in High-Density Lipoproteins: Structural Role and Biological Function. *International Journal of Molecular Sciences*, *14*(4), 7716–7741. https://doi.org/10.3390/IJMS14047716

Martínez-Ramírez, M., Madero, M., Vargas-Alarcón, G., Vargas-Barrón, J., Fragoso, J. M., Rodríguez-Pérez, J. M., Martínez-Sánchez, C., González-Pacheco, H., Bautista-Pérez, R., Carreón-Torres, E., & Pérez-Méndez, O. (2016). HDL-sphingomyelin reduction after weight loss by an energy-restricted diet is associated with the improvement of lipid profile, blood pressure, and decrease of insulin resistance in overweight/obese patients. *Clinica Chimica Acta*, *454*, 77–81. https://doi.org/10.1016/J.CCA.2015.12.039

Masana, L., Plana, N., Andreychuk, N., & Ibarretxe, D. (2023). Lipid lowering combination therapy: From prevention to atherosclerosis plaque treatment. *Pharmacological Research*, *190*. https://doi.org/10.1016/J.PHRS.2023.106738

Matsunaga, N., Tsuchimori, N., Matsumoto, T., & Ii, M. (2011). TAK-242 (resatorvid), a small-molecule inhibitor of Toll-like receptor (TLR) 4 signaling, binds selectively to TLR4 and interferes with interactions between TLR4 and its adaptor molecules. *Molecular Pharmacology*, *79*(1), 34–41. https://doi.org/10.1124/MOL.110.068064

Matzinger, P. (2002). The danger model: A renewed sense of self. *Science*, *296*(5566), 301–305. https://doi.org/10.1126/SCIENCE.1071059

McGovern, M. M., Avetisyan, R., Sanson, B. J., & Lidove, O. (2017). Disease manifestations and burden of illness in patients with acid sphingomyelinase deficiency (ASMD). *Orphanet Journal of Rare Diseases*, *12*(1). https://doi.org/10.1186/S13023-017-0572-X

McNelis, J. C., & Olefsky, J. M. (2014). Macrophages, Immunity, and Metabolic Disease. *Immunity*, *41*(1), 36–48. https://doi.org/10.1016/J.IMMUNI.2014.05.010

Medzhitov, R. (2007). Recognition of microorganisms and activation of the immune response. *Nature*, *449*(7164), 819–826. https://doi.org/10.1038/NATURE06246

Medzhitov, R., & Janeway, C. A. (1997). Innate immunity: The virtues of a nonclonal system of recognition. *Cell*, *91*(3), 295–298. https://doi.org/10.1016/S0092-8674(00)80412-2

Medzhitov, R., Preston-Hurlburt, P., & Janeway, C. A. (1997). A human homologue of the Drosophila toll protein signals activation of adaptive immunity. *Nature*, *388*(6640), 394–397. https://doi.org/10.1038/41131

Meikle, P. J., & Summers, S. A. (2017). Sphingolipids and phospholipids in insulin resistance and related metabolic disorders. *Nature Reviews Endocrinology*, *13*(2), 79–91. https://doi.org/10.1038/NRENDO.2016.169

Meunier, E., & Broz, P. (2017). Evolutionary Convergence and Divergence in NLR Function and Structure. *Trends in Immunology*, *38*(10), 744–757. https://doi.org/10.1016/J.IT.2017.04.005

Miller, Y. I., Choi, S. H., Wiesner, P., Fang, L., Harkewicz, R., Hartvigsen, K., Boullier, A., Gonen, A., Diehl, C. J., Que, X., Montano, E., Shaw, P. X., Tsimikas, S., Binder, C. J., & Witztum, J. L. (2011). Oxidation-specific epitopes are danger-associated molecular patterns recognized by pattern recognition receptors of innate immunity. *Circulation Research*, *108*(2), 235–248. https://doi.org/10.1161/CIRCRESAHA.110.223875

Mills, C. D., Kincaid, K., Alt, J. M., Heilman, M. J., & Hill, A. M. (2000). M-1/M-2 Macrophages and the Th1/Th2 Paradigm. *The Journal of Immunology*, *164*(12), 6166–6173. https://doi.org/10.4049/JIMMUNOL.164.12.6166

Min, B. K., Park, S., Kang, H. J., Kim, D. W., Ham, H. J., Ha, C. M., Choi, B. J., Lee, J. Y., Oh, C. J., Yoo, E. K., Kim, H. E., Kim, B. G., Jeon, J. H., Hyeon, D. Y., Hwang, D., Kim, Y. H., Lee, C. H., Lee, T., Jungwhan, K., … Lee, I. K. (2019). Pyruvate dehydrogenase kinase is a metabolic checkpoint for polarization of macrophages to the M1 phenotype. *Frontiers in Immunology*, *10*(MAY). https://doi.org/10.3389/FIMMU.2019.00944

Molteni, M., Gemma, S., & Rossetti, C. (2016). The Role of Toll-Like Receptor 4 in Infectious and Noninfectious Inflammation. *Mediators of Inflammation*, *2016*. https://doi.org/10.1155/2016/6978936

Mori, M. A., Bezy, O., & Kahn, C. R. (2011). Metabolic syndrome: Is Nlrp3 inflammasome a trigger or a target of insulin resistance? *Circulation Research*, *108*(10), 1160–1162. https://doi.org/10.1161/RES.0B013E318220B57B

Moser, V. A., Uchoa, M. F., & Pike, C. J. (2018). TLR4 inhibitor TAK-242 attenuates the adverse neural effects of diet-induced obesity. *Journal of Neuroinflammation*, *15*(1). https://doi.org/10.1186/S12974-018-1340-0

Mullarkey, M., Rose, J. R., Bristol, J., Kawata, T., Kimura, A., Kobayashi, S., Przetak, M., Chow, J., Gusovsky, F., Christ, W. J., & Rossignol, D. P. (2003). Inhibition of endotoxin response by E5564, a novel toll-like receptor 4-directed endotoxin antagonist. *Journal of Pharmacology and Experimental Therapeutics*, *304*(3), 1093–1102. https://doi.org/10.1124/JPET.102.044487

Murphy, S. A., & Nicolaou, A. (2013). Lipidomics applications in health, disease and nutrition research. *Molecular Nutrition and Food Research*, *57*(8), 1336–1346. https://doi.org/10.1002/MNFR.201200863

Murray, R. Z., & Stow, J. L. (2014). Cytokine secretion in macrophages: SNAREs, Rabs, and membrane trafficking. *Frontiers in Immunology*, *5*(OCT). https://doi.org/10.3389/FIMMU.2014.00538

Nagaev, I., Bokarewa, M., Tarkowski, A., & Smith, U. (2006). Human resistin is a systemic immune-derived proinflammatory cytokine targeting both leukocytes and adipocytes. *PLoS ONE*, *1*(1). https://doi.org/10.1371/JOURNAL.PONE.0000031

Navab, M., Reddy, S. T., Van Lenten, B. J., & Fogelman, A. M. (2011). HDL and cardiovascular disease: Atherogenic and atheroprotective mechanisms. *Nature Reviews Cardiology*, *8*(4), 222–232. https://doi.org/10.1038/NRCARDIO.2010.222

Netea, M. G., Domínguez-Andrés, J., Barreiro, L. B., Chavakis, T., Divangahi, M., Fuchs, E., Joosten, L. A. B., van der Meer, J. W. M., Mhlanga, M. M., Mulder, W. J. M., Riksen, N. P., Schlitzer, A., Schultze, J. L., Stabell Benn, C., Sun, J. C., Xavier, R. J., & Latz, E. (2020). Defining trained immunity and its role in health and disease. *Nature Reviews Immunology*, *20*(6), 375–388. https://doi.org/10.1038/S41577-020-0285-6

Netea, M. G., Quintin, J., & Van Der Meer, J. W. M. (2011). Trained immunity: A memory for innate host defense. *Cell Host and Microbe*, *9*(5), 355–361. https://doi.org/10.1016/J.CHOM.2011.04.006

Nixon, G. F. (2009). Sphingolipids in inflammation: Pathological implications and potential therapeutic targets. *British Journal of Pharmacology*, *158*(4), 982–993. https://doi.org/10.1111/J.1476-5381.2009.00281.X

Norris, G. H., & Blesso, C. N. (2017). Dietary and endogenous sphingolipid metabolism in chronic inflammation. *Nutrients*, *9*(11). https://doi.org/10.3390/NU9111180

Ohto, U., Fukase, K., Miyake, K., & Shimizu, T. (2012). Structural basis of species-specific endotoxin sensing by innate immune receptor TLR4/MD-2. *Proceedings of the National Academy of Sciences of the United States of America*, *109*(19), 7421–7426. https://doi.org/10.1073/PNAS.1201193109

O'Neill, L. A. J., Golenbock, D., & Bowie, A. G. (2013). The history of Toll-like receptors-redefining innate immunity. *Nature Reviews Immunology*, *13*(6), 453–460. https://doi.org/10.1038/NRI3446

O'Neill, L. A. J., Hennessy, E. J., & Parker, A. E. (2010). Targeting Toll-like receptors: emerging therapeutics? *Nature Reviews. Drug Discovery*, *9*(4), 293–307. https://doi.org/10.1038/NRD3203

Orecchioni, M., Ghosheh, Y., Pramod, A. B., & Ley, K. (2020). Corrigendum: Macrophage Polarization: Different Gene Signatures in M1(LPS+) vs. Classically and M2(LPS–) vs. Alternatively Activated Macrophages (Frontiers in Immunology,

(2019), 10, (1084), 10.3389/fimmu.2019.01084). *Frontiers in Immunology*, *11*. https://doi.org/10.3389/FIMMU.2020.00234

Ouimet, M., & Marcel, Y. L. (2012). Regulation of lipid droplet cholesterol efflux from macrophage foam cells. *Arteriosclerosis, Thrombosis, and Vascular Biology*, *32*(3), 575–581. https://doi.org/10.1161/ATVBAHA.111.240705

Panuganti, K. K., Nguyen, M., & Kshirsagar, R. K. (2023). Obesity. *StatPearls*. https://www.ncbi.nlm.nih.gov/books/NBK459357/

Park, B. S., & Lee, J. O. (2013). Recognition of lipopolysaccharide pattern by TLR4 complexes. *Experimental and Molecular Medicine*, *45*(12). https://doi.org/10.1038/EMM.2013.97

Park, B. S., Song, D. H., Kim, H. M., Choi, B. S., Lee, H., & Lee, J. O. (2009). The structural basis of lipopolysaccharide recognition by the TLR4-MD-2 complex. *Nature*, *458*(7242), 1191–1195. https://doi.org/10.1038/NATURE07830

Park, T. S., Panek, R. L., Mueller, S. B., Hanselman, J. C., Rosebury, W. S., Robertson, A. W., Kindt, E. K., Homan, R., Karathanasis, S. K., & Rekhter, M. D. (2004). Inhibition of sphingomyelin synthesis reduces atherogenesis in apolipoprotein E-knockout mice. *Circulation*, *110*(22), 3465–3471. https://doi.org/10.1161/01.CIR.0000148370.60535.22

Park, W. J., & Park, J. W. (2015). The effect of altered sphingolipid acyl chain length on various disease models. *Biological Chemistry*, *396*(6–7), 693–705. https://doi.org/10.1515/HSZ-2014-0310

Parrinello, M., & Rahman, A. (1981). Polymorphic transitions in single crystals: A new molecular dynamics method. *Journal of Applied Physics*, *52*(12), 7182–7190. https://doi.org/10.1063/1.328693

Peter Slotte, J. (2013). Molecular properties of various structurally defined sphingomyelins- Correlation of structure with function. *Progress in Lipid Research*, *52*(2), 206–219. https://doi.org/10.1016/J.PLIPRES.2012.12.001

Peters, L., Kuebler, W. M., & Simmons, S. (2022). Sphingolipids in Atherosclerosis: Chimeras in Structure and Function. *International Journal of Molecular Sciences*, *23*(19). https://doi.org/10.3390/IJMS231911948

Pizzuto, M., Hurtado-Navarro, L., Molina-Lopez, C., Soubhye, J., Gelbcke, M., Rodriguez-Lopez, S., Ruysschaert, J.-M., & Pelegrin, P. (2022). Ornithine Lipid Activates Both TLR4 and the non-canonical NLRP3 Inflammasome. *BioRxiv*, 2022.01.28.477396. https://doi.org/10.1101/2022.01.28.477396

Poltorak, A., He, X., Smirnova, I., Liu, M. Y., Van Huffel, C., Du, X., Birdwell, D., Alejos, E., Silva, M., Galanos, C., Freudenberg, M., Ricciardi-Castagnoli, P., Layton, B., & Beutler, B. (1998). Defective LPS signaling in C3H/HeJ and C57BL/10ScCr mice: Mutations in Tlr4 gene. *Science*, *282*(5396), 2085–2088. https://doi.org/10.1126/SCIENCE.282.5396.2085

Radzikowska, U., Rinaldi, A. O., Sözener, Z. Ç., Karaguzel, D., Wojcik, M., Cypryk, K., Akdis, M., Akdis, C. A., & Sokolowska, M. (2019). The influence of dietary fatty acids on immune responses. *Nutrients*, *11*(12). https://doi.org/10.3390/NU11122990

Raetz, C. R. H., & Whitfield, C. (2002). Lipopolysaccharide endotoxins. *Annual Review of Biochemistry*, *71*, 635–700. https://doi.org/10.1146/ANNUREV.BIOCHEM.71.110601.135414

Raghavan, B., Martin, S. F., Esser, P. R., Goebeler, M., & Schmidt, M. (2012). Metal allergens nickel and cobalt facilitate TLR4 homodimerization independently of MD2. *EMBO Reports*, *13*(12), 1109–1115. https://doi.org/10.1038/EMBOR.2012.155

Ridker, P. M., Everett, B. M., Thuren, T., MacFadyen, J. G., Chang, W. H., Ballantyne, C., Fonseca, F., Nicolau, J., Koenig, W., Anker, S. D., Kastelein, J. J. P., Cornel, J. H., Pais, P., Pella, D., Genest, J., Cifkova, R., Lorenzatti, A., Forster, T., Kobalava, Z., … Glynn, R. J. (2017). Antiinflammatory Therapy with Canakinumab for Atherosclerotic Disease. *New England Journal of Medicine*, *377*(12), 1119–1131. https://doi.org/10.1056/NEJMOA1707914

Roberts, L. D., Virtue, S., Vidal-Puig, A., Nicholls, A. W., & Griffin, J. L. (2009). Metabolic phenotyping of a model of adipocyte differentiation. *Physiological Genomics*, *39*(2), 109–119. https://doi.org/10.1152/PHYSIOLGENOMICS.90365.2008

Robinson, J., Swift-Scanlan, T., Salyer, J., & Jones, T. (2020). The Obesity Paradox in Sepsis: A Theoretical Framework. *Biological Research for Nursing*, *22*(2), 287–294. https://doi.org/10.1177/1099800420905889

Rocha, D. M., Caldas, A. P., Oliveira, L. L., Bressan, J., & Hermsdorff, H. H. (2016). Saturated fatty acids trigger TLR4-mediated inflammatory response. *Atherosclerosis*, *244*, 211–215. https://doi.org/10.1016/J.ATHEROSCLEROSIS.2015.11.015

Rogero, M. M., & Calder, P. C. (2018). Obesity, inflammation, toll-like receptor 4 and fatty acids. *Nutrients*, *10*(4). https://doi.org/10.3390/NU10040432

Ruggiero, A. D., Key, C. C. C., & Kavanagh, K. (2021). Adipose Tissue Macrophage Polarization in Healthy and Unhealthy Obesity. *Frontiers in Nutrition*, *8*. https://doi.org/10.3389/FNUT.2021.625331

Ruiz-Ojeda, F. J., Rupérez, A. I., Gomez-Llorente, C., Gil, A., & Aguilera, C. M. (2016). Cell models and their application for studying adipogenic differentiation in relation to obesity: A review. *International Journal of Molecular Sciences*, *17*(7). https://doi.org/10.3390/IJMS17071040

Ruysschaert, J. M., & Lonez, C. (2015). Role of lipid microdomains in TLR-mediated signalling. *Biochimica et Biophysica Acta - Biomembranes*, *1848*(9), 1860–1867. https://doi.org/10.1016/J.BBAMEM.2015.03.014

Saberi, M., Woods, N. B., de Luca, C., Schenk, S., Lu, J. C., Bandyopadhyay, G., Verma, I. M., & Olefsky, J. M. (2009). Hematopoietic Cell-Specific Deletion of Toll-like Receptor 4 Ameliorates Hepatic and Adipose Tissue Insulin Resistance in High-Fat-Fed Mice. *Cell Metabolism*, *10*(5), 419–429. https://doi.org/10.1016/J.CMET.2009.09.006

Sanin, D. E., Prendergast, C. T., & Mountford, A. P. (2015). IL-10 Production in Macrophages Is Regulated by a TLR-Driven CREB-Mediated Mechanism That Is Linked to Genes Involved in Cell Metabolism. *The Journal of Immunology*, *195*(3), 1218–1232. https://doi.org/10.4049/JIMMUNOL.1500146

Scheiblich, H., Schlütter, A., Golenbock, D. T., Latz, E., Martinez-Martinez, P., & Heneka, M. T. (2017). Activation of the NLRP3 inflammasome in microglia: the role of ceramide. *Journal of Neurochemistry*, *143*(5), 534–550. https://doi.org/10.1111/JNC.14225

Schlitt, A., Blankenberg, S., Yan, D., Von Gizycki, H., Buerke, M., Werdan, K., Bickel, C., Lackner, K. J., Meyer, J., Rupprecht, H. J., & Jiang, X. C. (2006). Further evaluation of plasma sphingomyelin levels as a risk factor for coronary artery disease. *Nutrition and Metabolism*, *3*. https://doi.org/10.1186/1743-7075-3-5

Schroder, K., Irvine, K. M., Taylor, M. S., Bokil, N. J., Le Cao, K. A., Masterman, K. A., Labzin, L. I., Semple, C. A., Kapetanovic, R., Fairbairn, L., Akalin, A., Faulkner, G. J., Baillie, J. K., Gongora, M., Daub, C. O., Kawaji, H., McLachlan, G. J., Goldman,

N., Grimmond, S. M., … Sweet, M. J. (2012). Conservation and divergence in Toll-like receptor 4-regulated gene expression in primary human versus mouse macrophages. *Proceedings of the National Academy of Sciences of the United States of America*, *109*(16). https://doi.org/10.1073/PNAS.1110156109

Schroder, K., & Tschopp, J. (2010). The Inflammasomes. *Cell*, *140*(6), 821–832. https://doi.org/10.1016/J.CELL.2010.01.040

Serhan, C. N., Yacoubian, S., & Yang, R. (2008). Anti-inflammatory and proresolving lipid mediators. *Annual Review of Pathology: Mechanisms of Disease*, *3*, 279–312. https://doi.org/10.1146/ANNUREV.PATHMECHDIS.3.121806.151409

Shi, H., Kokoeva, M. V., Inouye, K., Tzameli, I., Yin, H., & Flier, J. S. (2006). TLR4 links innate immunity and fatty acid-induced insulin resistance. *Journal of Clinical Investigation*, *116*(11), 3015–3025. https://doi.org/10.1172/JCI28898

Shimazu, R., Akashi, S., Ogata, H., Nagai, Y., Fukudome, K., Miyake, K., & Kimoto, M. (1999). MD-2, a molecule that confers lipopolysaccharide responsiveness on toll-like receptor 4. *Journal of Experimental Medicine*, *189*(11), 1777–1782. https://doi.org/10.1084/JEM.189.11.1777

Simopoulos, A. P. (2008). The importance of the omega-6/omega-3 fatty acid ratio in cardiovascular disease and other chronic diseases. *Experimental Biology and Medicine*, *233*(6), 674–688. https://doi.org/10.3181/0711-MR-311

Steppan, C. M., Bailey, S. T., Bhat, S., Brown, E. J., Banerjee, R. R., Wright, C. M., Patel, H. R., Ahima, R. S., & Lazar, M. A. (2001). The hormone resistin links obesity to diabetes. *Nature*, *409*(6818), 307–312. https://doi.org/10.1038/35053000

Stiban, J., Tidhar, R., & Futerman, A. H. (2010). Ceramide synthases: Roles in cell physiology and signaling. *Advances in Experimental Medicine and Biology*, *688*, 60–71. https://doi.org/10.1007/978-1-4419-6741-1_4

Stout, M. B., Justice, J. N., Nicklas, B. J., & Kirkland, J. L. (2017). Physiological aging: Links among adipose tissue dysfunction, diabetes, and frailty. *Physiology*, *32*(1), 9–19. https://doi.org/10.1152/PHYSIOL.00012.2016

Su, L., Athamna, M., Wang, Y., Wang, J., Freudenberg, M., Yue, T., Wang, J., Moresco, E. M. Y., He, H., Zor, T., & Beutler, B. (2021). Sulfatides are endogenous ligands for the TLR4–MD-2 complex. *Proceedings of the National Academy of Sciences of the United States of America*, *118*(30). https://doi.org/10.1073/PNAS.2105316118

Takeda, K., & Akira, S. (2004). TLR signaling pathways. *Seminars in Immunology*, *16*(1), 3–9. https://doi.org/10.1016/J.SMIM.2003.10.003

Takeuchi, O., & Akira, S. (2009). Innate immunity to virus infection. *Immunological Reviews*, *227*(1), 75–86. https://doi.org/10.1111/J.1600-065X.2008.00737.X

Takeuchi, O., & Akira, S. (2010). Pattern Recognition Receptors and Inflammation. *Cell*, *140*(6), 805–820. https://doi.org/10.1016/J.CELL.2010.01.022

Tan, Y., Zanoni, I., Cullen, T. W., Goodman, A. L., & Kagan, J. C. (2015a). Mechanisms of Toll-like Receptor 4 Endocytosis Reveal a Common Immune-Evasion Strategy Used by Pathogenic and Commensal Bacteria. *Immunity*, *43*(5), 909–922. https://doi.org/10.1016/J.IMMUNI.2015.10.008

Tan, Y., Zanoni, I., Cullen, T. W., Goodman, A. L., & Kagan, J. C. (2015b). Mechanisms of Toll-like Receptor 4 Endocytosis Reveal a Common Immune-Evasion Strategy Used by Pathogenic and Commensal Bacteria. *Immunity*, *43*(5), 909–922. https://doi.org/10.1016/J.IMMUNI.2015.10.008

Tarkowski, A., Bjersing, J., Shestakov, A., & Bokarewa, M. I. (2010). Resistin competes with lipopolysaccharide for binding to toll-like receptor 4. *Journal of Cellular and*

Molecular Medicine, *14*(6 B), 1419–1431. https://doi.org/10.1111/J.1582-4934.2009.00899.X

ter Horst, R., van den Munckhof, I. C. L., Schraa, K., Aguirre-Gamboa, R., Jaeger, M., Smeekens, S. P., Brand, T., Lemmers, H., Dijkstra, H., Galesloot, T. E., de Graaf, J., Xavier, R. J., Li, Y., Joosten, L. A. B., Rutten, J. H. W., Netea, M. G., & Riksen, N. P. (2020). Sex-specific regulation of inflammation and metabolic syndrome in obesity. *Arteriosclerosis, Thrombosis, and Vascular Biology*, *40*(7), 1787–1800. https://doi.org/10.1161/ATVBAHA.120.314508

Thomson, M. J., Williams, M. G., & Frost, S. C. (1997). Development of insulin resistance in 3T3-L1 adipocytes. *Journal of Biological Chemistry*, *272*(12), 7759–7764. https://doi.org/10.1074/JBC.272.12.7759

Turner, N., Kowalski, G. M., Leslie, S. J., Risis, S., Yang, C., Lee-Young, R. S., Babb, J. R., Meikle, P. J., Lancaster, G. I., Henstridge, D. C., White, P. J., Kraegen, E. W., Marette, A., Cooney, G. J., Febbraio, M. A., & Bruce, C. R. (2013). Distinct patterns of tissue-specific lipid accumulation during the induction of insulin resistance in mice by high-fat feeding. *Diabetologia*, *56*(7), 1638–1648. https://doi.org/10.1007/S00125-013-2913-1

Turpin, S. M., Nicholls, H. T., Willmes, D. M., Mourier, A., Brodesser, S., Wunderlich, C. M., Mauer, J., Xu, E., Hammerschmidt, P., Brönneke, H. S., Trifunovic, A., Losasso, G., Wunderlich, F. T., Kornfeld, J. W., Blüher, M., Krönke, M., & Brüning, J. C. (2014). Obesity-induced CerS6-dependent C16:0 ceramide production promotes weight gain and glucose intolerance. *Cell Metabolism*, *20*(4), 678–686. https://doi.org/10.1016/J.CMET.2014.08.002

Vaduganathan, M., Mensah, G. A., Turco, J. V., Fuster, V., & Roth, G. A. (2022). The Global Burden of Cardiovascular Diseases and Risk: A Compass for Future Health. *Journal of the American College of Cardiology*, *80*(25), 2361–2371. https://doi.org/10.1016/J.JACC.2022.11.005

Van den Bossche, J., Baardman, J., Otto, N. A., van der Velden, S., Neele, A. E., van den Berg, S. M., Luque-Martin, R., Chen, H. J., Boshuizen, M. C. S., Ahmed, M., Hoeksema, M. A., de Vos, A. F., & de Winther, M. P. J. (2016). Mitochondrial Dysfunction Prevents Repolarization of Inflammatory Macrophages. *Cell Reports*, *17*(3), 684–696. https://doi.org/10.1016/J.CELREP.2016.09.008

Van Der Spoel, D., Lindahl, E., Hess, B., Groenhof, G., Mark, A. E., & Berendsen, H. J. C. (2005). GROMACS: Fast, flexible, and free. *Journal of Computational Chemistry*, *26*(16), 1701–1718. https://doi.org/10.1002/JCC.20291

van der Vorst, E. P. C., Theodorou, K., Wu, Y., Hoeksema, M. A., Goossens, P., Bursill, C. A., Aliyev, T., Huitema, L. F. A., Tas, S. W., Wolfs, I. M. J., Kuijpers, M. J. E., Gijbels, M. J., Schalkwijk, C. G., Koonen, D. P. Y., Abdollahi-Roodsaz, S., McDaniels, K., Wang, C. C., Leitges, M., Lawrence, T., … Donners, M. M. P. C. (2017). High-Density Lipoproteins Exert Pro-inflammatory Effects on Macrophages via Passive Cholesterol Depletion and PKC-NF-κB/STAT1-IRF1 Signaling. *Cell Metabolism*, *25*(1), 197–207. https://doi.org/10.1016/J.CMET.2016.10.013

VanderLaan, P. A., Reardon, C. A., Thisted, R. A., & Getz, G. S. (2009). VLDL best predicts aortic root atherosclerosis in LDL receptor deficient mice. *Journal of Lipid Research*, *50*(3), 376–385. https://doi.org/10.1194/JLR.M800284-JLR200

Von Bank, H., Kirsh, C., & Simcox, J. (2021). Aging adipose: Depot location dictates age-associated expansion and dysfunction. *Ageing Research Reviews*, *67*. https://doi.org/10.1016/J.ARR.2021.101259

Wang, Y., Su, L., Morin, M. D., Jones, B. T., Whitby, L. R., Surakattula, M. M. R. P., Huang, H., Shi, H., Choi, J. H., Wang, K. W., Moresco, E. M. Y., Berger, M., Zhan, X., Zhang, H., Boger, D. L., & Beutler, B. (2016). TLR4/MD-2 activation by a synthetic agonist with no similarity to LPS. *Proceedings of the National Academy of Sciences of the United States of America*, *113*(7), E884–E893. https://doi.org/10.1073/PNAS.1525639113

Warren, H. S., Fitting, C., Hoff, E., Adib-Conquy, M., Beasley-Topliffe, L., Tesini, B., Liang, X., Valentine, C., Hellman, J., Hayden, D., & Cavaillon, J. M. (2010). Resilience to bacterial infection: Difference between species could Be due to proteins in serum. *Journal of Infectious Diseases*, *201*(2), 223–232. https://doi.org/10.1086/649557

Wculek, S. K., Dunphy, G., Heras-Murillo, I., Mastrangelo, A., & Sancho, D. (2022). Metabolism of tissue macrophages in homeostasis and pathology. *Cellular and Molecular Immunology*, *19*(3), 384–408. https://doi.org/10.1038/S41423-021-00791-9

Weisberg, S. P., McCann, D., Desai, M., Rosenbaum, M., Leibel, R. L., & Ferrante, A. W. (2003). Obesity is associated with macrophage accumulation in adipose tissue. *Journal of Clinical Investigation*, *112*(12), 1796–1808. https://doi.org/10.1172/JCI19246

Wickramasinghek, K., Williams, J., Rakovac, I., Grosso, G., & Heinen, M. (2022). Key messages of the WHO European Regional Obesity Report. *The European Journal of Public Health*, *32*(Suppl 3). https://doi.org/10.1093/EURPUB/CKAC129.354

Wilmanski, J. M., Petnicki-Ocwieja, T., & Kobayashi, K. S. (2008). NLR proteins: integral members of innate immunity and mediators of inflammatory diseases. *Journal of Leukocyte Biology*, *83*(1), 13–30. https://doi.org/10.1189/JLB.0607402

Wong, S. W., Kwon, M. J., Choi, A. M. K., Kim, H. P., Nakahira, K., & Hwang, D. H. (2009). Fatty acids modulate toll-like receptor 4 activation through regulation of receptor dimerization and recruitment into lipid rafts in a reactive oxygen species-dependent manner. *Journal of Biological Chemistry*, *284*(40), 27384–27392. https://doi.org/10.1074/JBC.M109.044065

Wymann, M. P., & Schneiter, R. (2008). Lipid signalling in disease. *Nature Reviews Molecular Cell Biology*, *9*(2), 162–176. https://doi.org/10.1038/NRM2335

Yan, L. R., Wang, D. X., Liu, H., Zhang, X. X., Zhao, H., Hua, L., Xu, P., & Li, Y. S. (2014). A pro-atherogenic HDL profile in coronary heart disease patients: An iTRAQ labelling-based proteomic approach. *PLoS ONE*, *9*(5). https://doi.org/10.1371/JOURNAL.PONE.0098368

Yao, J., Wu, D., & Qiu, Y. (2022). Adipose tissue macrophage in obesity-associated metabolic diseases. *Frontiers in Immunology*, *13*. https://doi.org/10.3389/FIMMU.2022.977485

Yeo, H. J., Kim, T. H., Jang, J. H., Jeon, K., Oh, D. K., Park, M. H., Lim, C. M., Kim, K., & Cho, W. H. (2023). Obesity Paradox and Functional Outcomes in Sepsis: A Multicenter Prospective Study. *Critical Care Medicine*, *51*(6), 742–752. https://doi.org/10.1097/CCM.0000000000005801

Yunna, C., Mengru, H., Lei, W., & Weidong, C. (2020). Macrophage M1/M2 polarization. *European Journal of Pharmacology*, *877*. https://doi.org/10.1016/J.EJPHAR.2020.173090

Zamyatina, A., & Heine, H. (2020). Lipopolysaccharide Recognition in the Crossroads of TLR4 and Caspase-4/11 Mediated Inflammatory Pathways. *Frontiers in Immunology*, *11*. https://doi.org/10.3389/FIMMU.2020.585146

Zanoni, I., Ostuni, R., Marek, L. R., Barresi, S., Barbalat, R., Barton, G. M., Granucci, F., & Kagan, J. C. (2011). CD14 controls the LPS-induced endocytosis of toll-like receptor 4. *Cell*, *147*(4), 868–880. https://doi.org/10.1016/J.CELL.2011.09.051

Zanoni, I., Tan, Y., Di Gioia, M., Springstead, J. R., & Kagan, J. C. (2017a). By Capturing Inflammatory Lipids Released from Dying Cells, the Receptor CD14 Induces Inflammasome-Dependent Phagocyte Hyperactivation. *Immunity*, *47*(4), 697-709.e3. https://doi.org/10.1016/J.IMMUNI.2017.09.010

Zanoni, I., Tan, Y., Di Gioia, M., Springstead, J. R., & Kagan, J. C. (2017b). By Capturing Inflammatory Lipids Released from Dying Cells, the Receptor CD14 Induces Inflammasome-Dependent Phagocyte Hyperactivation. *Immunity*, *47*(4), 697-709.e3. https://doi.org/10.1016/J.IMMUNI.2017.09.010

Zhong, Y., Kinio, A., & Saleh, M. (2013). Functions of NOD-Like Receptors in Human Diseases. *Frontiers in Immunology*, *4*. https://doi.org/10.3389/FIMMU.2013.00333

9 ACKNOWLEDGEMENTS

First and foremost I would like to thank my primary supervisors Prof. Dr. Eicke Latz and PD Dr. Peter Düwell for the opportunity to work on such an exciting project in a great laboratory. I am grateful that you always believed in my capabilities, pushed me to the best and offered your guidance, while also letting me pursue my own ideas. Moreover, I can't express enough, how much I appreciate your support in procuring a collaboration with Jan, and allowing me to spend the major part of my PhD in his laboratory in the Netherlands.

I would like to thank Dr. Jan Van den Bossche from the bottom of my heart for agreeing to a collaboration between Bonn and Amsterdam, making it possible for me to work on my project in his group. Your enthusiasm for the topic, "out-of-the-box" perspectives and close supervision immensely facilitated the success of this project in such a short time.

Furthermore I would like to acknowledge all members of my PhD examination committee in Bonn including PD Dr. Peter Düwell, Prof. Dr. Geyer, Prof. Dr. Eicke Latz and Prof. Dr. Zimmer.

It is important to me to acknowledge Dr. Anette Christ, not only for providing relevant preliminary data that served as a basis for this project, but also for guiding me in the first year of my PhD.

In addition, a big thank you goes to the organizing team of the Immunosensation Cluster of Science for organizing courses, expert talks as well as other science-related events.

I would like to express my gratitude to all of our collaborators including all of the clinical study coordinators for providing me with samples to include in my studies. Without you, this project would not have been successful. Thank you to everyone who contributed in preparation of our manuscript; it was an immense team effort that I am extremely proud of!

Further, I would like to express my gratitude to Eisai for gifting us their compound Eritoran (E5564) for use in this study.

I want to acknowledge all of my fellow MCBI colleagues and especially past and present members of "Group Jan" for all the discussions, help in and out of the lab, after-work "borrels" and much needed coffee breaks during long days. A special thanks at this point to my former colleague Kyra for introducing me to the MCBI lab when I started in 2020, and now being there for me as an

extremely supportive friend. Karl, although you drove me crazy with your chaos in the lab, I have come to appreciate you so much not only as a fellow “soon-to-be” PhD, but as one of my best friends. We made it (…almost)! Also, Henrique, you will always remain the happiest face one could ask for at the opposite office desk – you made me smile even on the bad days – thank you!

I am also deeply thankful for the support I got while working in Bonn in transitioning from a Master student to a PhD, during my first PhD year, and while regularly visiting the lab. Specifically, I want to thank Guddi and Andrea for their organizational talent and Max for his support in the lab and sending me countless lab “goodie” packages. In addition, a big thank you goes to Eike G. for not only helping me kick off this whole project, but also always being interested in my scientific and personal progress.

I want to thank my friends, especially Vanessa and Marcel, for always hearing me out and sharing bliss but also worries from a distance. You had my back every time I needed it!

Finally, I couldn’t be more grateful for having a family that always believes in me and provides their unconditional support. Foremost, I am deeply thankful to my sisters: Isi and Thea, you have not only directly contributed to this work - I am glad to have two other “science nerds” by my side… – but you have always motivated me, told me that I got this and celebrated my successes with me. Last but not least, I can’t express enough how much I appreciate the support of my parents. You have always encouraged me to pursue my dreams and go for what feels right for me, not only professionally, but personally. Without my family, I would not have been able to enjoy life outside of my PhD journey as much as I did, and this work would surely not have turned out the way that it did. You taught me to be proud of myself – thank you!